5-17-2017 3:00 PM

Numerical and Experimental Analysis of a Retrofit System for Light-Framed Wood Structures Under Wind Loading

Joshua D. Rosenkrantz
The University of Western Ontario

Supervisor
Prof. A. A. El Damatty
The University of Western Ontario

Graduate Program in Civil and Environmental Engineering
A thesis submitted in partial fulfillment of the requirements for the degree in Master of Engineering Science

Abstract

Load paths in light-frame wood structures have historically been nailed connections between the sheathing and rafters, and toenail connections between the rafters and stud walls. However, these connections have poor resistance to uplifting forces, as occurs in high wind speed events, causing sheathing or roof-to-wall-connection (RTWC) failures. The improvements made to building codes after Hurricane Andrew affected only new construction, and the economic losses caused by roof failures in homes built prior to 1993 from Hurricane Katrina pointed to a need to retrofit older structures. This paper will investigate the design, analysis, and testing of a temporary cable-netting roof harness as an alternative to other relatively expensive and invasive retrofitting options. To do this, a non-linear finite element analysis (FEA) is performed to model a typical light-frame wood structure with the roof harness, which is then validated through results derived from destructively testing a reduced scale LFWS. To demonstrate the comparative benefit of the roof harness, an identical reduced scale LFWS with the retrofit system applied is numerically modeled and destructively tested in the same manner as the unretrofitted LFWS. The comparison of the resulting numerical and experimental data both validates the numerical models used for predicting structural behaviour of the model, and demonstrates significant improvement in the capacity of the structure when the retrofit system is applied.

Keywords: Light-Framed Wood Structures, Finite-Element Modeling, Hurricane Damage Mitigation, Roof to Wall Connection, Retrofit, Roof Harness, Structural Scaling, Wind Tunnel

Co-Authorship Statement

This thesis has been prepared in accordance with the regulations for an Integrated-Article format thesis stipulated by the School of Graduate and Postdoctoral Studies at the University of Western Ontario and has been co-authored as:

Chapter Two: Comparative Testing of a Reduced Scale LFWS Using Wind Load

The initial numerical model was developed by A. Dessouki. Modifications to the numerical model and the numerical analysis were completed by R. Jacklin under the supervision of Dr. A. A. El Damatty. Further modifications to the numerical model and the numerical analysis were completed by A. Enajar and J. Rosenkrantz under the supervision of Dr. A. A. El Damatty. Drafts of the work were prepared by A. Enajar and J. Rosenkrantz and modifications were completed under the supervision of Dr. A. A. El Damatty. A paper co-authored by J. Rosenkrantz, A. Enajar, R. Jacklin, A. Dessouki, and A. A. El Damatty will be submitted to the *Journal of Wind and Structures.*

Chapter Three: Comparative Testing of a Reduced Scale LFWS Using Wind Load

The initial numerical model was developed by A. Dessouki. Modifications to the numerical model and the numerical analysis were completed by R. Jacklin under the supervision of Dr. A. A. El Damatty. Further modifications to the numerical model and the numerical analysis were completed by A. Enajar and J. Rosenkrantz under the supervision of Dr. A. A. El Damatty. Drafts of the work were prepared by A. Enajar and J. Rosenkrantz and modifications were completed under the supervision of Dr. A. A. El Damatty. A paper co-authored by J. Rosenkrantz, A. Enajar, R. Jacklin, A. Dessouki, and A. A. El Damatty will be submitted to the *Journal of Wind and Structures.*

Acknowledgments

I would like to first thank my supervisor, Dr. A. A. El Damatty for his valuable guidance and expertise throughout my time working under his supervision. I would also like to thank M. A. Steelcon Engineering Limited for the financial support of the research, and the WindEEE and IRLBH facilities for their assistance with the experimental program. I wish to extend gratitude to my research partner, Adnan Enajar, as well as all the volunteers who participated in the experimental work. Finally, I would like to thank my mother Pat and sister Leah for their unwavering support, and my father David for encouraging me to do what I love.

Table of Contents

List of Tables

List of Figures

1 Introduction

1.1 Motivation

Light frame wood structures (LFWSs) are the most popular choice of construction for residential buildings in North America. The relative abundance of products have led to the wide spread adoption of light framing wood as an inexpensive and efficient building material. Most LFWSs do not require exceedance of span and load limits set out by building codes, and therefore referral to standard details for essential building components without structural analysis is acceptable.

LFWSs have historically been vulnerable to the effects of high speed wind events. Relatively light components and building envelope materials can be breached and allow damage such as water intrusion, or catalyze more serious structural failure. A particularly common point of building envelope breach is the roof system, which accounted for approximately 95% (Baskaran and Dutt, 1997) of the 20-25 billion USD in economic losses incurred by Hurricane Andrew in Florida during 1992 (HUD, 1993). Figure 1.1 shows extensive damage to roofs from Hurricane Andrew.

Figure 1.1 Roof damage from Hurricane Andrew, www.floridadisaster.org

Standard details outlined in building codes were changed to address this issue, and following Hurricane Katrina in 2005, were deemed to have a positive effect on LFWS resilience, despite the persistence of some issues with the vertical load path (van de Lindt et al., 2007). However, significant economic loss was still observed, particularly in structures where non-structural elements allowed for breach of the building envelope and where the vertical load path was inadequate (van de Lindt et al., 2007). Expected annual hurricane damage in the United States is predicted to increase 12 billion USD by 2075, as both climate change and coastal development expose more infrastructure to greater risk (cbo.gov, 2016). The goal of this research is to address this apparent need for mitigation strategy that specifically focusses on reducing or eliminating the issue of damage to the roof system of LFWSs in high speed wind events.

During a high speed wind event, flow separation occurs over low-pitch roofs creating large areas of suction. This suction can then be amplified if the building envelop is breached, by increasing the pressure inside the house and adding to the global uplift pressure on the roof. Failure in the roof system then occurs where the vertical load path is unable to transfer the force applied. Critical failure locations have been roof-to-wall connections (RTWCs) and sheathing-to-truss connections (STTCs), as both have historically relied on nailed connections with poor uplift resistance to transfer load between components (FEMA, 1993; van de Lindt et al., 2007). Figure 1.2 and Figure 1.3 show STTC and RTWC failure respectively, the latter being an example of catastrophic failure.

Figure 1.2 STTC failure, www.fema.gov

Figure 1.3 RTWC failure and full roof collapse, www.floridadisaster.org

There is an obvious need for investigating and mitigating the way in which LFWS roofs fail in high speed wind events. Existing research has examined RTWCs and STTCs at the component level and has led to more robust connection devices mandated by code for new structures, as well as an assortment of retrofit options for already built structures. Past research has also investigated numerical methods of structural behavior analysis, validated experimentally with both full scale and simulated full scale testing.

1.2 Background

1.2.1 Numerical and Experimental Studies of LFWS Behaviour

Past numerical and experimental studies of the behaviour of LFWSs have largely sought to investigate full-scale structures in order to fully capture the system behaviour. Experimental testing of individual and connected RTWCs have also been conducted to characterize their non-linear behaviour, and study its combined effect with load sharing.

The numerical studies by Jacklin and El Damatty (2014) and Dessouki and El Damatty (2010) focused on creating numerical models of a full scale LFWS that was experimentally tested by Morrison (2010). Known as the 'Three Little Pigs' project, a single storey gable roof LFWS was constructed according to the Ontario Building Code, and tested at the University of Western Ontario (UWO) under realistic wind loads. These loads were applied to the roof of the structure via 58 airbags that were evacuated to simulate the characteristic fluctuating suction induced by flow separation. RTWCs were subjected to loads exceeding their individual capacity, but load sharing in the roof structure was found to have distributed the uplift force over adjacent RTWCs. The toe-nails were found to have failed incrementally with the fluctuating load, where peak gust loads corresponded with spikes in permanent withdrawal. The severity of these spikes, or damaging peaks, increased corresponding to wind speed.

A precursor to the numerical models developed of the 'Three Little Pigs' house, Li et. al. (1998) created a numerical model that had many unique features, some of which were borrowed in the initial numerical models of the 'Three Little Pigs' house. The sheathing was modelled as lateral beams between trusses, the top chords of the trusses had artificially

increased stiffness to account for the composite effect of the connected sheathing, and the gusset plates connecting the truss members were allowed to release moment. Agreement between numerical and literature derived values of deflection, load distribution and axial force were deemed realistic and provided confidence in the model.

The first numerical model of the 'Three Little Pigs' house created by Dessouki and El Damatty (2013) consisted of frame and shell elements to model the structure, and non-linear links using a stiffness relationship defined by Reed et. al. (1997) to simulate the toe-nail connections. Uniform surface loads where applied across the surface of the roof to model the airbags used in the experimental test. Since LFWS roofs have typically low periods of vibration, the non-linearity of the roof is chiefly attributed to the RTWCs. Given that the RTWCs were characterized by a user-defined relationship, there was no non-linearity expected from the roof and a quasi-static analysis was conducted considering a number of time-steps from the time-history of the experimental test. The numerically predicted RTWC displacement results had good agreement with those collected experimentally, and the model was concluded to be therefore validated. Further examination of this model identified that the gable end trusses attracted a significant portion of the load within the tributary area of adjacent trusses. For this reason, as well as non-linear nature of load sharing within the structure, the tributary area method of allocating load to RTWCs was deemed inaccurate.

Jacklin and El Damatty (2014) developed a successive numerical model to the one developed by Dessouki and El Damatty (2010), which focused on modelling only the roof of the experimentally tested structure and included inset RTWCs to allow for overhanging eaves. Similar to the first numerical model, Jacklin and El Damatty (2014) validated the

second model by observing good agreement between numerically derived RTWC deflections and those collected experimentally. The numerical investigation also concluded the unsuitability of the tributary area method in accounting for load at RTWCs, again due to the inability of the method to consider both the load attraction to the much stiffer gable end trusses and load sharing between the trusses. It was also found that the behaviour of the roof structure was highly dependent on the type of load, either uniform or realistic, that was applied.

Individual toe-nail connection testing was undertaken by Morrison (2010) and used fluctuating simulated wind loads to assess hysteretic behaviour of the connection. Though this differed from the ramp load approach undertaken by Reed et al. (1997), the way in which load was applied was deemed to have a negligible effect on the overall capacity of the nail. Hysteresis was observed in the toe-nail connections, and initial stiffness was found to be similar to stiffness after successive loading and unloading cycles.

Khan and Kopp (2012) continued experimental testing of individual toe-nail connections, and of a system toe-nail connections linked by a steel angle section that loosely simulated lateral roof stiffness. It was found that in both individual and in interconnected configurations, toe-nail connections had higher variation in failure displacement than failure capacity, though more so individually. Additionally, since the difference in stiffness between toe-nail connections is relatively small prior to yield, the difference in load across the connections was at a minimum. Conversely, just prior to failure of the system, load difference was found to be greatest as individual connections began to rapidly loose stiffness.

Similar conclusions regarding load sharing were reached by running a sensitivity analysis on the stiffness of elements in a numerical model developed by Shivarudrappa and Nielson (2013). This model was validated by the experimental results of Datin and Prevatt (2013) and concluded that increased withdrawal stiffness in the RTWCs and bending stiffness in the sheathing panels had a significant effect on load sharing.

The past research detailed, both experimental and numerical, can be used to understand the sensitivity of structural behaviour to certain component and loading parameters, allow for the development of more accurate models, and outlines the boundaries of current knowledge on how LFWSs behave under high speed wind loads.

1.2.2 Current State of Technology

1.2.2.1 Building Code and Construction Products

Products such as ring shank nails and hurricane clips were developed to replace or add to existing construction products and methods for use in new construction, responding to the need to enhance the tensile resistance of vertical load paths in LFWSs. Similarly, building code changes have been developed to address advances in knowledge, and to respond to catastrophic losses incurred by past high speed wind events. The most significant of these with respect to the improvement of roof performance were enacted by the 1994 South Florida Building Code in response to the heavy losses incurred there by Hurricane Andrew in 1992.

Though the use of new building products are suggested in these codes, it is not always mandated. For example, though the 2014 Florida Building Code mentions that both 8D common nail and ring shank nails of the same size can be used, tests have revealed that the

use of ring shank nails improved the mean uplift capacity of a typical sheathing panel by 32% (IHRC, 2012).

1.2.2.2 Retrofitting Technology

Though newly constructed LFWSs incorporate new building products and are built in accordance to modern code provisions, older LFWSs are remain particularly susceptible to damage in high wind speed events. A number of mainly internal retrofitting options have been developed in response to this issue, such as adhesives, straps, hurricane ties, and the installation of additional studs (FEMA, 2010). However, these methods often require invasive renovations and are therefore expensive, estimated between 15 – 50 % of the cost of an existing structure (Stewart et al, 2003). Since retrofitting RTWCs is not required by the FBC if Further, insurance providers may not renew policies for roofs older than 20 years, and will only pay current value once damage has already occurred (insurance.com, 2016). Leaving the financial burden to the consumer increases the likelihood that roofs will not be adequately maintained to withstand high speed wind events.

An idea to significantly lessen the cost of retrofitting old roofs is the roof harness. Consisting of tension elements placed over the roof and pretensioned to either the foundation or anchor piles independent of the structure, the roof harness is a temporary method of providing an alternate load path to resist uplift forces. It requires little if any alteration of the underlying structure, and similar to other damage mitigation practices, it can be applied to the structure in the event of a high wind speed warning and removed thereafter. The roof harness is designed to prevent structural damage to RTWCs and STTCs, damage to roof cladding elements, and theoretically prohibits a total loss of roof.

There exist a number of patents for various roof harnesses, which can be categorized as chiefly fabric or cable based systems. Bachynski (2007), Gaffney (1998), Gitlin and Maloney (1998), and Watson Jr. (2008) have filed patents on systems using a pretensioned fabric mesh with integrated straps that serve to connect the system to anchor piles. These systems have all of the potential benefits of the most robust roof harnesses, while providing extra coverage of windows and other fenestration from windborne debris. However, these systems all have very complex strapping configurations, many tie-down points, and consist of one large sheet. This makes the application of such systems cumbersome and time consuming, likely requiring professional assistance.

Alternatively, patents filed by Bimberg and Bimberg (1997) and Luzzi (1999) rely on simpler, cable and strap-based systems respectively. Bimberg and Bimberg (1997) proposed a system consisting of a series of cables applying compressive force to the roof through wooden bearing pads and attached on either side of the structure to pile, while Luzzi (1999) proposed an array of ratchet straps spanning the roof and anchored to the foundation. Though the simplicity of these designs allow for low cost and ease of application, depending on the density of cables only RTWC failure is prevented, leaving the structure vulnerable to sheathing and cladding damage that is likely to cause the most damage. Therefore, further iterations of this technology should seek to combine the protection offered by fabric-based systems with the simplicity and ease of application of the strap and cable-based system.

1.2.3 Numerical and Experimental Studies of Roof Harness Behaviour

The current research program began with the work of Dessouki and El Damatty (2010), with the goal of minimizing own weight and number of external cables, while maximizing

RTWC and STTC protection. The resulting retrofit configuration, pictured in Figure 1.4 below, consisted of an orthogonal mesh of interior cables connected to rigid carbon fibre rods around the perimeter of the structure and anchored through external cables to piles.

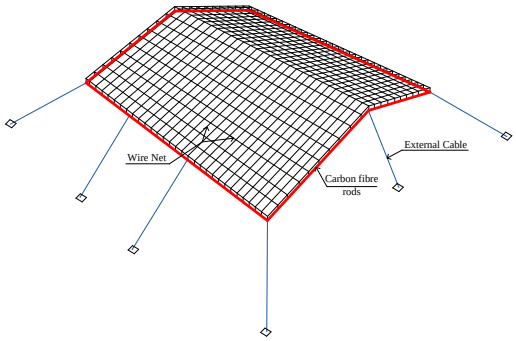

Figure 1.4 Restrofit system proposed by Dessouki and El Damatty (2010)

Using the previously developed numerical model of the 'Three Little Pigs' structure, a parametric optimization of the size and configuration of the various retrofit components was conducted with the goal of minimizing weight and maximizing stiffness. The retrofit system was included in the numerical model of the original LFWS by treating rigid bars as three dimensional frame elements, and the cables as non-linear cable objects with a target force acting as a pretension in the external cables. Using a static non-linear analysis, a uniform suction of 2 kN/m^2 was applied over the surface of the roofs of both the original numerical model, and the one including the retrofit system. A comparison of the results revealed a 40 % reduction in the average RTWC deflection, providing the motivation for further investigation of the technology.

Given these encouraging results, Jacklin and El Damatty (2014) refined the previously developed retrofit concept as a series of modular sections that can be easily applied and stored, and replaced the costly carbon fibre bars with more cost-effective aluminum. A picture of the new design is shown in Figure 1.5 below.

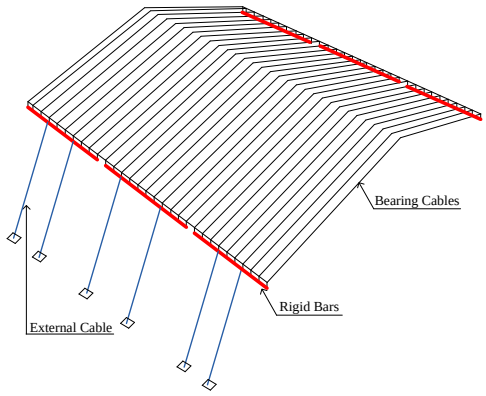

Figure 1.5 Retrofit system proposed by Jacklin and El Damatty (2014)

This new design of the retrofit system was incorporated into the updated numerical model similarly to the previous exercise, where a non-linear static analysis was used to incrementally apply a more realistic load to the underlying LFWS. The load applied simulated winds in excess of 25 m/s such that the RTWCs would exhibit plastic deformation to observe the load sharing behaviour between the two load paths. A parametric study was conducted to optimize the sizes of the various components.

Jacklin and El Damatty (2014) also conducted the first experimental tests of the retrofit system, by subjecting a 9 m by 1.2 m strip of a full scale roof without overhang to an uplift force produced by a hydraulic jack located under the test section. A photo of the test setup is shown in Figure 1.6 below.

Figure 1.6 Sample roof strip and retrofit tested by Jacklin and El Damatty (2014)

The roof had a slope of 4:12, used 3-16D spiral nails in the RTWCs, and consisted of three trusses spaced at 0.6 m. The retrofit system used 3/16 in. and 1/2 in. diameter aircraft cable for the interior and exterior cables respectively, as well as a 2 in. by 4 in. by 1/4 in. hollow aluminum section as the rigid bar. This experiment concluded that the presence of the retrofit system decreased the expected deformation at the RTWCs by approximately 40 %, validating the results of the numerical model.

1.3 Objectives

Furthering the experimental research of Jacklin and El Damatty (2014), the current study compares the performance of a reduced scale LFWS with and without a reduced scale retrofit system subject to wind loading. The primary objectives of this investigation are to better understand the interaction between the retrofit and the underlying LFWS, and to evaluate the effectiveness of the retrofit as a means of preventing roof damage. In this investigation roof damage is constrained to the RTWCs, and retrofit improvement is

defined as the increase in velocity required to achieve: (i) initial separation, (ii) initial RTWC failure, (iii) windward RTWC failure. However, the use of wind to generate destructive failure in a reduced scale LFWS requires additional objectives for the development and validation of an appropriate testing environment, and the development of an appropriate scaling method to scale component strength.

The objectives of each chapter in this investigation can then be summarized as follows:

- Design a simple, reduced scale destructive testing environment that produces a sufficiently great wind speed over a suitably large wind field. This should demonstrate the viability of similar additions to improving wind tunnel capabilities.

- Characterize the resulting wind field and determine the resulting pressure coefficient and RTWC load distributions.

- Design a reduced scale test specimen that approximates the behaviour of a full scale LFWS and meets the geometric constraints as set out by the testing environment.

- Predict the behaviour of the test specimen using a numerical model.

- Observe total windward RTWC failure in the test specimen at a desired failure velocity, and optimize the numerical model to better correspond with the recorded failure mode.

- Predict the behaviour of the test specimen and a reduced scale version of the retrofit system using a numerical model.

- Observe comparative improvement to the test specimen and retrofit system under similar wind load, and optimize the numerical model to better correspond with the recorded response.

1.4 Thesis Structure

This thesis has been prepared in the 'Integrated Article' format. The current chapter discusses the motivation for the following research by investigating the inherent susceptibility of older LFWSs to wind induced uplift loads. The chapter further investigates previously developed measures to protect these vulnerabilities such as building code changes, and retrofitting methods. An evaluation of retrofitting methods is then conducted with a specific focus on proposed roof harness designs. The retrofit design and research developed and conducted by Jacklin and El Damatty (2014) are reviewed and assessed. The primary objectives of the thesis are then defined to expand on this research and the requirements of the current research, to be addressed in subsequent chapters, are then outlined. The final chapter provides a summary of the key findings of the current research and suggested improvements for future research.

1.4.1 Structural Behaviour Analysis of a Reduced Scale LFWS Subject to Wind Load

The second chapter recounts prior work regarding development of an outdoor testing environment for reduced scale applications at the WindEEE dome, as well as the associated uplift load imparted to a reduced scale structure. It then describes the development of the reduced scale LFWS, corresponding numerical model, results of the destructive test, and post-failure numerical model. The chapter first introduces the scaling process by which the strength of components in the one third length scaled LFWS were reduced. A numerical

model is generated and a non-linear static analysis is performed to assess the roof behaviour over a range of wind speeds. The experimental test is then discussed and the results presented. The numerical model is updated to reflect the observed experimental roof response, and the results of the initial and updated numerical models are then compared with the experimental results to determine accuracy. Importantly, this chapter presents the behaviour of the LFWS as the control variable.

1.4.2 Structural Behaviour Analysis of a Reduced Scale Retrofitted LFWS Subject to Wind Load References

Similar to the previous chapter, the third chapter discusses development of the reduced scale retrofit system, addition of the retrofit to the numerical model, results of the experimental test, and a post-failure adaptation of the initial model. However, this chapter also compares the numerical and experimental results of the retrofitted and unretrofitted structures, and suggests an alternate configuration to the retrofit system to improve performance. As before, the chapter describes the same process for decreasing the strength and size of the retrofit components, as well as the incorporation of the system into the existing numerical LFWS model. The experimental test and results are then presented, followed by a description of the adaptations made to the numerical model from post-failure analysis and corresponding results. Again, the accuracy of the initial and post-failure models are compared and recommendations are made as to improvement measures. The third chapter then uses the results of the previous chapter to compare the benefit of applying the retrofit system, and an alternate retrofit configuration is produced and analyzed to assess potential performance improvement.

1.5 References

Baskaran, A. and Dutt, O., 1997. Performance of roof fasteners under simulated loading conditions. Journal of Wind Engineering and Industrial Aerodynamics, 72(0), 389-400

Bimberg, U., and Bimberg, O. (1997), U.S Patent No. 5623788. Washington, DC: U.S. Patent and Trademark Office.

Bitsuamlak, G.T., et al 2009, Computational assessment of blockage and wind simulator proximity effects for a new full-scale testing facility, Wind and Structures, Vol. 13 No. 1, 21-36

Cook, N. J., 1985. The designer's guide to wind loading of building structures. Garston, Watford: Building Research Establishment, Dept. of the Environment. USA

Dagnew, A., 2012. Computational Evaluation of Wind Loads on Low and High- Rise Buildings (Doctoral Dissertation).

Federal Emergency Management Agency (FEMA), 1993. Building Performance: Hurricane Iniki in Hawaii - Observations, Recommendations, and Technical Guidance. Federal Emergency Management Agency.

Federal Emergency Management Agency (FEMA), 2010. Wind Retrofit Guide for Residential Buildings. Federal Emergency Management Agency.

Jacklin, R., El Damatty A. A., Dessouki, A. A., 2014. Finite-Element Modeling of a Light-Framed Wood Roof Structure. Wind and Structures, Vol. 19 No. 6, 603-621

Morrison, M. J. (2010). *Response of a Two-Story Residential House Under Realistic Fluctuating Wind Loads*. (PhD Thesis). London, Ont.: Department of Engineering, The University of Western Ontario.

Luzzi, J., 1999. U.S Patent No. 5881499. Washington, DC: U.S. Patent and Trademark Office.

Reed, T. D., Rosowsky, D. V. and Schiff, S. D. (1997). Uplift capacity of light-frame rafter to top plate connections. *Journal of Architectural Engineering, 3*(4), 156-163.

Roof Damage and Insurance., 2016, July 29, Retrieved December 25, 2016, from http://www.insurance.com/home-and-renters-insurance/coverage/have-a-20-year-old-roof-you-may-lose-your-homeowners-insurance.html

States, Congress Of The United, and Congressional Budget Office. "Potential Increases in Hurricane Damage in the United States: Implications for the Federal Budget." CBO (2016), cbo.gov. June 2016. Web. 25 Dec. 2016.

Stewart, M. G., 2003. Cyclone damage and temporal changes to building vulnerability and economic risks for residential construction. Journal of Wind Engineering and Industrial Aerodynamics, 91(5), 671-691

Tsoumis, G. 1991. Science and technology of wood: structure, properties, utilization. New York: Van Nostrand Reinhold.

van de Lindt, J., Graettinger, A., Gupta, R., Skaggs, T., Pryor, S., and Fridley, K., 2007. Performance of wood-frame structures during Hurricane Katrina. Journal of Performance of Constructed Facilities, 21(2), 108-116.

2 Structural Behaviour Analysis of a Reduced Scale LFWS Subject to Wind Load

2.1 Introduction

Connections in the vertical load path of light-frame wood structures (LFWSs) allows the sheathing to transfer vertical forces imposed on the roof to the trusses beneath, then further to the stud walls and through to the foundation. Historically, sheathing connections to roof trusses and the roof truss connections to stud walls are typically nailed, with poor withdrawal resistance (FEMA, 1993; van de Lindt et al., 2007). After Hurricane Andrew in 1993 caused considerable economic losses, largely due to the failure of roofing system components (Baskaran and Dutt, 1997), building codes across North America began to reflect the need for increased capacity in these connections. Since the building code changes only affected new construction, it left older structures prone to damage during high speed wind events. This became evident in the aftermath of Hurricane Katrina, where older structures experienced considerable damage (van de Lindt et al., 2007).

Though there exist retrofitting options for older structures such as adhesives, straps, hurricane ties, and the installation of additional studs (FEMA, 2010), these options are relatively invasive and are approximately 15-50 % of the cost of the structure to implement (Stewart et al, 2003). This points to a need for a low-cost, and minimally invasive method of improving vertical load paths.

One such method is the roof harness, where a mesh of cabling or fabric covers the roof and is tethered to either the foundation of the structure or surrounding piles. The harness is designed for temporary application in the event of a high wind speed event warning, and does not require the applicator to be a contractor or construction professional. Though there

exist various patents for roof harness systems (Bimberg 1997; Luzzi 1999), the system developed by Jacklin and El Damatty (2014) shown in Figure 2.1 seeks to address issues apparent in their design through improving modularity, increasing stiffness, and reducing the weight of the retrofit system. The proposed roof harness retrofit system consists of modular strips of bearing cables connected through rigid bars to two external cables which are anchored to piles surrounding the structure.

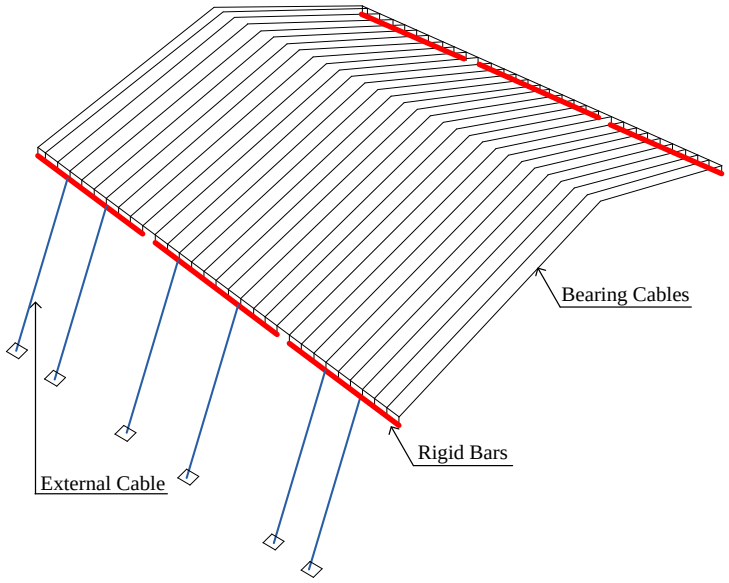

Figure 2.1 Retrofit system proposed by Jacklin and El Damatty (2014)

Finite element analysis (FEA) and experimental testing are performed to understand the structural behaviour of this roof harness configuration and the underlying roof. The primary objective of the experimental testing is to first determine the capacity of the roof through RTWC failure, and then comparatively examine the performance of the roof with the harness.

Experimental testing involves subjecting a whole structure to a range of wind speeds, allowing for a robust examination of the effects of spatially and temporally varying suction

on inter-truss load sharing and non-linear roof-to-wall connection behaviour. The WindEEE Dome in London, Canada is chosen as the testing facility as the exterior platform can accommodate a large test specimen that is loaded until failure. A three-dimensional contraction is used to increase the incident wind velocity and direct the flow at the test specimen.

The test specimen is designed such that (i) failure occurs at a sufficiently small fraction of the maximum available wind velocity, (ii) RTWC failure is the primary failure mode, (iii) its geometry is sufficiently within the wind-field generated by the contraction, and (iv) the demand-capacity ratios of structural members are similar to the full scale structure.

To reduce the capacity of the RTWC connections while maintaining a ductile failure mode similar to full scale nailed connections, smaller nails are evaluated as potential candidates. Using a simple displacement controlled apparatus, the average force-displacement relationship is determined for a variety of smaller candidate nails. FEA models of potential configurations for the reduced scale structure are then generated using non-linear springs to model the RTWCs and loaded with the pressure coefficient distribution generated from Rosenkrantz and El Damatty (2016). However, due to minimum bounds in observed nail candidate capacity, the number of trusses are reduced in the final test specimen configuration to promote failure at the target velocity.

Once the configuration of the reduced scale structure is determined according to the capacity of the reduced RTWC, a static non-linear analysis of the structure using the newly developed RTWC constitutive relationship is conducted assuming full scale members cross-sections. A uniform suction is incrementally applied until the solution does not

converge. Iteratively, the cross-section dimensions are optimized such that the demand capacity ratios of each structurally pertinent member are the similar to those in the full scale structure loaded at the same fraction of the failure load.

Length and strength scaling can be valuable tools to destructive experimental research by reducing the amount of space and load required of testing apparatuses. The primary goal of this paper is to demonstrate the ability of these techniques applied to a LFWS in accurately replicating the failure mode observed in full scale structures. The secondary goals are to prove the accuracy in which the FEA can model the recorded failure mode, and to assess the sensitivity of structural behaviour to various RTWC constitutive relations.

2.2 Testing Environment, Initial Specimen Geometry and Load Effects

2.2.1 Testing Environment

This section focusses on prior work by Rosenkrantz and El Damatty (2016). The WindEEE Dome at the University of Western Ontario is selected as the testing venue as its ability to accommodate outdoor testing greatly reduces the risk of facility damage when performing destructive tests. Outdoor testing requires the dome to act as an open circuit wind tunnel where two garage doors on opposite ends of the hexagonal structure open to allow air to pass through. However, since reverse flow from the fans produced relatively low wind velocities, a three dimensional linear contraction is employed to increase the incident wind velocity.

The dimensions of the resulting wind field cover a 1.9 m height and a 6 m width. The mean velocity and turbulence intensity factor contour plots shown in Figure 2.2 below are

measured via cobra probes, measuring the wind profile and assess the propagation of the jet flow through the incident portion of the wind field.

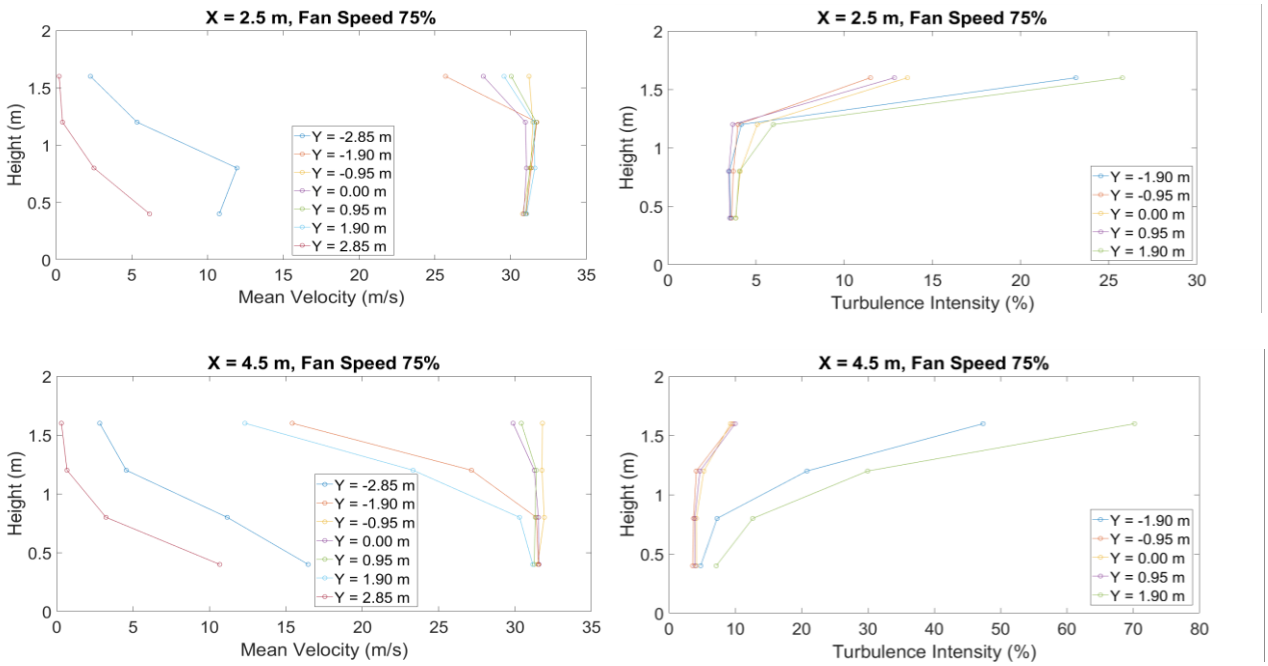

a) b)

Figure 2.2 Measured velocity and turbulence intensity profiles respectively

Decay in both wind velocity and flow smoothness is noticeable near the sides and top of the wind field, where the jet mixes with the relatively stagnant outdoor air. The dimensions of the proposed test specimen are designed to be within the uniform range of the contour plots, resulting in uniform flow across the windward face of the specimen. Though uniform flow produces different pressure distributions over a structure than a more realistic boundary layer flow, it is important to note that the wind field in this experiment is not intended to simulate reality. As such, it is used as a structural loading mechanism used to conveniently compare suction induced behaviour over complex test specimens under similar loading conditions.

2.2.2 Specimen Geometry

The geometry of the test specimen was designed to (i) fit within the uniform area of the wind field and (ii) promote failure in the RTWC at a suitably low wind velocity. The latter criteria is to allow the retrofitted structure to have a substantial margin of velocity with which to demonstrate a performance improvement. To determine the geometry of the test specimen, a variety of augmentations are applied to the FEM developed by Jacklin and El Damatty (2014). At the outset, the size of the structure is reduced to 3 m square by 0.9 m at the eave height to fit within the wind field. Additionally, since the house is tested at an incident angle of 0˚, the roof pitch is decreased from 4:12 to 3:12 to promote greater flow separation and consequently greater suction across the roof. The RTWCs are then modelled as pin connections simply to assess the load attributed to each model, and all member sizes are left as in the full scale model. Using the C_P distribution developed from wind tunnel tests by Dagnew et al (2012) for a similar roof shape, a static pressure distribution is applied over the roof corresponding to 30 m/s, produced by the contraction apparatus at approximately 75% fan speed. A linear static analysis is performed, indicating a need to reduce the number of trusses from 16 to 4 such that tributary area allocated to each RTWC can be maximized. Given the relatively small number of trusses, the end trusses are designed to simulate interior trusses to prevent significant load attraction to much stiffer gable end trusses. This is done by replacing plywood cladding with reinforced plastic sheeting and removing stud wall supports along the truss length, ensuring that the end trusses have no added in-plane stiffness from cladding while sealing the building envelope, and that all the trusses are supported similarly.

2.2.3 Wind Load Effects

From this analysis, the geometry of the structure is set and a rough estimate of the RTWC uplift forces are generated and deemed suitable. A prototype specimen then is built and tested in the apparatus at a variety of fan speeds to establish the effects of the applied wind field, namely the suction distribution across the roof and the RTWC uplift forces.

The roof is outfitted with 40 differential pressure transducers distributed across the roof. One port on each pressure transducer is directly exposed to the exterior and interior of the roof. A schematic of the instrumentation is shown in Figure 2.3 below.

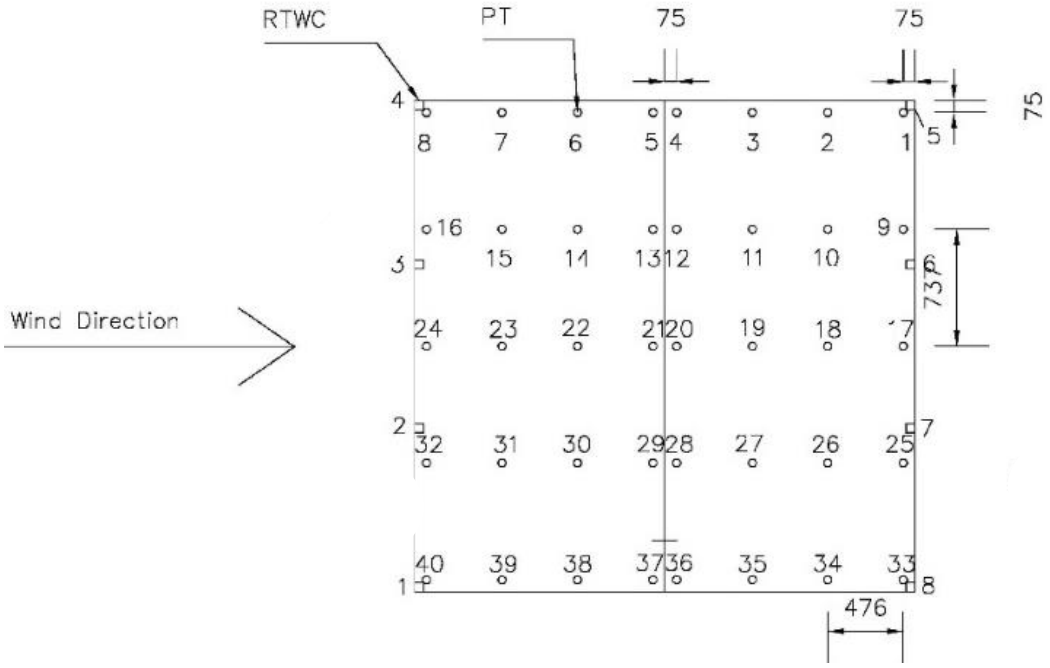

Figure 2.3 Diagram of pressure transducer and load cell layout

The wind profile used in this experiment is very uniform, and produces atypically even pressure distributions over the roof of the specimen. Borrowed from Cook (1985), Figure 2.4 a) and b) show the difference in pressure distribution over the top of a cube in uniform and boundary layer profiles respectively.

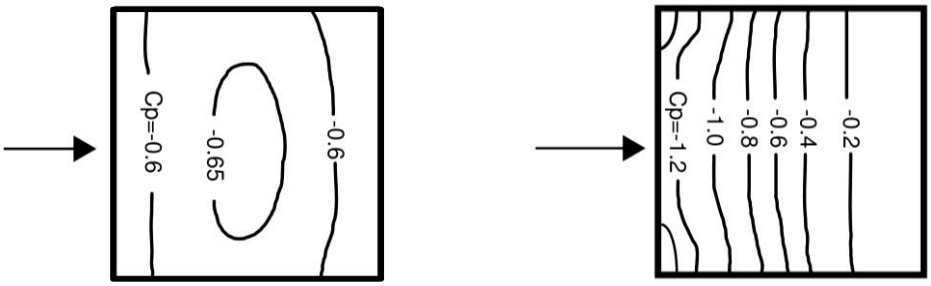

a) b)

Figure 2.4 C_P distributions over flat roof in a) uniform and b) boundary layer flows

The uniform profile produces a comparatively even pressure distribution since there is a lack of Reynolds stresses encouraging flow reattachment (Cook, 1985). Similarly, the pressure distribution observed from the test is notably uniform. Figure 2.5 shows the test results compared to experimental results of a specimen with a similar 3:12 slope gable roof tested in boundary layer flow with a roughness length of $z_0 = 0.23$ m, similar to suburban exposure (Dagnew, 2012).

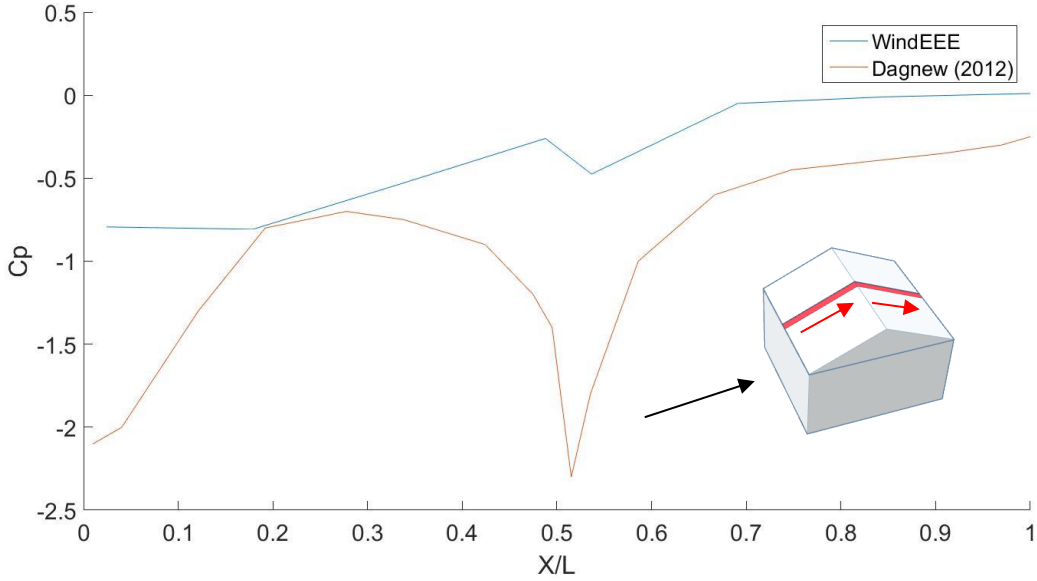

Figure 2.5 Pressure coefficient in the direction of flow along the centre of the roof

The shape of the two curves are qualitatively similar, however the separation and reattachment of flow at the windward edge and peak of the roof are significantly less in uniform flow. Though undetected along the centre of the roof, since the eave height of the test specimen is relatively high, erosion of the wind field may introduce pressure variation near the edges of the roof towards the leeward half. Though the pressure profile does not simulate reality, it does impart the required pressure to generate failure.

Uplift forces are measured by push-button style load cells under each RTWC. Since these load cells can only measure compression, weights are hung between the roof trusses near the RTWCs. This imparts an initial compressive force at the RTWCs greater than the maximum expected value of uplift, so that the load cells are constantly in compression and the roof remains fixed to the walls. RTWC reactions are then measured as a decrease in the initial load. Table 2.1 shows the average RTWC reaction recorded at each fan speed. The location of each RTWC is as outlined in section 2.2 previously.

Fan Speed	**RTWC 1**	**RTWC 2**	**RTWC 3**	**RTWC 4**	**RTWC 5**	**RTWC 6**	**RTWC 7**	**RTWC 8**
50%	101.5	206.9	184.2	101.5	43.9	86.8	81.9	26.1
60%	153.1	290.8	265.1	153.1	68.3	123.0	118.4	40.8
75%	229.5	430.5	408.1	229.5	99.9	173.3	158.5	65.6

Table 2.1 Average RTWC reaction (N)

RTWCs 1-4 recorded larger uplift due to the localized effects of flow separation in this area. Further, the RTWCs experience uplift proportional to the tributary area allocated to them, since there is no failure-induced load redistribution experienced in this test. Consequently, end truss RTWCs 1, 4, 5, and 8 recorded approximately half the load experienced at the interior truss RTWCs.

At 50% fan speed, the RTWC uplift force of approximately 207 N was chosen as the criterion regarding average maximum ultimate failure capacity for selection of a smaller nail for the reduced RTWC. Assuming that failure of the unretrofitted structure initiates at 50% fan speed, this offers the retrofitted structure a margin of 50% fan speed to demonstrate performance enhancement.

2.3 Strength Scaling and the Design of a Reduced Strength Scaled LFWS

2.3.1 Concept of Structural Scaling

In cases where the dynamic effects of loading can be neglected, as in the case of a typical LFWS subject to wind loading, strength scaling can be applied to mimic the structural behavior of a full scale structure on a reduced length scale. This is achieved by preserving the demand-capacity ratios of individual structural members relative to each other. To provide a basis for comparison, the demand-capacity ratios of individual structural members are compared to the ratio of the current wind velocity to the velocity that initiates failure.

The reduced length scaled test specimen is designed such that failure mode of interest initiates at the desired velocity and that the structural behavior resembles that of the full scale structure. Since RTWC failure is isolated as the governing failure mode, alternatives for full scale RTWCs are sought to reduce the capacity of the connection while maintaining a similarly ductile constitutive relation. Once the properties of a suitable reduced capacity RTWC are established, an iterative comparison of the full and reduced scale FEMs are carried out using incrementally increased uniform loads using a static non-linear analysis. The goal of this exercise is to optimize the size of the roof truss members such that their

demand capacity ratios at any given fraction of the failure loading conditions are similar to those in the full scale structure. RTWC demand capacity ratios are also compared in the same manner with the expectation that these values are unity when failure loading conditions are applied.

2.3.2 RTWC Scaling

2.3.2.1 Literature Review

The RTWC research regarding toe-nail connection withdrawal behaviour is sourced from studies that used both load and displacement controlled approaches. Reed et al. (1997) provided a ramp load used to induce a continuous rate of displacement between 2.54 mm/min. and 5.08 mm/min. The resulting deflection curve shown below was established from load-deflection measurements collected every 3.2 mm up to 12.7 mm, 1/5 of the total nail length. The most common failure mode of the toenail connection was pullout from the top plate.

More detailed testing of test samples focusing solely on toe-nail connections was conducted by Morrison (2010) and Khan and Kopp (2012). These studies compared the effects of withdrawal using ramp loading and simulated wind loading. Morrison (2010) provide Table 2.2 shown below comparing the distribution of failure types among the tested specimens, and the correlation of failure type to mean failure capacity.

Failure Mode	**% of Failures**
All Nails Split	8 %
D-Side Split	21 %
S-Side Split	6 %
All Nails Pull Out	65 %

Table 2.2 Failure mode statistics (Khan and Kopp, 2012)

Khan and Kopp (2012) have performed further testing on toe-nailed connections and have produced an average load displacement curve, shown in Figure 2.6 below, for 35 samples subjected to an 8 kN/min ramp load.

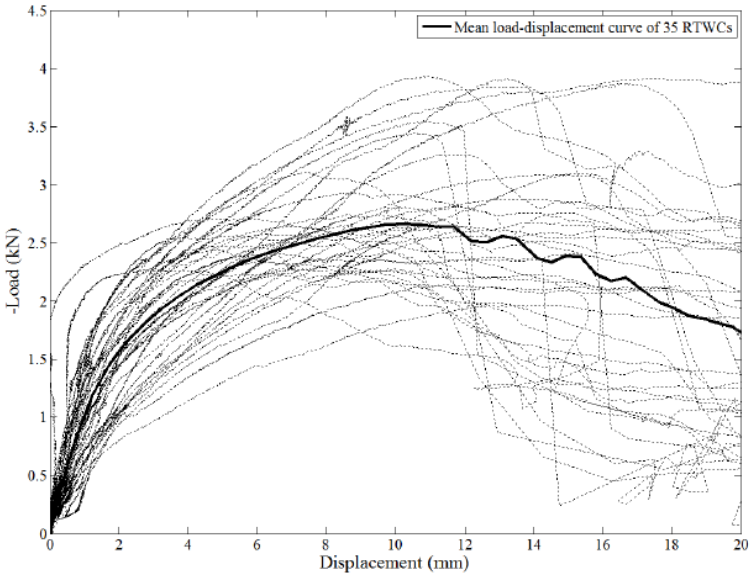

Figure 2.6 Typical force – displacement relationship (Khan and Kopp, 2012)

Further, statistics of the parameters from both bi-linear and curvi-linear fits were generated to assess the non-linear response. The bi-linear statistics, shown in the Table 2.3 below, are used for simplicity as a benchmark for assessing behaviour similarity.

Statistics	**Yield Capacity, F_y (kN)**	**Yield Displacement, D_y (mm)**	**Initial Slope, K_0 (mm)**	**Failure Capacity, F_c (kN)**	**Failure Displacement, D_c (mm)**	**Secondary Slope, K_1 (mm)**
Mean	1.17	1.22	1.06	2.84	10.57	0.19
Maximum	2.26	2.15	2.61	3.93	17.48	0.28
Minimum	0.59	0.55	0.46	1.97	5.06	0.05
Std. Dev.	0.36	0.41	0.47	0.57	3.41	0.06
COV	0.31	0.33	0.45	0.20	0.32	0.31

Table 2.3 Bi-linear statistics for force – displacement curves (Khan and Kopp, 2012)

2.3.2.2 Test Description

The criteria governing nail size selection for the reduced scale RTWCs is simply to reduce the capacity of the connection as much as possible while maintaining similarity in withdrawal response to a full scale toe-nail connection. Therefore, testing began with ten connection samples using 2D common nails, the smallest size framing nail available that had no supplementary shank features to improve withdrawal strength such as spiraling or rings. However, before connections using the 2D nail are tested, ten connection samples using 12D spiral shank are tested and the results were compared to those from literature to verify the testing method and identify any skewness in the data.

All test specimens consist of a 1' long 2" x 4" segment simulating the roof truss and two 1½' long 2" x 4" segments simulating the top plate. The segments simulating the top plate were fastened together with six 1½" long deck screws to ensure that any relative displacement would occur exclusively between the roof truss and the top plate segments. Further, two metal contact points are installed on either end of the roof truss segment where displacement from the jacks is applied. Three nails are hand driven through the roof truss to the top plate in according to the schematic shown in Figure 2.7 below. There is an s-side and a d-side, corresponding to the side of the sample with a single nail and double nails respectively. The wood used was No. 1 grade SPF, and was qualitatively dry. The moisture content was not quantitatively verified as this parameter is known to have a negligible effect on withdrawal behaviour, when compared to factors such as fabrication (Khan and Kopp, 2012).

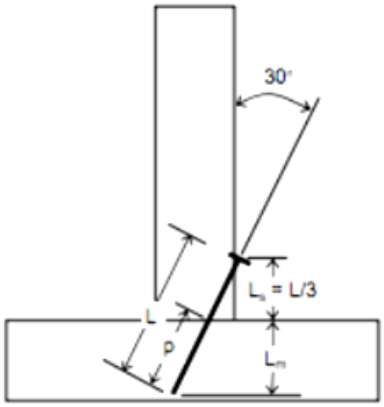

Figure 2.7 Toe-nail connection schematic (AWC, 2007)

The test apparatus used two hand operated hydraulic jacks to induce discrete displacement between rates of approximately 6 mm/min to 12 mm/min. This is slightly faster than the rate of displacement used by Reed et al (1997) but within the envelope specified by ATSM D1761. There are four load cells that act as a force balance, and are located on top of the jack crossheads and at either end of the top plate segment. An average of the sum of forces recorded at the load cells above the crossheads less the own weight of the specimen and instruments and of the sum of forces recorded at the load cells at either end of the top plate are what is used to determine the force the total uplift force on the test specimen. Displacement was recorded with a linear variable displacement transducer installed above the roof truss segment. The configuration shown in Figure 2.8 below allows top plate segment to be braced against the inside of the hollow steel section while the roof truss segment is lifted by the jacks.

Figure 2.8 Toe-nail connection test setup

2.3.2.3 Compare Observed 12D Results to Literature

The typical force-displacement curve is the calculated as the average withdrawal force in eight of the tested toe-nail connection samples, where the curves with the highest and lowest ultimate capacity are removed. As displacement was applied in discrete increments, removing the effect of relaxation was done by fitting smoothing spline with a smoothing parameter value of 0.9 to the force-displacement relations of each sample, as shown in Figure 2.9 below.

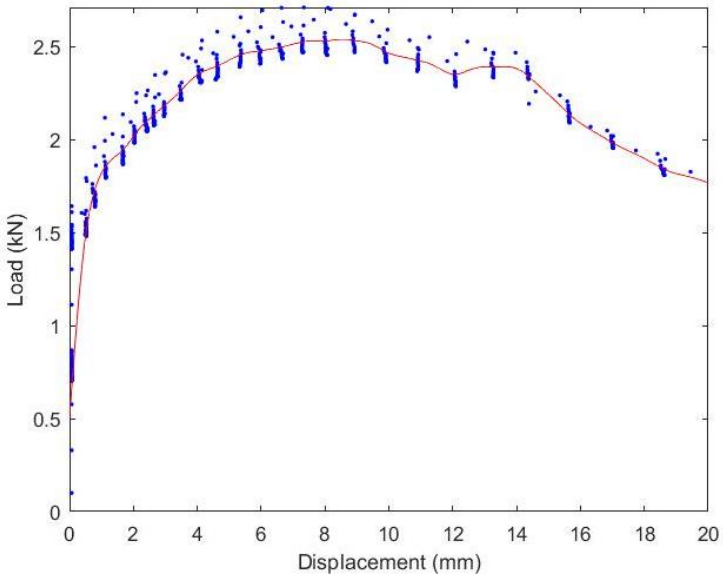

Figure 2.9 RTWC test sample 2 with and without smoothing

As the force-displacement curves are fitted as functions of displacement, the typical curve is then simply the average of the fitted withdrawal force for each sample for every value of displacement between 0 mm and 20 mm, or approximately half the embedment length. The calculated average curve is shown in Figure 2.10 below.

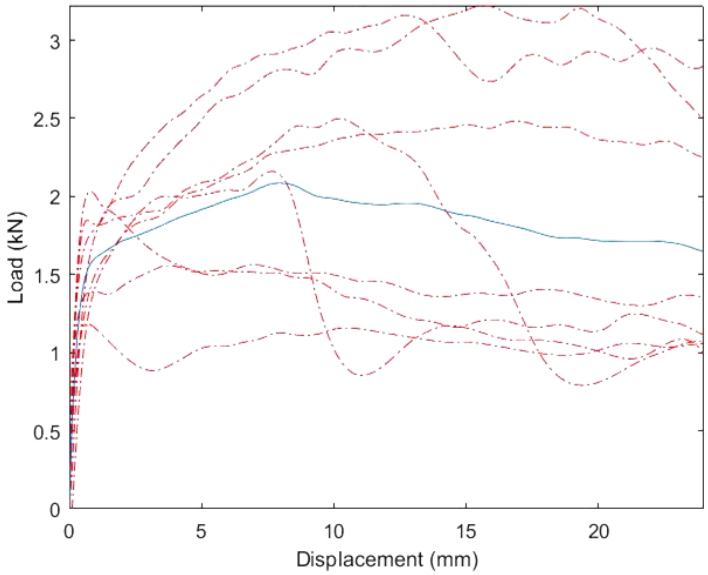

Figure 2.10 Typical 12D spiral nail force – displacement curve from test

12D spiral nails were specifically chosen as a test control, to be compared to the data produced by Khan and Kopp (2012) using the same nail in a similar set of tests. This data will be referred to in this paper as the 'literature'. To quantitatively assess behavioural similarity to the literature, the bi-linear statistics for the above figure are presented in Table 2.4 below. As in the literature, an arbitrary selection method is used to determine the yield point.

Statistics	**Yield Capacity, F_y (kN)**	**Yield Displacement, D_y (mm)**	**Initial Slope, K_0 (mm)**	**Failure Capacity, F_c (kN)**	**Failure Displacement, D_c (mm)**	**Secondary Slope, K_1 (mm)**
Mean	1.50	1.24	1.21	2.05	8.24	0.16
Maximum	2.10	1.35	1.60	3.43	16.10	0.09
Minimum	1.20	1.05	1.14	1.27	1.50	0.16
Std. Dev.	0.31	0.11	0.24	0.68	5.66	0.06
COV	0.20	0.09	0.20	0.33	0.69	0.40

Table 2.4 Typical bi-linear force – displacement statistics from displacement test

Though the range of the test statistics is somewhat small compared to the literature, the failure capacity and displacement are both still highly dependent on the type of failure initiated. The difference between these test values and the values produced by Khan and Kopp (2012) as a percentage of the latter are presented in Table 2.5 below.

Percent Difference	**Yield Capacity**	**Yield Displacement**	**Initial Slope**	**Failure Capacity**	**Failure Displacement**	**Secondary Slope**
Mean	28.21 %	1.64 %	14.15%	27.82 %	22.04 %	15.79 %
Maximum	7.08 %	37.21 %	38.70 %	12.72 %	7.89 %	67.86 %
Minimum	103.39 %	90.91 %	147.83 %	35.53 %	70.36 %	220.00 %
Std. Dev.	13.89 %	73.17 %	48.94 %	19.30 %	65.98 %	0.00 %
COV	35.48 %	72.73 %	55.56 %	65.00 %	115.63 %	29.03 %

Table 2.5 Difference in bi-linear statistics between test and Khan and Kopp, 2012

Given the highly variable nature of wood product performance, the difference between the mean bi-linear test statistics and those from Khan and Kopp (2012) demonstrate a good agreement. Further, the failure mode of each sample are documented in Table 2.6 below.

Failure Mode	% of Failures
All Nails Split	10 %
D-Side Split	30 %
S-Side Split	20 %
All Nails Pull Out	40 %

Table 2.6 Failure mode statistics from test

Though this distribution is more even across all failure modes than as recorded in the literature, the two obvious modes of the data correspond with similar modes in the literature. As the population of this test includes only ten specimens, the expectation is that an increase in the number of specimens would allow the current distribution to approach that of the literature.

The agreement between both the distributions of failure mode and characteristics of the force displacement relationships indicate that the test design is valid and that it is suitable for determining the behaviour of similar toe-nail connections using different nail sizes.

2.3.2.4 Compare 2D Curve and Types of Failure Observed to Literature

The same method of generating the typical force displacement relationship of connections using the 12D spiral nail is used for connections using the 2D common nail. However, while loading the apparatus one of the specimens broke due to the small size of nail used, resulting in a total population size of nine specimens for the test.

Again, a smoothing spline was fitted to the force displacement relationship for each specimen with a smoothing parameter of 0.9 to remove the effects of relaxation. Then, an average of each of the fitted functions is determined over the interval of 0 mm to 7 mm, approximately half the embedment length of the nail. The typical force displacement curve is shown in Figure 2.11 below.

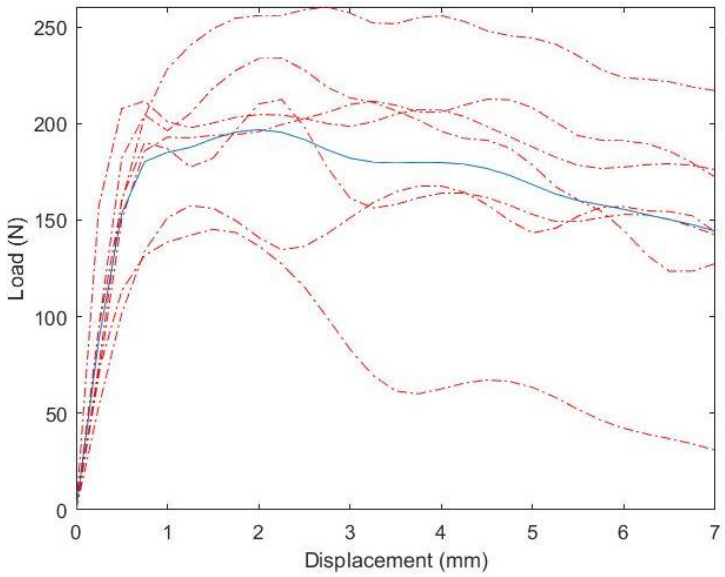

Figure 2.11 Typical 2D force – displacement curve from test

Importantly, the above 2D withdrawal curve demonstrates an approximate tenfold reduction of ultimate failure capacity compared to a connection using 12D nails. However, to compare the behaviour of the curves from the 12D and 2D nails, both sets of data need to be normalized. Therefore, the withdrawal load is normalized to the average failure capacity and the displacement is normalized to the vertical embedment length of the toenail connection. Figure 2.12 below shows both the 12D and 2D normalized force displacement relationships.

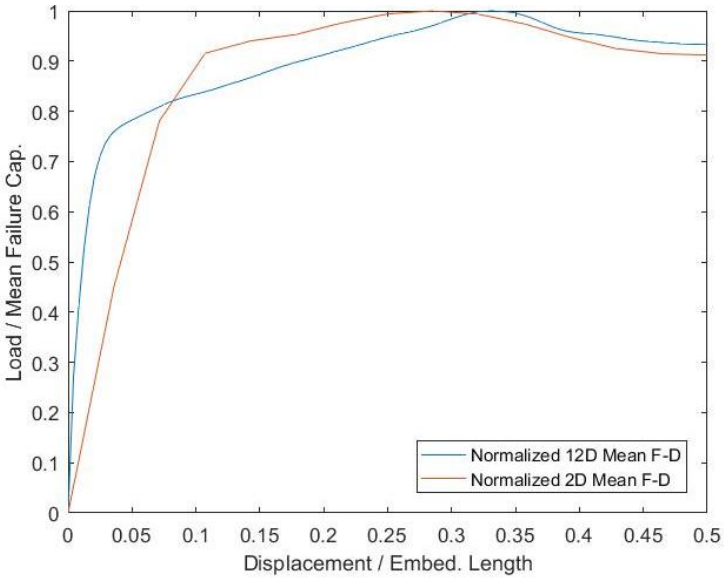

Figure 2.12 Normalized mean force-displacement curves

The statistics of the normalized mean curves are described in Table 2.7 below.

Normalized Mean Statistics	Yield Capacity	Yield Displacement	Initial Slope	Failure Capacity	Failure Displacement	Secondary Slope
2D	0.85	0.10	8.50	1.00	0.28	0.83
12D	0.75	0.03	25.00	1.00	0.33	0.83
% Diff.	11.76%	70.00%	194.12%	–	17.00%	0.00%

Table 2.7 Bi-linear parameters for 2D and 12D normalized typical force – displacement

The most apparent difference in behaviour between the two nail sizes is the mean normalized initial slope. The 12D connections tended to have a much greater initial stiffness, possibly due the spiraled shank. However, the secondary slope is virtually identical and there are only small differences in both the yield capacity and ultimate failure displacement.

The failure modes of the two tests and the test from the literature are compared in Table 2.8 below.

Failure Mode	2D % of Failures	12D % of Failures	12D (Khan and Kopp, 2012) % of Failures
All Nails Split	0 %	10 %	8 %
D-Side Split	11 %	30 %	21 %
S-Side Split	44 %	20 %	6 %
All Nails Pull Out	44 %	40 %	65 %

Table 2.8 Comparison of failure modes by nail type

Notably, the s-side split failure mode occurred the same number of times as all nails pulling out, which was not nearly as common in both 12D studies. It is observed that when roof truss penetration length L_a is small, the bottom corner of the roof truss tends to delaminate along the grain and split easily. This behaviour is magnified when even small asymmetries in loading increase force through a particular side of the connection, leaving the s-side with only one nail notably vulnerable to sharp increases in local stress. Though the 2D connections have a different failure mode distribution than that of 12D connections, nail pullout still remains the dominant failure mode. Further, given that the normalized typical withdrawal curves of the two types of nail are similar, it is reasonable to conclude that greater number of s-side failures has a negligible effect on the average withdrawal behaviour of the 2D nail. Considering the inherent variability of wood products, the both the response and failure mode make the 2D common nail a suitable candidate to structurally scale a full scale toe-nail RTWC.

2.3.3 Member Scaling

Scaling the individual roof truss members is done by iteratively changing their dimensions and then comparing their response as a part of the reduced scale roof to that of similar

members in the full scale roof. In this way, the behaviour of the RTWCs can also be assessed to ensure good agreement.

Once the 2D connection typical withdrawal behaviour is established, it is used to determine the size of the roof truss members. To scale these members according to strength, an adaptation of a FEM produced by Jacklin and El Damatty (2014) is used to model the reduced scale test specimen at full scale. To do this, the gable end trusses are simply replaced with interior trusses to simulate the reduced scale structure that have no gable end trusses. However, as before, there are still 16 trusses in the full scale FEM. An image of the model is shown in Figure 2.13 below.

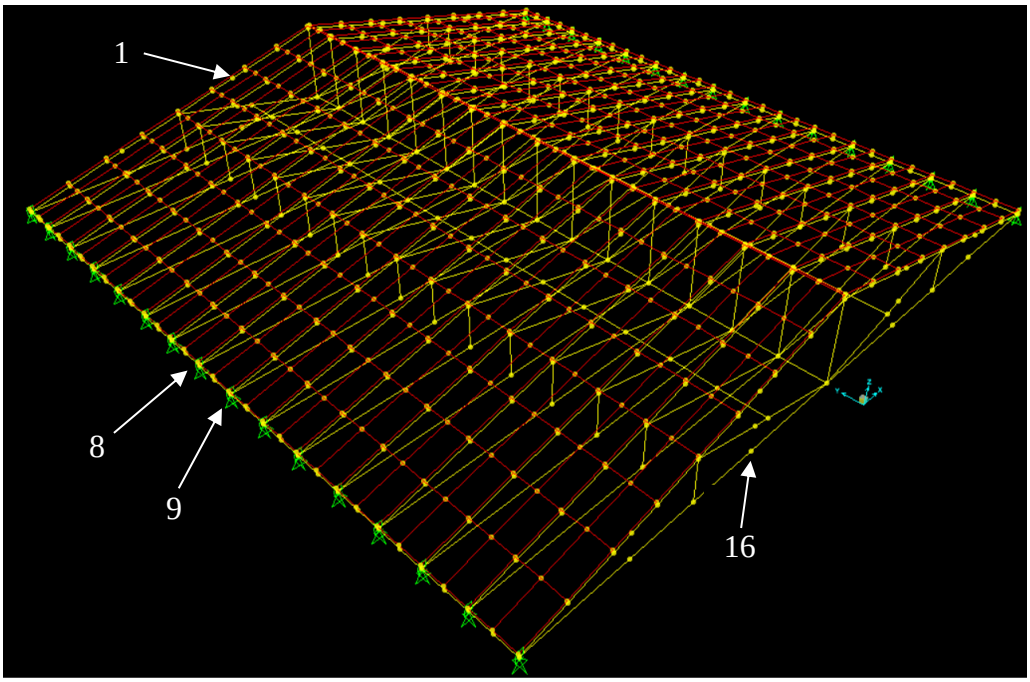

Figure 2.13 Full scale FEM with trusses of interest identified

The model is then incrementally loaded using a non-linear static analysis. A uniform pressure distribution is applied over the roof corresponding to $^1/_2\,\rho v^2$ for values of v increasing every 0.5 m/s from 0 m/s until the solution does not converge. This point in the

analysis is where failure is deemed to occur. The demand-capacity ratios for the truss members are then determined at every 0.5 m/s increment.

Similarly, a reduced scale adaptation of the full scale FEM is produced where the geometry and number of trusses are reduced, and the RTWCs are idealized as non-linear plastic deformation link elements. An image of the FEM is shown in Figure 2.14 below.

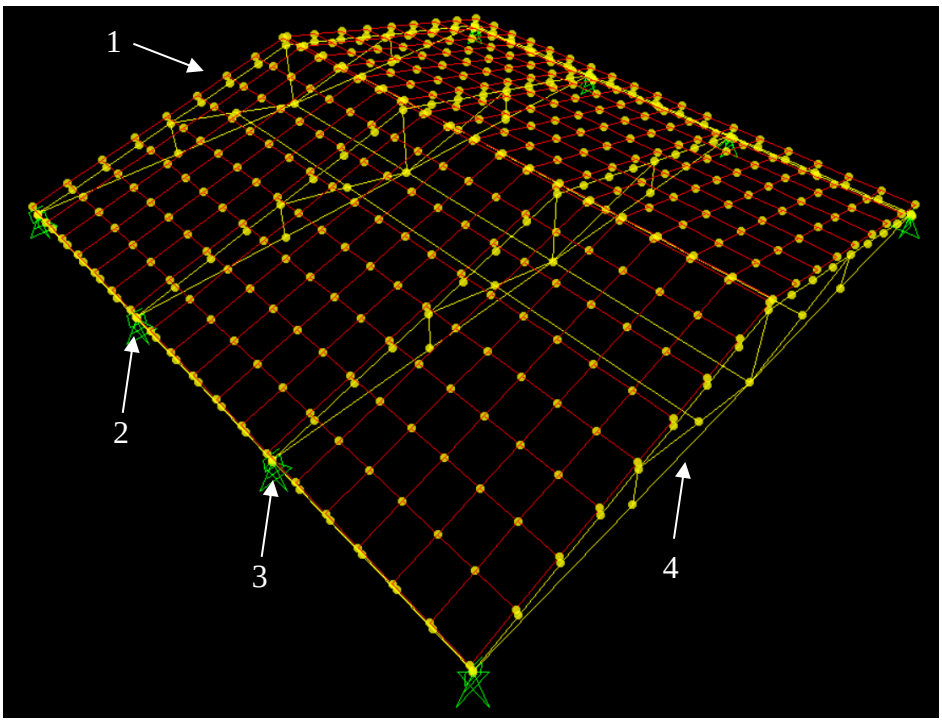

Figure 2.14 Reduced scale FEM with trusses of interest identified

These links elements follow the typical force displacement relationship established for the 2D toe-nail connection. The model is then subject to the same loading and analysis as the full scale FEM, and again the demand-capacity ratios for every member and connection are then determined at every 0.5 m/s increment.

To compare the two different structures with similar trusses, only the exterior trusses 1 and 16 as well as the two middle trusses 8 and 9 of the large scale FEM are investigated. These

are then compared to the response of their reduced scale counter parts 1 and 4 as well as 2 and 3 respectively.

To compare the resulting two sets of data, the demand-capacity ratios for each member and connection are plotted against the system demand-capacity ratio, which is the proportion of the current velocity increment to the failure velocity. Comparing the results in this way allows for the normalization of the failure velocity, unique to both models.

Once a method of comparison is established, member sizes are iteratively altered to better match the response of members in the full scale structure. The average response of the RTWCs in the final configuration of the reduced model are plotted in Figure 2.15 below.

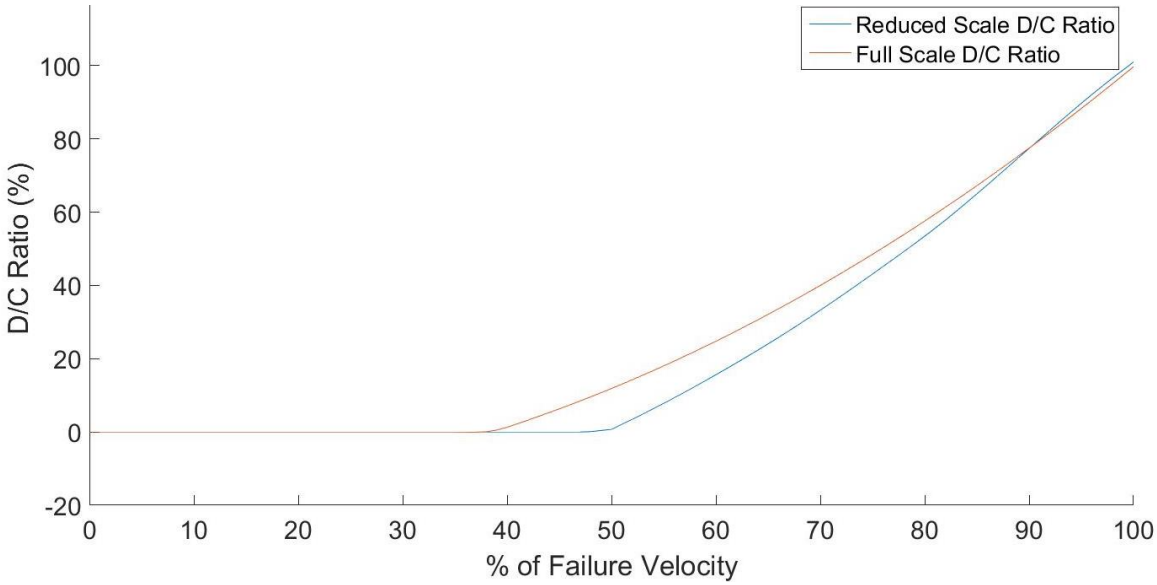

Figure 2.15 Average windward RTWC demand – capacity ratios

For the RTWCs, the capacity is chosen as the average ultimate failure capacity of the connection. Since these connections govern failure, it is logical that when system demand meets system capacity, so too do the RTWCs. The two distinct areas of the curve are the net compression area where the own weight of the structure is not yet overcome, and the

net uplift phase. There exists a small difference between full and reduced scale RTWCs where the point of net uplift initiates. This is due to differences in own weight of the structure and the size of tributary areas allocated to RTWCs. However, there is good agreement between the responses.

Given that wood is an orthotropic material, for this exercise it is assumed that all truss members are cut such that the principle axis is in line with the radial direction of the wood grain. This is taken into account when preparing the reduced scale model truss. As such, for SPF of 12% moisture content, the yield capacity is approximately 41.4 MPa (Tsoumis, 1991). The observed behaviour of the truss members in both the full and reduced scale FEMs is, at every load increment, well within the very linear elastic range of response. Therefore, simply assessing the demand-capacity ratios of the individual truss members at the system failure loading condition is adequate. Notation of the different truss members are presented in Figure 2.16 below.

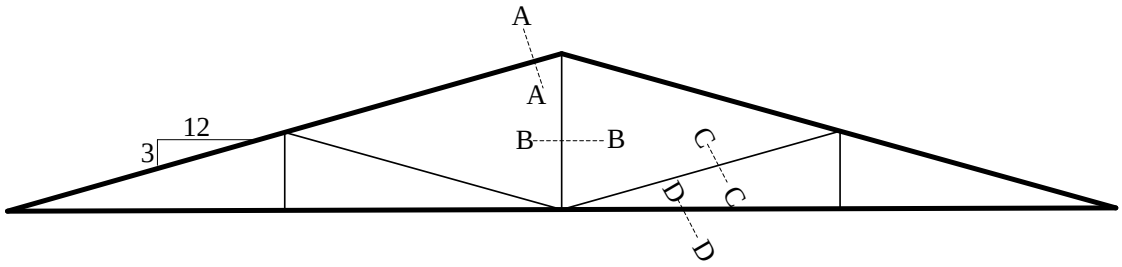

Figure 2.16 Truss member schematic

The following Table 2.9 uses this notation to compare the demand-capacity ratios of the full scale truss members and the final iteration of the reduced scale truss members.

Section	Reduced Scale	Full Scale

	Dimension	Demand (MPa)	Capacity (MPa)	*D/C (%)*	Dimension	Demand (MPa)	Capacity (MPa)	*D/C (%)*
A-A Top	1” x 1-1/2”	1.15	29.29	*3.9*	2” x 4”	2.92	29.29	*9.9*
A-A Bottom	1” x 1-1/2”	0.79	12.23	*6.4*	2” x 4”	2.78	12.23	*22.8*
B-B	1” x 1”	0.062	12.4	*0.5*	2” x 3”	0.001	5.67	*0.02*
C-C	1” x 1”	0.238	8.53	*2.7*	2” x 3”	0.1143	8.53	*1.3*
D-D	1” x 1”	0.372	5.53	*6.7*	2” x 4”	0.094	0.971	*9.7*

Table 2.9 Demand – capacity ratios for reduced and full scale truss members at failure

The difference in the demand-capacity ratios between the reduced scale and full scale truss members are relatively small and remain well within the elastic range, indicating that any variance over the range of loading is less than what is present at failure.

In addition to decreasing the size of the truss members, the sheathing thickness is also decreased. Since sheathing contributes minimally to the lateral stiffness of the roof truss, 3/8” OSB is used to reduce the own weight of the structure, compared to 5/8” in the full scale structure. The sheathing-to-truss connections (STTs) are fixed using a robust screwed connection, such that failure is restricted to the failure mode of interest in the RTWCs.

The use of system demand-capacity ratio as a basis for comparing the demand-capacity ratios of individual truss members and RTWCs is the primary means of ensuring response correlation in strength scaled structures. By setting the full scale relationship as a target for the reduced scale structure, the size of the truss members are then optimized. Using the optimal sized members and connections, the structure should now behave similar to a full scale structure under similar loading conditions.

2.4 Analysis of FEM Behaviour Subjected to Realistic Wind Load

Subjecting the model to a simple uniform pressure is sufficient to observe whether an adapted structure behaves like the original when scaling the structurally relevant components by strength. However, to understand response of the model to the loading conditions applied by the testing apparatus, pictured in Figure 2.17 below as outlined in Rosenkrantz and El Damatty (2016), it is necessary to provide the model with a spatially varying pressure.

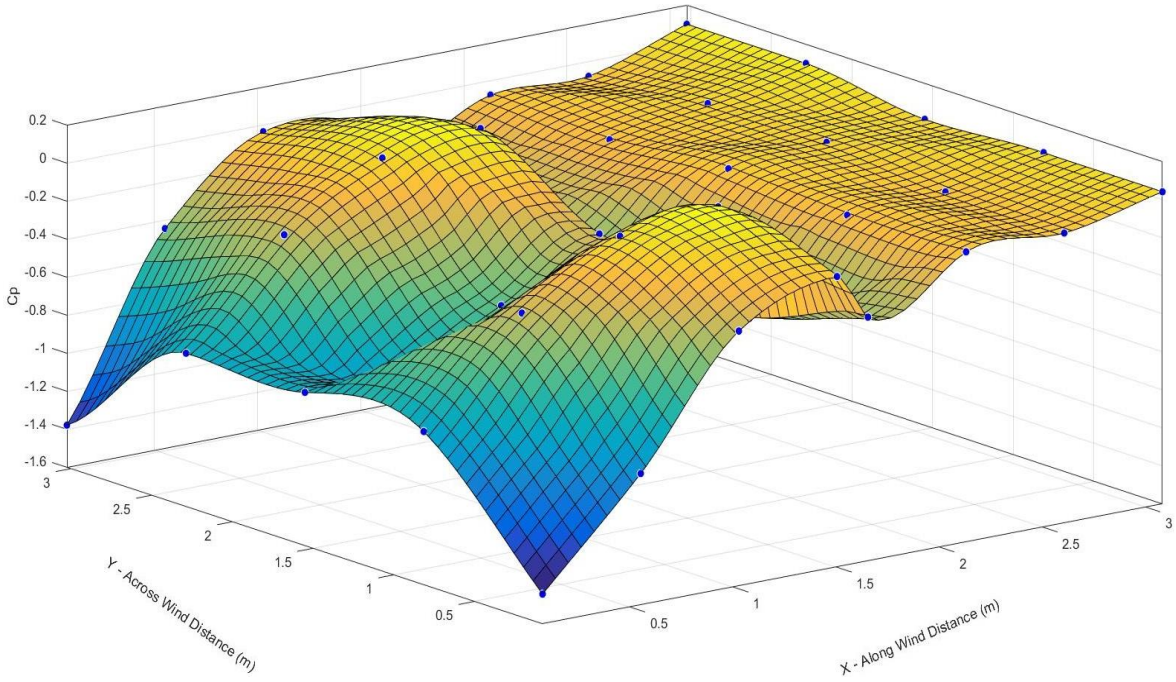

Figure 2.17 C_P distribution over test specimen roof

For this exercise, the roof pressure on the FEM is varied spatially according to the mean C_P distribution. As mentioned, since low-rise wood structures are not significantly affected by their dynamic response, a static non-linear analysis is sufficient to model the test specimen. In this analysis, the roof pressure is incrementally increased by $P = {}^{1}/_{2}\, C_P \rho v^2$ from $v = 0$ m/s every 0.1 m/s until the solution becomes unstable and first failure occurs.

Using the average force-displacement relationship for toenail connections with 2D nails to model the RTWCs, full withdrawal of either RTWC 2 or 3 is predicted to occur at $v = 31$ m/s. Due to the high flow separation over the windward edge of the roof, the system failure mechanism is such that the initial failure of the windward RTWCs causes overturning of the roof. The failure of the windward RTWCs is subsequently investigated by examining displacement and uplift of the non-linear link elements, to be compared to the experimental results.

2.4.1 Displacement – Velocity Curves

The structure and loading are symmetric about the house centerline, so the following behaviours of RTWCs 1 and 2 are identical to those of 3 and 4 respectively, and are therefore overlain by the latter two. The results shown are then a comparison of the interior and exterior RTWC behaviour, RTWCs 2, 3 and 1, 4 respectively.

Figure 2.18 below describes displacement as a function of velocity for the windward RTWCs.

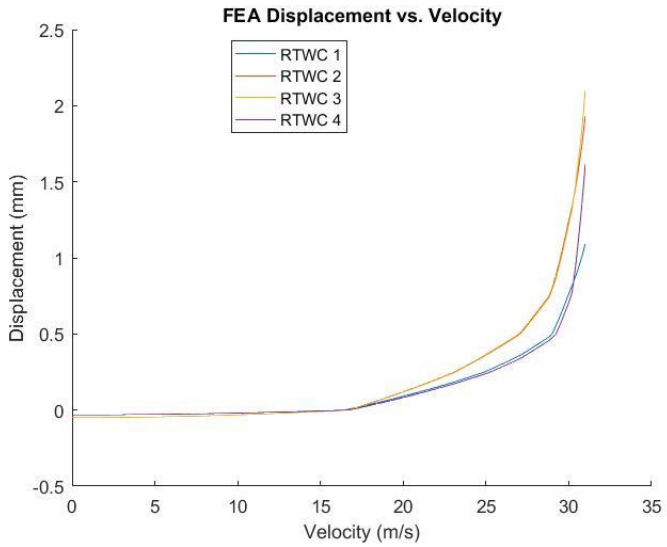

Figure 2.18 FEA generated displacement – velocity curve

The most remarkable feature of the above figure is the difference in displacement between the interior and exterior windward RTWCs. In construction of the prototype, it is found that the framing angles used to affix the lateral bracing and sheathing panels to the trusses allow for small rotations before the full stiffness of the connection is engaged. When magnified by the 1 m distance between trusses, these rotations can produce a significant difference in displacement between RTWCs before the total lateral stiffness of the roof is regained. This behaviour is suitably modelled using pinned connections to affix the lateral bracing members to the trusses, and translation-only body constraints to connect the edges of the sheathing. This means that the RTWC stiffness in both compression and tension is greater than the lateral stiffness of the roof, allowing the roof to behave as three separate spans of simply supported beams and concentrating load on the interior trusses. As seen in the above figure, this generates a difference in displacement between the interior and exterior windward RTWCs that increases with velocity.

This effect is unique to the small scale model, as the lateral bracing in the full scale structure is shorter, permitting smaller deflection for a given rotation. Coupled with the longer embedment length of nail used in a full scale toenail connection, this allows for the lateral bracing to fully engage prior to any meaningful displacement in the RTWC, resulting in the relatively equal load sharing observed by Jacklin and El Damatty (2014). However, since the small scale structure acts as a control variable for further testing, a difference in load distribution behaviours between the small and full scale structures is unimportant.

The above displacement – velocity relationship is primarily composed of three sections: (i) compression, (ii) pre-yield tension, and (iii) post-yield tension. Prior to approximately 17 m/s, the windward RTWCs experience net compression and therefore exhibit negative

displacement. This compression displacement increases to zero over a relatively large change in wind velocity as the compression region of the force – displacement relationship is governed by the stiff compressibility of wood. Between approximately 17 m/s and 27 m/s for the interior RTWCs, or 29 m/s for the exterior RTWCs, the stiffness of the non-linear link changes and displacement increases from zero to the yield displacement of 0.5 mm. Here, the difference in displacement between the interior and exterior RTWCs becomes increasingly pronounced. Much like the region of negative displacement, the stiffness is constant and the curvature of the displacement – velocity relationship in this region is only because uplift is proportional to the square of velocity. Finally, after the yield displacement occurs in the windward RTWCs, a rapid increase in displacement is recorded until ultimate failure has occurred. This occurs at some fraction of a velocity step between the last stable step, and the step causing solution non-convergence.

2.4.2 Uplift – Velocity Curves

The behaviour of the displacement – velocity relationship is reflected in the uplift – velocity relationship, and further illustrates the effect of the small rotations allowed by the lateral bracing on the distribution of uplift between the interior and exteriors RTWCs. Figure 2.19 below shows the various uplift – velocity relationships of the windward RTWCs.

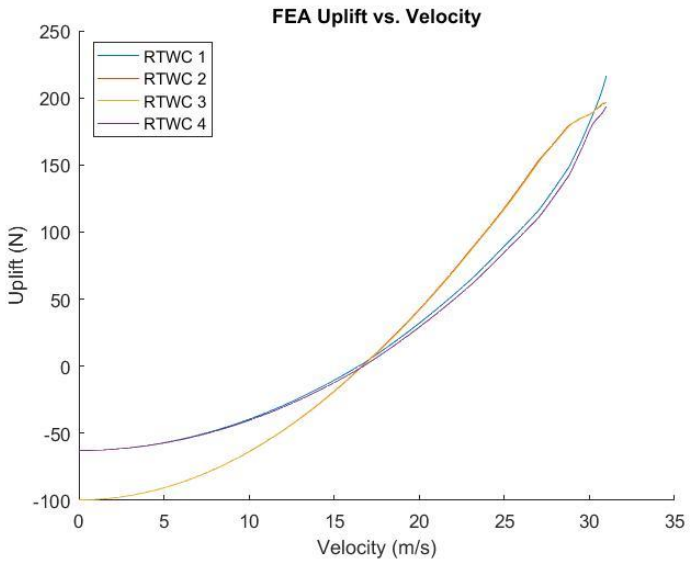

Figure 2.19 FEA generated uplift – velocity curve

As observed in Figure 4.2, prior to $v = 17$ m/s the windward RTWCs experience compression from the weight of the roof that progressively decreases as wind velocity increases. The initial compression of the interior RTWCs is not exactly double that experienced by the exterior RTWCs, as the weight of the roof trusses is wholly transferred to the RTWC below them. However, given that the weight of the sheathing is uniformly distributed across all spans and represents the majority of the roof weight, the difference in initial compression between the interior and exterior RTWCs evidently displays the expected behaviour of three simply supported spans. Since the wind-induced suction is relatively uniform over the width of the roof, the uplift experience by the interior RTWCs should be approximately double that of the exterior RTWCs over the same change in velocity. This behaviour is observed between 0 m/s and 17 m/s, where the interior RTWCs recover, with only a small difference, twice the uplift as the exterior RTWCs to intersect at 0 N. This small difference is due to the concentration of suction near the windward corners that allocated slightly more uplift to the exterior RTWCs.

Examining the pre-yield region between approximately 17 m/s and 27 m/s for the interior RTWCs, or 29 m/s for the exterior RTWCs, the ratio of load difference between interior and exterior RTWCs stays constantly at 2:1. Again, despite having constant stiffness in both compression and pre-yield tension, since uplift is proportional to the square of velocity, the uplift – velocity relationship is curved accordingly.

At 27 m/s, the interior RTWCs begin to approach the ultimate failure capacity and shed stiffness according to the input force – displacement relationship. As wind-induced suction increases with velocity, the interior RTWCs cannot acquire load at the pre-yield rate and transfer it to the exterior RTWCs. This consequently accelerates the failure of the exterior RTWCs, reducing the difference in uplift experienced and precipitating ultimate failure in the interior RTWCs at approximately 200 N. Though the velocity was increased in fine increments of 0.1 m/s, the resolution is still not small enough to observe ultimate failure in the exterior RTWCs, however it can be assumed that this occurs at some velocity between 31 m/s and 31.1 m/s.

2.4.3 Uplift – Displacement Curves

The force displacement relationship for the windward RTWCs, presented in Figure 2.20 below, is produced as the result of relating the displacement and uplift at the corresponding velocities from Figures 2.18 and 2.19 respectively.

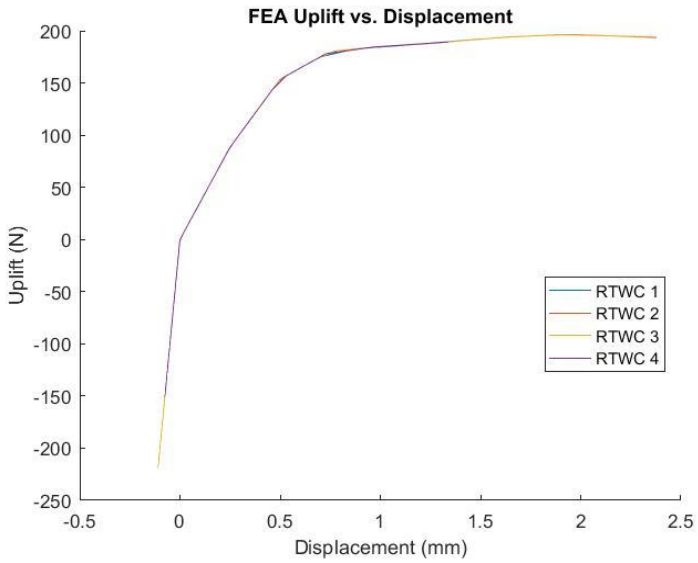

Figure 2.20 FEA generated uplift – displacement curve

As input, the demonstrated behaviour replicates the 2D force-displacement relationship, where yield occurs at approximately 0.5 mm and 150 N, and ultimate failure occurs at approximately 2 mm displacement and 200 N. The interior RTWC behaviour can be seen to occupy a larger range than that of the exterior RTWCs in both initial compression and at failure as discussed.

2.5 Analysis of Experimental Behaviour

2.5.1 Model and Test Description

The experimental test consists of subjecting the scale model to wind load produced by the contraction apparatus. Figure 2.21 shows the model and contraction setup.

Figure 2.21 Model and contraction setup

The scale model used a system of interchangeable sacrificial RTWC elements in order to reuse the roof truss in multiple failure tests. A system of harnessing straps were used from the interior to the roof from overturning after failure in the windward RTWCs. A three dimensional CAD model is featured in Figure 2.22 below to show the position of the displacement transducer and the configuration of the sacrificial blocks.

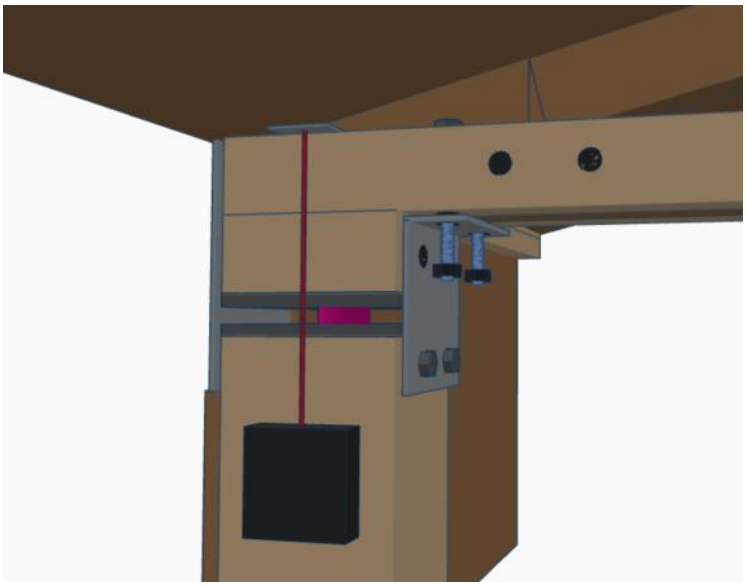

Figure 2.22 CAD model of connection and laser displacement sensor

Using the blockage considerations outlined in Rosenkrantz and El Damatty (2016), the structure is located 4.5 m from the aperture of the contraction at an incident angle of 0˚. Test measurements were collected via laser displacement sensors for RTWC displacement, and a pitot tube placed in the free stream to collect wind velocity data. The fan speed is increased to 40% and maintained to observe possible issues before increasing by 5% over 5 seconds and holding for 20 seconds until RTWC failure becomes obvious. The resulting velocity time history, shown in Figure 2.23 below, indicates this pattern.

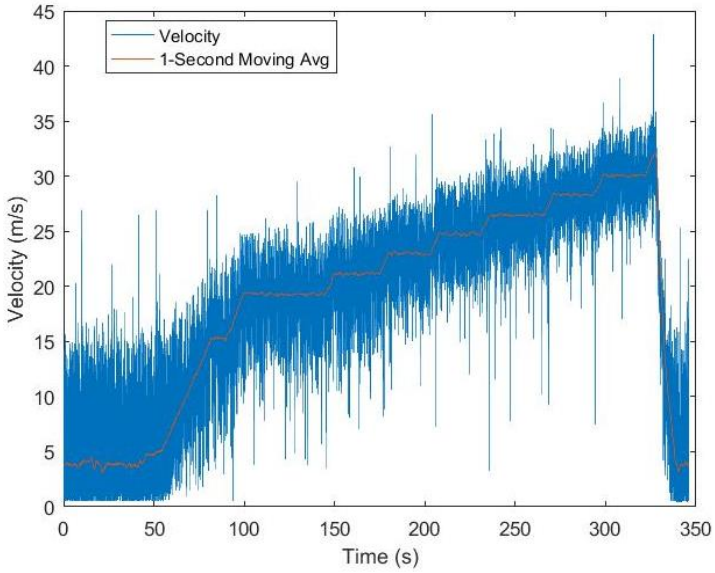

Figure 2.23 Experiment velocity time history

The fan speed was increased much past failure, to approximately 35 m/s, such that the safety harnesses became fully engaged and displacement at the roof to wall connections became obvious. A moving-average is plotted for clarity. Since this test was conducted outdoors, the ambient wind velocity is recorded at approximately 4 m/s. This is deemed insignificant as, the velocity of the generated wind flow is comparatively much greater than the ambient conditions, and has no meaningful interaction with the resulting jet.

2.5.2 RTWC Displacement Analysis

The displacement time history, shown below in Figure 2.24, records the sequence of displacement events leading to failure.

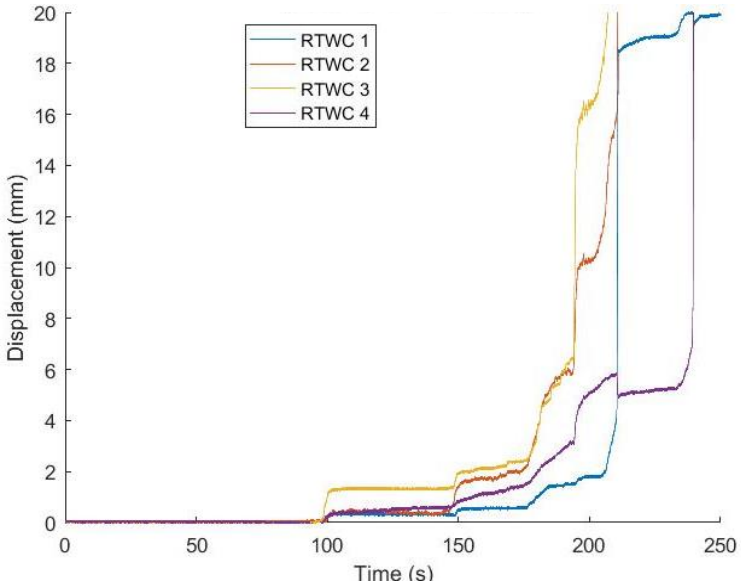

Figure 2.24 Experiment displacement time history

The laser displacement sensors measure absolute displacement, including initial displacement due to the own weight of the structure. Therefore, the displacement used in analysis is normalized to the displacement experienced at 90 seconds or 15.3 m/s, the point at which net tension in the windward RTWCs is predicted to occur from FEA results. Combining the displacement and velocity time histories produces the displacement – velocity relationship for the windward RTWCs shown in Figure 2.25 below.

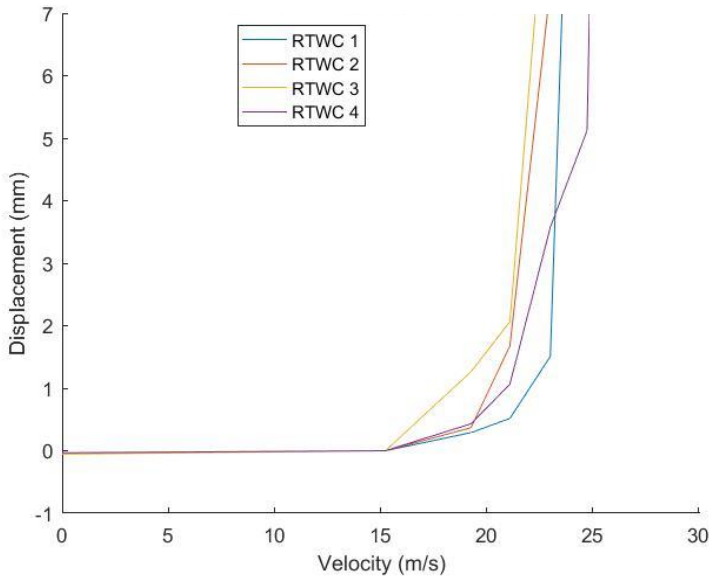

Figure 2.25 Experimental displacement – velocity curves

The sequence of displacements demonstrates the system behaviour prior to failure. As the wind velocity increases beyond 15.3 m/s, RTWCs 1, 2, and 4 have almost the same displacement. However, RTWC 3 has a marked increase in displacement, possibly surpassing the yield point. Investigating the failure mode of these connections, RTWCs 1, 2, and 4 failed by nail pullout, while RTWC 3 failed by a wood split along the D-side. This was due to an initial split in the wood during installation, and is likely the cause of the initial displacement separation at that RTWC. For the other RTWCs the small separation of displacements likely due to a combination of varying stiffnesses and the minor rotations permitted by the lateral bracing members. These connections consist of angle plates screwed on either side of the lateral bracing member to the truss, and behave as modelled in the FEM by pinned connections, adding flexibility to the lateral roof stiffness. This means that small differences in displacement can occur between the RTWCs.

As in the FEM, the interior RTWCs 2 and 3 experience greater displacement at a lower velocity. After approximately 21.1 m/s, the displacement of RTWCs 2-3 increases

indicating that the connections are near their ultimate failure capacities. Since the load in this region is constant, stiffness must be approaching zero such that small fluctuations in the wind loading increase displacement. At approximately 23 m/s, the failure capacity of RTWCs 2 and 3 is surpassed and displacement greatly increases, causing both RTWC 4 to approach ultimate failure capacity.

However, as the wind speed is constant at 23 m/s, RTWCs 2 and 3 approach the plastic hinge regime in their stiffness pausing the increase in the displacement at RTWCs 1 and 4. Once the wind speed is increased to 24.8 m/s RTWCs 2 and 3 achieve ultimate failure, whereby both RTWCs 1 and 4 should logically fail as well. However, friction from the safety harnesses tightening in addition to some residual strength in the connections at RTWCs 2 and 3 allowing for a pause in the displacement at these locations. Consequently, displacement at RTWC 4 increases approaching the plastic hinge regime, stabilizing until the wind speed reached 26.5 m/s, at which point RTWC 1 fails.

Movement of RTWC 4 is verified by internal video to have become accidentally restricted by the safety harness, causing a small decrease in displacement and a tilt in the roof due to the now asymmetric height of the supports. Another increase in wind velocity to 28.3 m/s allows for the harness at RTWC 4 to be released and all RTWCs are observed to have failed.

2.5.3 RTWC Uplift Estimation

Though RTWC uplift is not recorded for this test, solving the typical force-displacement relationship of the 2D toe-nailed connections for the recorded displacement allows for an

estimate of the uplift the average RTWC would experience. The experimental uplift – velocity relationship for the windward RTWCs is presented in Figure 2.26.

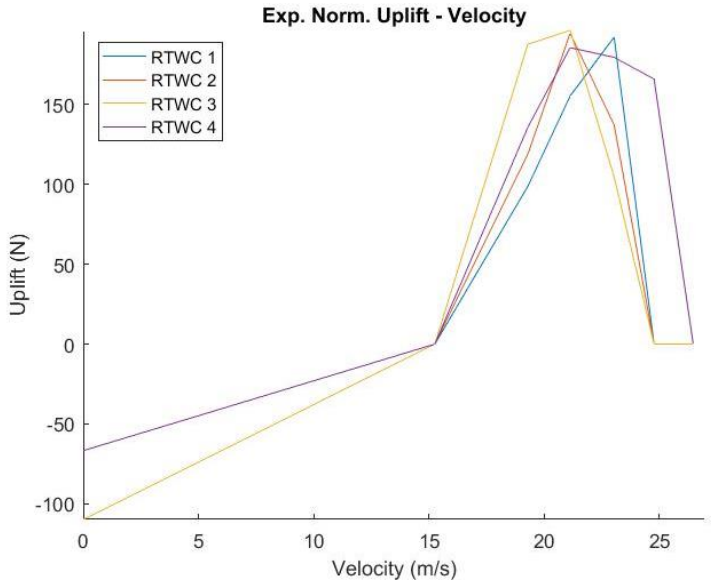

Figure 2.26 Experiment uplift – velocity curves

It is important to note that though the typical force – displacement relationship for 2D toenail connections is used to derive Figure 3.26, the individual RTWCs likely do not behave as such given the inherent variability in materials and construction. Therefore, the uplift – velocity relationship simply provides a means of understanding the potential differences in stiffness between RTWCs. Using the same reasoning, the force – displacement relationship using the inferred uplift data would be unable to indicate the true stiffness differences between RTWCs and is therefore not included in the investigation of the experimental data.

The difference by a factor of approximately 2 in initial load between the interior and exterior RTWCs demonstrate the expected simply supported beam behaviour in the compression region of the uplift – velocity relationship. However, upon examining the pre-

yield tension region, the difference in rates of uplift accumulation are marked departure from the FEA results, indicating that the stiffnesses of the RTWCs are dissimilar. From Figure 3.26 it appears that RTWC 3 has little stiffness and easily deforms, likely due to the split noticed during construction. Since RTWC 3 experiences a rapid increase in displacement and the stiffness of the lateral supports fully engage, RTWC 2 and 4 bear approximately the same load. Since they also experience similar displacement, reflected in the uplift – velocity and displacement – velocity relationships, these two RTWCs must have similar stiffnesses. Finally, as RTWC 1 fails after the rest of the windward RTWCs approach failure and shed stiffness, it can be said that RTWC 1 has a comparatively greater stiffness and ultimate failure capacity.

2.6 Post-Failure Analysis

Due to the nature of wood products and wood construction, it is unlikely that toe-nail behaviour is the same for every RTWC in a structure. To understand the effect of different RTWC behaviours on the response of the structure, and to better simulate the experimental results, toe-nail connection force – displacement relationships are created to simulate the RTWC response. To facilitate a parametric study, these relationships are reduced to piecewise linear function of a toenail connection force – displacement relationship, consisting of a series of points representing the negative force – displacement regime, yield, ultimate failure, residual plasticity, and full withdrawal.

The negative stiffness regime and full withdrawal length are relatively constant parameters, and the point at which residual plasticity leads to full withdrawal cannot be fully examined by the FEA due to negative stiffness. Therefore, to reduce the number of variables, only the yield and ultimate failure were chosen to be manipulated. The values of deformation

and load at both yield and ultimate failure for all four windward RTWCs in the FEA are then iteratively changed until the results of the displacement – velocity relationship acceptably match that observed in the destructive test. The results can then approximate the actual behaviour of the RTWCs and be used to examine the validity of the uniform average force – displacement FEA behaviour prediction method.

2.6.1 Displacement – Velocity Curves

The objectives of yield and ultimate failure parameter manipulation were chiefly (i) to allow RTWC 3 displacement preceded the displacement of the other windward RTWCs, (ii) to provide RTWCs 2 and 4 with similar displacement – velocity relationships, (iii) to ensure that yield and ultimate failure in RTWC 1 followed the other windward RTWCs, and (iv) that ultimate failure of the whole roof occurs at a similar velocity.

To verify that post-failure parametric study is successful, a comparison of the experimental and post-failure FEA displacement – velocity curves are featured in Figure 2.27 below.

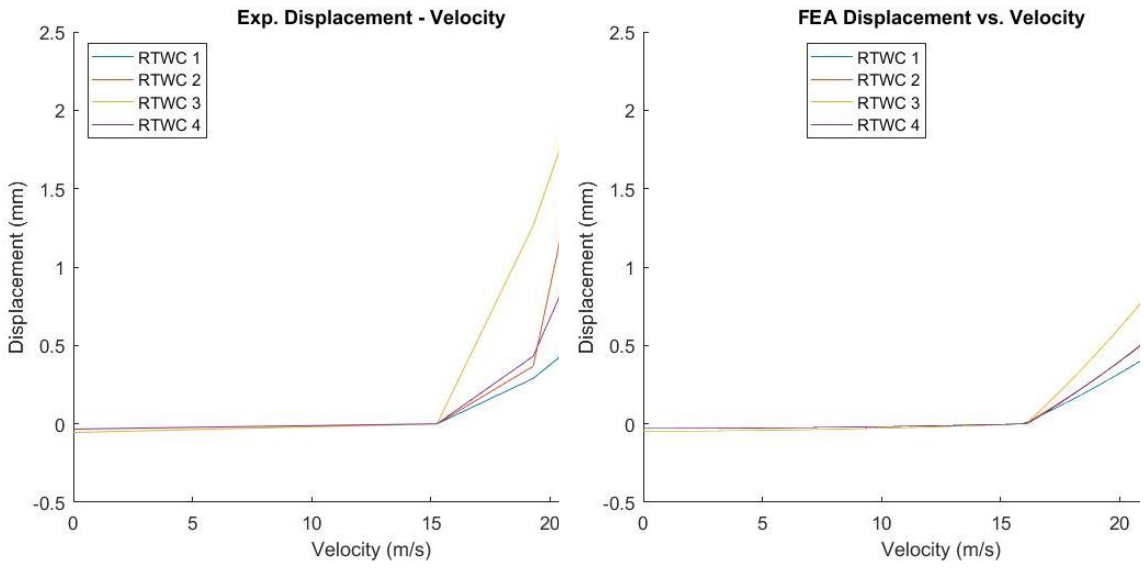

a) b)

Figure 2.27 Displacement – velocity curves from a) experimental and b) FEA results

A comparison of the above figures indicate that indeed, these objectives are satisfactorily met. However, due to model and manual parameter manipulation limitations, some minor aspects of experimental displacement – velocity curves proved difficult to replicate. Chief among these is the observable load sharing near failure. In the FEA results, as system approaches ultimate failure, the rate of displacement accumulation in RTWCs 2-4 tends to decrease such that all the RTWCs fail at a similar velocity, whereas the experimental results indicate that displacement for all RTWCs becomes unbounded at different velocities.

The primary cause of this effect is the result of the FEA being unable to permit sufficient rotation of lateral bracing members at trusses 1 and 4, to allow large enough deflections to the interior RTWCs. In the FEA, as the system approaches failure, the full stiffness of the lateral bracing system engages and load is distributed through stiff beam – weak spring behaviour. However, this effect can be seen to be almost negligible when considering Figure 3.25, as the extended displacement axis allows for a near convergence of the displacement of RTWCs 1-3 to occur near 22 m/s. Further, RTWC 4 is not technically unbounded and diverging only because of the accidental restriction of movement from the safety harness.

In addition to the load and displacement parameters of both yield and ultimate failure, the unit weight of the sheathing and roof truss materials were reduced such that the velocity at which the windward RTWCs began to experience net tension was decreased to match the experimental results. The resulting unit weights of the materials remain realistic and typical for low moisture content, where the SPF in the roof truss members was reduced to 4.0 kN/m^3 and the plywood sheathing reduced to 5.0 kN/m^3.

2.6.2 Uplift – Velocity Curves

Once the displacement – velocity curves have satisfactorily met the objectives of the parametric optimization, an estimate of the RTWC uplift can be produced. Figure 2.28 below shows the resulting uplift – velocity curve for the windward RTWCs.

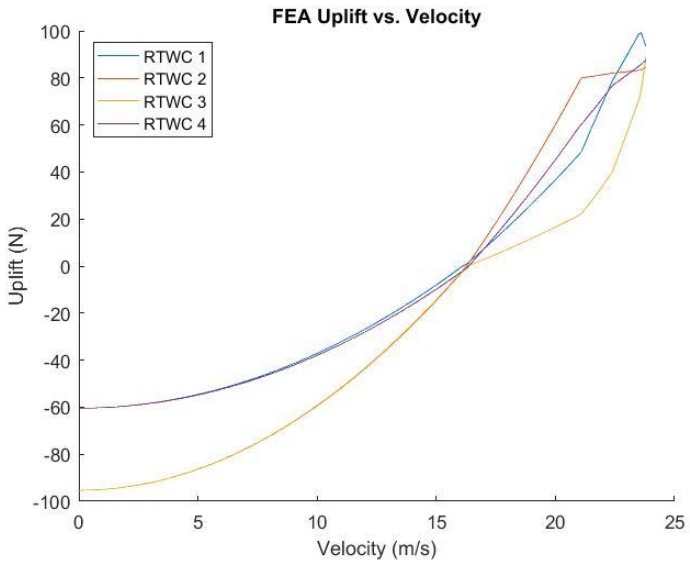

Figure 2.28 Uplift – displacement for RTWCs simulating experimental failure modes

The most obvious difference between the above figure and both of the preceding uplift – velocity curves is value of uplift, or tension, at which yield and ultimate failure occurs. The load parameters of these points were reduced significantly to initiate failure at approximately 23 m/s, and are much smaller than the results of testing individual toenail samples. There are two possible explanations for the apparent weakness of the RTWCs, likely acting simultaneously.

Firstly, the construction of test samples for assessing the typical 2D toenailed connection force – displacement properties was performed in controlled laboratory conditions, with specific attention paid to constructing each sample in a uniform manner. However, despite

best efforts, construction of the toenail connections for the test specimen was performed on site in less than optimal conditions, resulting in higher variability in connection quality. It is recommended that in future testing a suitable factor be introduced to artificially reduce the expected tensile resistance of these connections when constructed on site.

The second reason for the apparent RTWC weakness concerns the suction pressure applied in the FEA rather than the toenail connections. The pressure coefficient distribution over the roof, as provided in Rosenkrantz and El Damatty (2016), was measured on during the load control session of testing. For this test, the house roof was secured with weights to prevent any movement and was therefore able to be sealed to prevent any changes to the interior pressure. However, in the displacement controlled session of the test, investigated in this paper, the windward edge of the roof required freedom of movement and prohibited the use of previously used restrictive sealing methods. Consequently, as the test progressed the windward edge of the roof separated from the top plate exposing a significant gap in the building envelope, made larger by deflections across the width of the sheathing panels. This gap then likely allowed for an increase in the internal pressure, amplifying the uplift experienced at the RTWCs. Since the pressure coefficient distribution provided in Rosenkrantz and El Damatty (2016) does not include the effect of this increased internal pressure, it is likely that the RTWCs experienced greater tension than applied in the FEA. It is therefore recommended that the differential pressure distribution be measured continuously throughout the test.

2.6.3 Uplift – Displacement Curves

Despite the reasons for the lower than expected values of the load parameters, the uplift – displacement curves of the windward RTWCs, shown below in Figure 2.29, accurately portray the relative difference in stiffness between the connections.

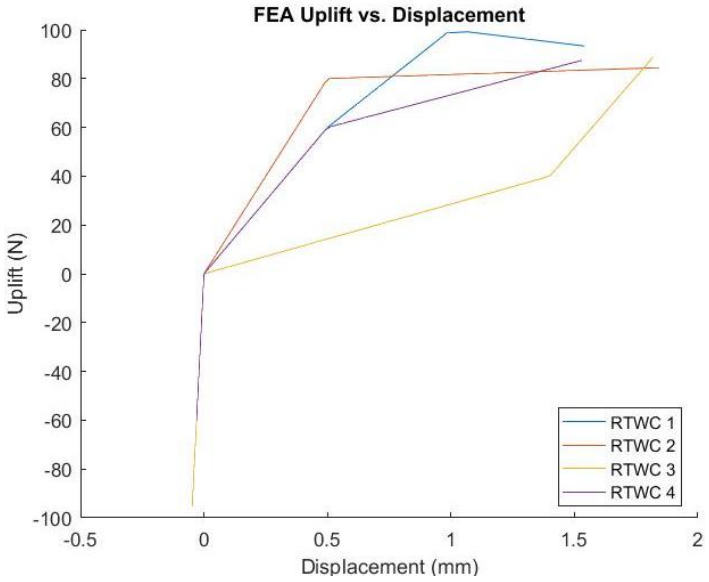

Figure 2.29 Force – displacement relationships simulating experimental failure modes

The characteristics of each windward RTWC piecewise linear force – displacement relationship are shown in Table 2.10 below.

Stage Demarcation Point	**RTWC 1**		**RTWC 2**		**RTWC 3**		**RTWC 4**	
	F (N)	**D (mm)**	**F (N)**	**D (mm)**	**F (N)**	**D (mm)**	**F (N)**	**D (mm)**
Compressive Stiffness	-1000	-0.5	-1000	-0.5	-1000	-0.5	-1000	-0.5
Zero	0	0	0	0	0	0	0	0
Yield	60	0.5	80	0.5	40	1.4	60	0.5
Ultimate Failure	100	1	85	2	110	2	100	2
Residual	20	7.5	20	7.5	20	7.5	20	7.5
Full Withdrawal	0	10	0	10	0	10	0	10

Table 2.10 Windward RTWC piecewise linear force – displacement relationships

The optimized force – displacement relationships as outlined confirm important observations made during post-failure inspection of the test specimen.

The first and most apparent observation is the crack identified during the construction of RTWC 3 that severely compromised yield strength, as reflected in the small value assigned to this parameter. Further, since this connection had the highest ultimate failure load value, an unexpected increase in in stiffness occurs after yield. However, RTWC 3 was observed to have subsequently failed through a d-side split. Given that observations from small scale toenail connection testing and from the full scale testing of Khan and Kopp (2012) indicate that this type of failure has typically greater tensile resistance, this behaviour is reasonable.

The optimized stiffness profiles also revealed the load sharing behaviour of the windward RTWCs. For RTWCs 2 and 4 to have similar displacement – velocity curves, the pre-yield stiffness of RTWC 2 needed to be greater than that of RTWC 4 to accommodate a larger tributary area.

The final significant observation is the comparatively high failure velocity of RTWC 1. Analysis of the experimental displacement – velocity curves indicates that this due to the distance between RTWC 1 and the initially weak RTWC 3. Prior to yield in RTWC 3, the difference between the tension allocated to this connection through tributary area and the tension actually transmitted through the connection is transferred to adjacent RTWCs 2 and 4. As only a small proportion of this difference is transferred to RTWC 1, it is assumed that this connection need not be stiffer than the other windward RTWCs to achieve the highest failure velocity. A validation of this assumption can be made by comparing the optimized stiffness profile of RTWC 1 to RTWC 2.

2.7 Comparison of FEA to Experimental Results

The comparison of results for both initial and post-failure FEAs to experimental results is required to determine the accuracy of these methods, and validate them for future use in determining test specimen behaviour. Given the large variability of toenail connection behaviour, the ability to examine failure modes for use in post-failure FEA will invariably give this method an accuracy advantage when compared to simply assuming the average force – displacement relationship of a toenail connection applies all RTWCs, as in the initial FEA. However, the ability to reliably predict the behaviour of the test specimen is of far greater use. Therefore, this section will seek to validate both methods of analysis as accurate, and provide suggestions for improvement.

To measure how accurately each analysis method predicted total applied load, a ratio comparing the total uplift due to wind load to the sum of RTWC tension is determined, where the measure of accuracy can be interpreted as the proximity of the ratio to unity. Calculation of the ratio is as outlined in the equation below.

$$Eq.\ Ratio\ (V_i) = \frac{{}^{1}/_{2}\,\rho V_i \iint C_p(x,y)\cdot dxdy}{\sum RTWC(V_i)}$$

The ratio is calculated for each velocity step, V_i, recorded in the test. To determine the total applied force, the dynamic pressure is multiplied by the area integral of the pressure coefficient distribution over the area of the roof, adjusted to consider roof inclination. The total force measured is the summation of the solution to the force – displacement curves assigned to the RTWCs by the two analysis methods for the average displacement during

a particular velocity step. From this equation, Figure 2.30 can be constructed, as shown below.

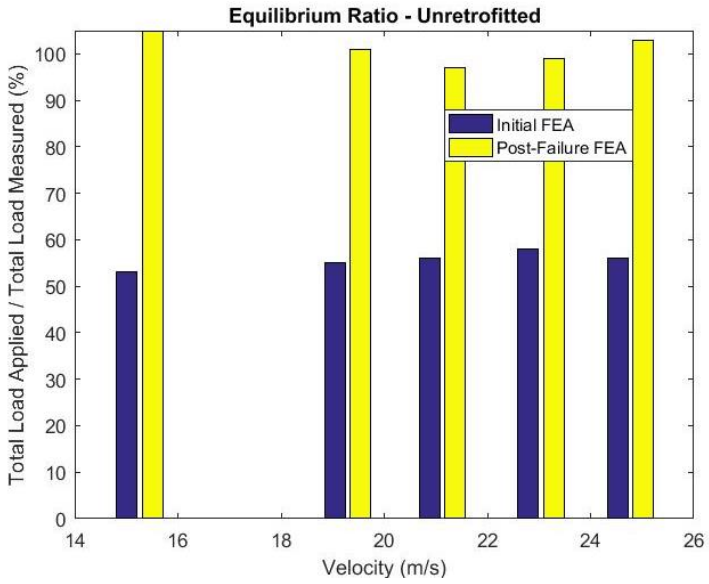

Figure 2.30 Equilibrium ratio from both initial and post-failure FEAs

The presented bar chart indicates a significant apparent difference in the accuracy of these analysis methods. This difference is due to the previously discussed effects of material weight, reduced RTWC construction quality on site, and windward edge separation.

Though the presented challenges significantly affect the accuracy of the model, they are theoretical systematic errors, and can be significantly reduced through better modelling. This is encouraging as the post-failure analysis method appears to be highly accurate, and the difference between the two methods are fairly constant, suggesting that the use of one force – displacement relationship to model all RTWCs can produce results consistent with methods that use different relationships. Though the post-failure FEA proved much more accurate than the initial FEA in this exercise, better modelling of the identified systematic errors can significantly improve the accuracy of the more useful initial method.

2.8 Conclusions

A scaling exercise is conducted to reduce the RTWC and roof component strength such that the test specimen fails at a velocity predicted from FEA results, and behaves similarly to a full scale structure. Though there are differences between the predicted and observed failure velocity, as well as the full and small scale truss load sharing behaviour, the cause of these differences are understood and suggestions are made for future improvement. Further, the failure mode of the test specimen is used to approximate the relative stiffness of the windward RTWCs, resulting in a highly accurate means of modeling the behaviour.

The specific results of the study are as follows:

- Scaling exercise for the roof components, while thorough, neglects the cross-bracing members and corresponding connections. In the reduced scale model, these connections prove weaker than expected, resulting in a difference between full and reduced scale RTWC load sharing behaviour. Further investigation into improving the lateral roof stiffness of the reduced scale model would improve this, but is not necessary if used purely for comparative purposes.

- Test specimen successfully fails along the windward RTWCs as expected, however at a lower velocity than predicted in the initial FEA. The cause of this is attributed to a reduction in on-site RTWC construction quality, and the inability to account for increases in internal pressure from windward edge separation. Application of a reduction factor to RTWC strength and continuous monitoring of differential pressure throughout the test can improve this.

- Post-failure analysis succeeds in numerically approximating the observed behaviour of the test specimen by optimizing the windward RTWC properties. However, as the potential increase in internal pressure is not recorded, the load parameters of the resulting RTWC properties are likely lower than reality, though relative stiffness is unaffected.

Despite a discrepancy between the predicted and observed failure velocities, the response of the test specimen is markedly similar to that of the FEM. The experimental results show consistency with the predicted failure sequence of the interior RTWCs followed by the exterior RTWCs, effectively capturing the behaviour of the roof. Further, FEA is useful in observing load-sharing when performing the analysis using different force – displacement relationships based on observed failure modes.

The presented method of reducing the strength of a small scale structure to approximate the behaviour of the full scale original has proved an efficient and viable means to destructively test and analyze large whole structures where the infrastructure is not available. Implementation of the recommendations made will further enhance this process.

2.9 References

Baskaran, A. and Dutt, O., 1997. Performance of roof fasteners under simulated loading conditions. Journal of Wind Engineering and Industrial Aerodynamics, 72(0), 389-400

Bimberg, U., and Bimberg, O. (1997), U.S Patent No. 5623788. Washington, DC: U.S. Patent and Trademark Office.

Computers and Structures, Inc. (2009). SAP 2000 V. 14: Integrated Software for Structural Analysis and Design. Berkley, California, USA.

Cook, N. J., 1985. The designer's guide to wind loading of building structures. Garston, Watford: Building Research Establishment, Dept. of the Environment. USA

Dagnew, A., 2012. Computational Evaluation of Wind Loads on Low and High- Rise Buildings (Doctoral Dissertation).

Federal Emergency Management Agency (FEMA), 2010. Wind Retrofit Guide for Residential Buildings. Federal Emergency Management Agency.

Jacklin, R., El Damatty A. A., Dessouki, A. A., 2014. Finite-Element Modeling of a Light-Framed Wood Roof Structure. Wind and Structures, Vol. 19 No. 6, 603-621

Khan, M., (2012). *Load-Sharing of Toe-Nailed, Roof-to-Wall Connections under Extreme Wind Loads in Wood-Frame Houses*. (PhD Thesis). London, Ont.: Department of Engineering, The University of Western Ontario.

Morrison, M. J. (2010). *Response of a Two-Story Residential House Under Realistic Fluctuating Wind Loads*. (PhD Thesis). London, Ont.: Department of Engineering, The University of Western Ontario.

Luzzi, J., 1999. U.S Patent No. 5881499. Washington, DC: U.S. Patent and Trademark Office.

Reed, T. D., Rosowsky, D. V. and Schiff, S. D. (1997). Uplift capacity of light-frame rafter to top plate connections. *Journal of Architectural Engineering, 3*(4), 156-163.

Rosenkrantz, J. D., El Damatty, A. A., 2016. Wind load parameters of a structural test using real wind load at the WindEEE Dome. 4th American Association for Wind Engineering Workshop, May 31st 2016

Stewart, M. G., 2003. Cyclone damage and temporal changes to building vulnerability and economic risks for residential construction. Journal of Wind Engineering and Industrial Aerodynamics, 91(5), 671-691

van de Lindt, J., Graettinger, A., Gupta, R., Skaggs, T., Pryor, S., and Fridley, K., 2007. Performance of wood-frame structures during Hurricane Katrina. Journal of Performance of Constructed Facilities, 21(2), 108-116.

3 Structural Behaviour Analysis of a Reduced Scale Retrofitted LFWS Subject to Wind Load

3.1 Introduction

Connections in the vertical load path of light-frame wood structures (LFWSs) allows the sheathing to transfer vertical forces imposed on the roof to the trusses beneath, then further to the stud walls and through to the foundation. Historically, sheathing connections to roof trusses and the roof truss connections to stud walls are typically nailed, with poor withdrawal resistance (FEMA, 1993; van de Lindt et al., 2007). After Hurricane Andrew in 1993 caused considerable economic losses, largely due to the failure of roofing system components (Baskaran and Dutt, 1997), building codes across North America began to reflect the need for increased capacity in these connections. Since the building code changes only affected new construction, it left older structures prone to damage during high speed wind events. This became evident in the aftermath of Hurricane Katrina, where older structures experienced considerable damage (van de Lindt et al., 2007).

Though there exist retrofitting options for older structures such as adhesives, straps, hurricane ties, and the installation of additional studs (FEMA, 2010), these options are relatively invasive and are approximately 15-50 % of the cost of the structure to implement (Stewart et al, 2003). This points to a need for a low-cost, and minimally invasive method of improving vertical load paths.

One such method is the roof harness, where a mesh of cabling or fabric covers the roof and is tethered to either the foundation of the structure or surrounding piles. The harness is designed for temporary application in the event of a high wind speed event warning, and does not require the applicator to be a contractor or construction professional. Though there

exist various patents for roof harness systems (Bimberg 1997; Luzzi 1999), the system developed by Jacklin and El Damatty (2014), shown in Figure 3.1 below, seeks to address issues apparent in their design through improving modularity, increasing stiffness, and reducing the weight of the retrofit system. The proposed roof harness retrofit system consists of modular strips of bearing cables connected through rigid bars to two external cables which are anchored to piles surrounding the structure.

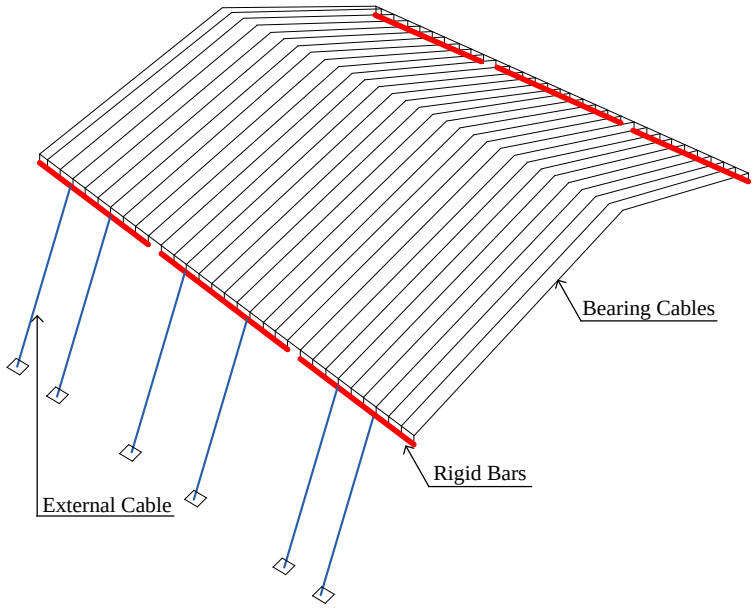

Figure 3.1 Retrofit system proposed by Jacklin and El Damatty (2014)

3.2 Prior Research

Currently, finite element analysis (FEA) and experimental testing are carried out to understand the structural behaviour of this roof harness configuration and the underlying roof. The primary objective of the experimental testing is to first determine the capacity of the roof through RTWC failure, and then comparatively examine the performance of the roof with the harness.

Experimental testing involves subjecting a whole structure to wind load, allowing for a robust examination of the effects of spatially and temporally varying suction on inter-truss load sharing and non-linear roof-to-wall connection behaviour. The WindEEE Dome in London, Canada is chosen as the testing facility as the exterior platform can accommodate a large test specimen that is loaded until failure. A three-dimensional contraction is used to increase the incident wind velocity and direct the flow at the test specimen.

The test specimen is designed such that (i) failure occurs at a sufficiently small fraction of the maximum available wind velocity, (ii) RTWC failure is the primary failure mode, (iii) its geometry is sufficiently within the wind-field generated by the contraction, and (iv) the demand-capacity ratios of structural members are similar to the full scale structure.

To reduce the capacity of the RTWC connections while maintaining a ductile failure mode similar to full scale nailed connections, smaller nails are evaluated as potential candidates. Using a simple displacement controlled apparatus, the average force-displacement relationship is determined for a variety of smaller candidate nails. FEA models of potential configurations for the reduced scale structure are then generated using linear springs to model the RTWCs and loaded with the pressure coefficient distribution generated from Rosenkrantz and El Damatty (2016). However, due to minimum bounds in observed nail candidate capacity, the number of trusses are reduced in the final test specimen configuration to promote failure at the target velocity.

Once the configuration of the reduced scale structure is determined according to the capacity of the reduced RTWC, a static non-linear analysis of the structure using the newly developed RTWC constitutive relationship is conducted assuming full scale members

cross-sections. A uniform suction is incrementally applied until the solution does not converge. Iteratively, the cross-section dimensions are optimized such that the demand capacity ratios of each structurally pertinent member are the similar to those in the full scale structure loaded at the same fraction of the failure load.

Destructive experimental tests are carried out on the reduced scale structure without the retrofit to observe the failure mode and assess RTWC displacement parameters. The data is then compared with the FEM data and, through post-failure analysis, improvements are made to the FEM to improve accuracy.

This paper focusses on the behaviour of the reduced scale structure when the strength scaled retrofit system is applied, under the same wind loading conditions. The primary objective is to investigate the potential benefits of the retrofit system, namely (i) the delay in onset of RTWC displacement, (ii) the delay in onset of RTWC ultimate failure, and (iii) prevention of total failure. This is done by comparing the behaviour of the reduced scale structure without the retrofit system to an identical structure with the system under the same wind load. The secondary is to prove the accuracy in which the FEA models the recorded failure mode and use post-failure analysis to improve this. Finally, a proposed method of further improving the system is evaluated.

3.3 Strength Scaling and the Design of a Reduced Strength Scaled Retrofit System

3.3.1 Concept of Structural Scaling

In cases where the dynamic effects of loading can be neglected, as in the case of a typical LFWS subject to wind loading, strength scaling can be applied to mimic the structural

behavior of a full scale structure on a reduced length scale. This is achieved by preserving the demand-capacity ratios of individual structural members relative to each other. To provide a basis for comparison, the demand-capacity ratios of individual structural members are compared to the ratio of the current wind velocity to the velocity that initiates failure.

The reduced length scaled test specimen is designed such that failure mode of interest initiates at the desired velocity and that the structural behavior resembles that of the full scale structure. Since RTWC failure is isolated as the governing failure mode, alternatives for full scale RTWCs are sought to reduce the capacity of the connection while maintaining a similarly ductile constitutive relation. Once the properties of a suitable reduced capacity RTWC are established, an iterative comparison of the full and reduced scale FEMs are carried out using incrementally increased uniform loads using a static non-linear analysis. Rosenkrantz and El Damatty (2016) have previously optimized the size of the roof truss members such that their demand capacity ratios at any given fraction of the failure loading conditions are similar to those in the full scale structure. RTWC demand capacity ratios are also compared in the same manner with the expectation that these values are unity when failure loading conditions are applied. This allows the base model to behave similar to the full scale structure under comparable loading conditions.

Given the prior validation of the underlying LFWS model, this section presents a brief description of the optimization results for the underlying roof components and focus on those results pertaining to the retrofit system.

3.3.2 Retrofit Component Scaling

3.3.2.1 Description of the Retrofit Addition to the Finite Element Models

The full scale retrofit system consists of three modular assembly units spanning the width of the roof. Each unit consists of ten ¼ in. diameter internal cables spaced center on center at 1 ft. to alternate between resting along and between the roof trusses. The internal cables are consolidated through a 2 in. x 4 in. x ¼ in. hollow rectangular aluminum section to two 3/8 in. diameter cables spaced equally at 6 ft. center on center, transferring uplift force to piles installed around the structure. The piles are offset from the structure such that the external cables make a 15˚angle with the side of the structure. Each external cable is then pretensioned to 2 kN. The finite element model of the full scale retrofitted structure is shown in Figure 3.2 below.

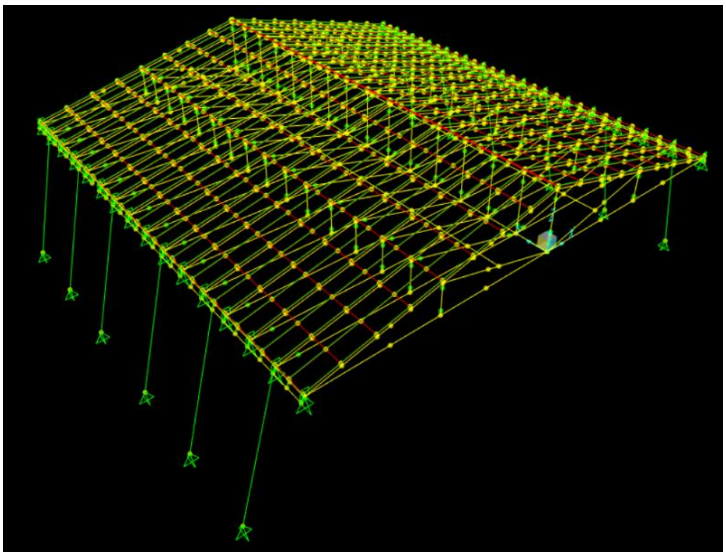

Figure 3.2 Full scale finite element model with retrofit

To simulate the retrofit on a reduced scale, some modifications were made to the geometry. Given the limited number of trusses used in the reduced scale roof, only 7 internal cables were required to alternate between resting on and between trusses when spaced at 1 2/3 ft.

Two external cables were used to keep the ratio of internal to external cables as close as possible, meaning that only one module of the retrofit system was needed for the reduced scale structure. Despite the different number of internal cables, the external cables are spaced at 6 ft. to keep the same geometric proportionality as a module from the full scale retrofit system. The component sizes of the reduced scale retrofit system are defined as per the strength scaling optimization outlined in the following section, and are initially set as the full scale component sizes. Additionally, the amount of pretension is initially set as 2 kN and is reduced through FEA such that the load sharing as a function of relative velocity is similar to that of the full scale structure. The finite element model of the reduced scale retrofitted structure is shown in Figure 3.3 below.

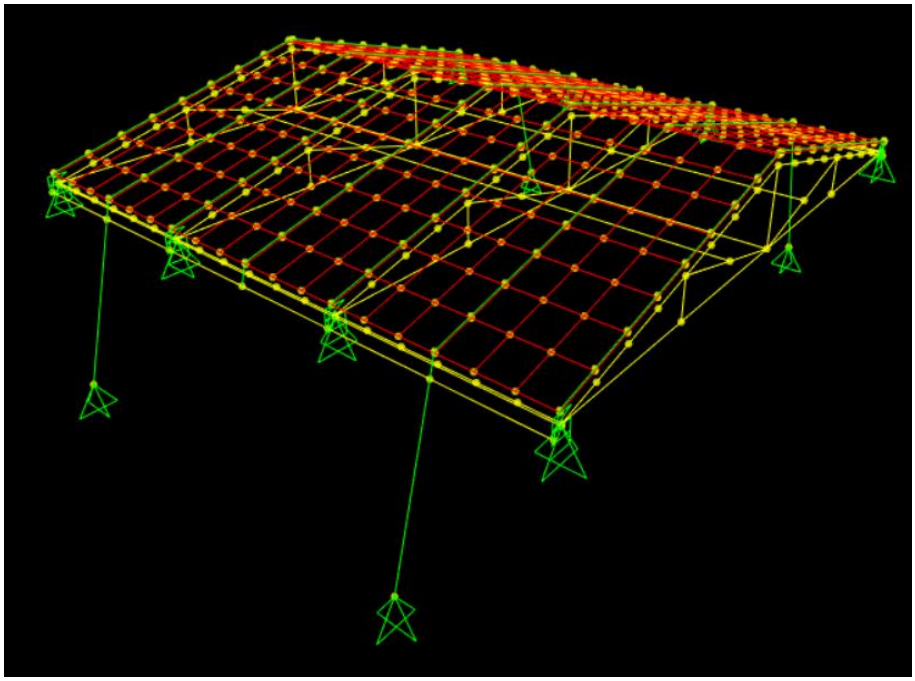

Figure 3.3 Reduced scale finite element model with retrofit

The full scale finite element model is directly borrowed from Jacklin and El Damatty (2014), while the reduced scale finite element model simply adjusts the geometry,

configuration, size of components and external cable target force. The base model and loading for the retrofit scaling exercise are as outlined in the previous chapter.

Given the differences in model configuration, some components of the full scale model lack corresponding components in the reduced scale model. Similar to the exercise conducted in the previous chapter, components analogous in function are chosen for comparison.

3.3.2.2 External Cable

Figure 3.4 presents the component demand capacity ratios to system demand capacity ratio for the external cables in both the reduced and full scale FEMs.

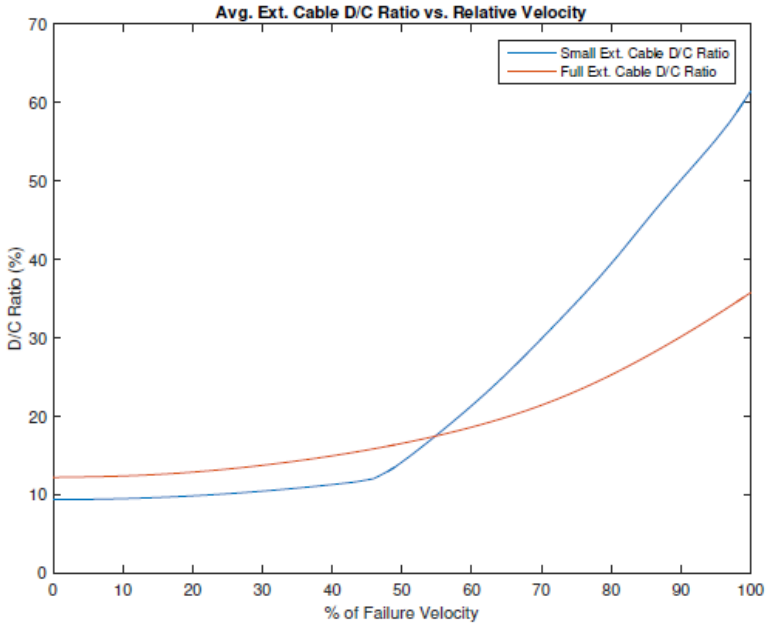

Figure 3.4 External cable demand-capacity ratio comparison

The cable was reduced from 3/8 in. to 1/8 in. diameter in the reduced scale FEM. The dramatic increase in demand capacity ratio in the reduced scale member near approximately 50 % of failure load is cause by the reduced number of RTWCs and retrofit

modules present in the reduced scale FEM. Though the difference is large near failure, given this inherent difference in load applied to the external cables, the region largely governed by pretension at less than 50 % of failure velocity is where the behaviour of the two cables can be reasonably compared. Here, the two behaviours are similar over most of the regime, and the reduced size cable is appropriate for the scaled model.

3.3.2.3 Internal Cable

Given the limited number of commercially available wire rope sizes, the optimization process concludes that the internal cable size should remain the same at 1/8 in. diameter between full and reduced scale retrofits to provide the closest approximation of behaviour. Figure 3.5 presents the component demand capacity ratios to system demand capacity ratio for the internal cables in both the reduced and full scale FEMs.

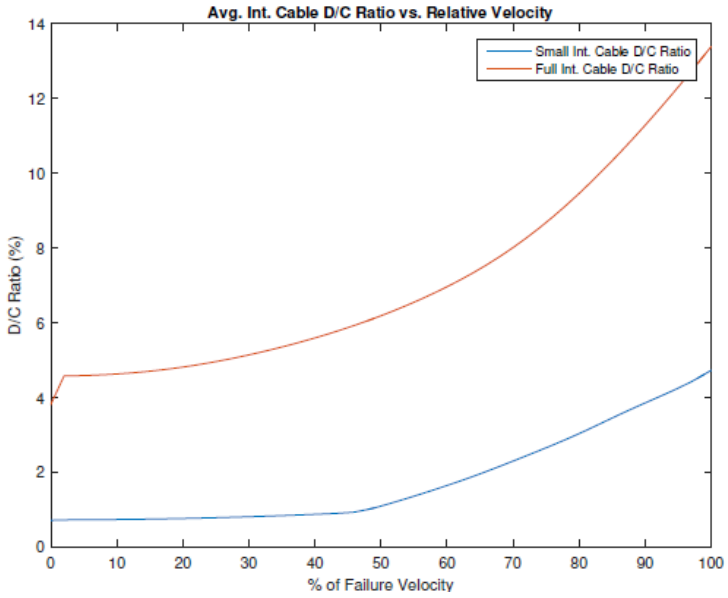

Figure 3.5 Internal cable demand-capacity ratio comparison

Though using the same sized cable does not provide the same behaviour under different loading conditions, it is important to note the small absolute difference between demand

capacity ratios. Given that these cables are well within the elastic range, this small difference is relatively inconsequential.

3.3.2.4 Aluminum Beam

Though the issue of commercial availability is present in the selection of the reduced aluminum beam section, more selection allowed for the reduction of the full scale 2 in. x 4 in. x ¼ in. hollow rectangular beam to a 1 in. x 1 in. x 1/8 in. hollow beam for the reduced scale retrofit. Figure 3.6 below shows the component demand capacity ratios to system demand capacity ratios for the full and reduced scale aluminum beams.

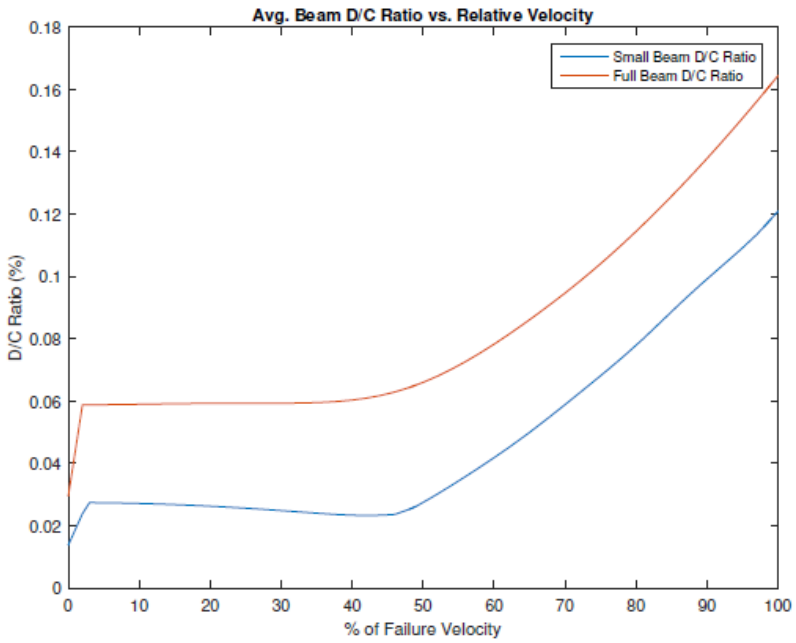

Figure 3.6 Aluminum beam demand-capacity ratio comparison

The reduced beam demonstrates qualitative similarity in behaviour. Further, since the demand – capacity ratios are small, the difference between those for full scale and reduced scale are minimal and inconsequential.

3.3.2.5 Load Sharing

Given that the reduced scale RTWC and retrofit are designed to behave similarly to those in the full scale, adjusting the initial conditions allows these elements to act in phase. To assess the impact of pretension, the change in total RTWC uplift and the change in external total cable tension are divided by their sum to determine the load sharing behaviour of the system through a range of velocities. Figure 3.7 below shows the load sharing – relative velocity curves for both the reduced and full scale FEMs.

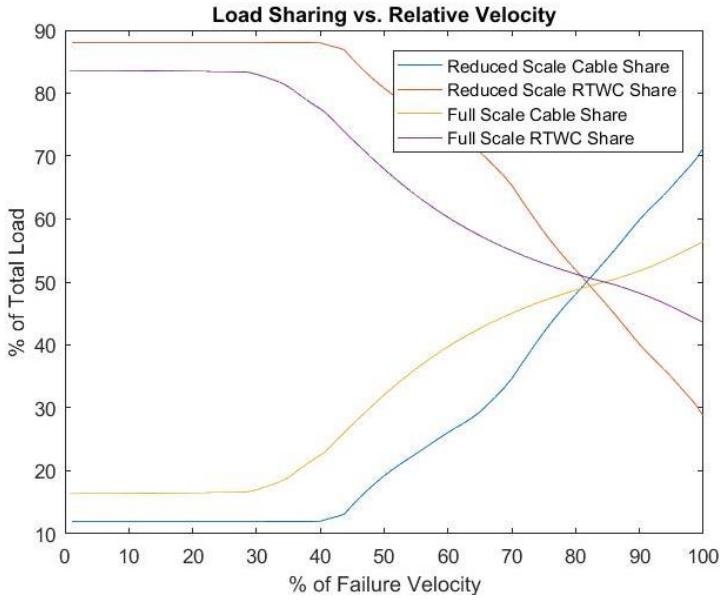

Figure 3.7 Load sharing – relative velocity for full and reduced scale FEMs

Working within the geometric constraints of the reduced scale structure, the pretension of the retrofit system is adjusted to best approximate the initial difference in load sharing between the retrofit and the RTWCs, and the point at which the windward RTWCs experience net tension. The optimized pretension for the retrofit system is then 200 N.

3.4 Analysis of FEM Behaviour Subjected to Realistic Wind Load

3.4.1 Description of Exercise

Subjecting the model to a simple uniform pressure is sufficient to observe whether an adapted structure behaves like the original when scaling the structurally relevant components by strength. However, to understand response of the model to the loading conditions applied by the testing environment, pictured in Figure 3.8 below as outlined in Rosenkrantz and El Damatty (2016), it is necessary to provide the model with a spatially varying pressure.

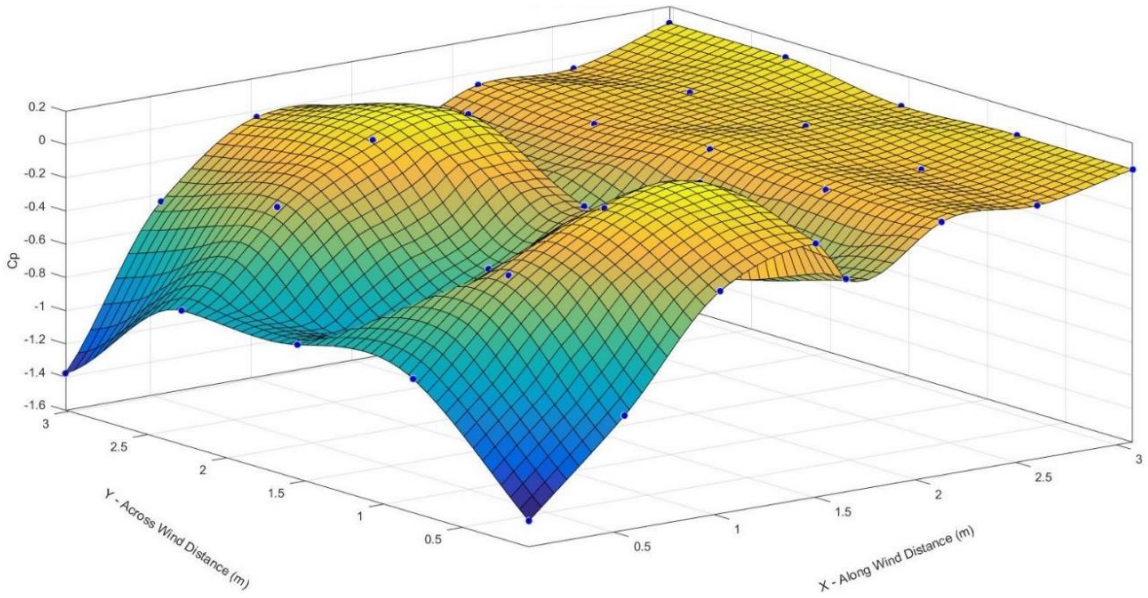

Figure 3.8 C_P distribution over test specimen roof

For this exercise, the roof pressure on the FEM is varied spatially according to the mean C_P distribution. As mentioned, since low-rise wood structures are not significantly affected by their dynamic response, a static non-linear analysis is sufficient to model the test specimen. In this analysis, the roof pressure $P(x,y) = {}^{1}/_{2}\, C_P(x,y)\rho v^2$ is increased

incrementally from $v = 0$ m/s by 0.5 m/s until 50 m/s, well after the ultimate failure capacities of the windward RTWCs have been achieved. Unlike the exercise conducted in the previous chapter, the solution is stable after this point due to the presence of the retrofit system. Using the average force-displacement relationship for toenail connections with 2D nails to model the RTWCs, first failure occurs at $v = 40$ m/s demonstrating an approximate 40 % increase in velocity compared to the unretrofitted FEM. The increase in performance is subsequently investigated by examining displacement, uplift, and external cable tension as a function of velocity. Additionally, load sharing is also assessed to determine the role of the retrofit system in preventing failure.

3.4.2 Uplift – Displacement Curves

The structure and loading are symmetric about the centerline of the roof, producing a relatively symmetric RTWC response. For this section, those curves displaying RTWC response demonstrate indistinguishably different responses for RTWCs 2 and 3, and a slight difference in the responses for RTWCs 1 and 4. The apparent asymmetry in response of the latter RTWCs is caused by a corresponding small asymmetry in cable pretension, from a numerical approximation of initial cable target force.

The uplift – displacement curves in Figure 3.9 below, are compiled from the displacement and force data from each velocity increment until failure.

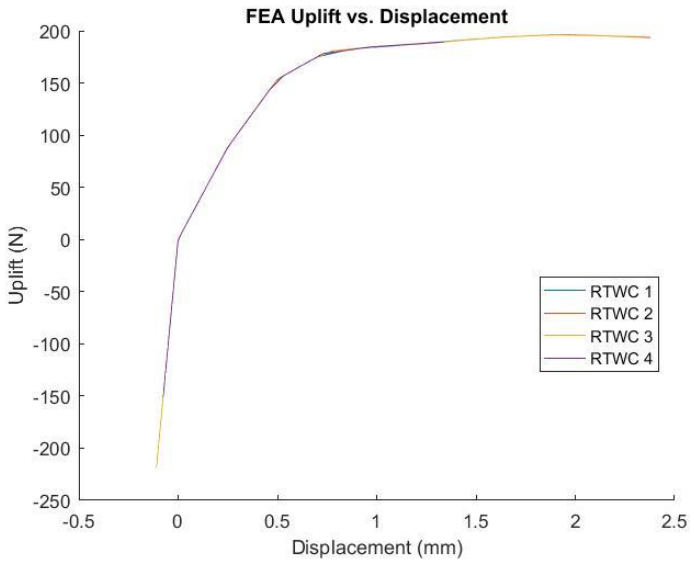

Figure 3.9 FEA generated uplift – displacement curves

Each RTWC response is constrained to the typical force-displacement relationship for toenail connections with 2D nails. The compression region in the above figure is larger than the corresponding figure from the FEA results of the unrestrained structure, due to added pretension from the retrofit system.

The interior RTWC response extends further than the exterior RTWC response, indicating the difference in load and displacement between these connections initially and at failure. The difference in load and displacement conditions at failure between the interior and exterior trusses is due to load sharing among the RTWCs. The FEA model releases moment and torsion where the roof truss cross-bracing connects to the trusses, to simulate the small rotations at these locations permitted by the test specimen. This means that the RTWC stiffness in both compression and tension is greater than the lateral stiffness of the roof, allowing the roof to behave as three separate spans of simply supported beams and concentrating load on the interior trusses.

This behavior is further evidenced in examining the uplift – velocity and displacement – velocity relationships for windward RTWCs.

3.4.3 Uplift – Velocity Curves

The structure and loading are symmetric about the centerline of the roof, eliciting a relatively symmetric RTWC response. For this section, those curves displaying RTWC response demonstrate indistinguishably different responses for RTWCs 2 and 3, and a slight difference in the responses for RTWCs 1 and 4. The apparent asymmetry in response of the latter RTWCs is caused by a corresponding small asymmetry in cable pretension, from numerical approximation of initial cable target force.

Figure 3.10 below describes uplift as a function of velocity for the windward RTWCs.

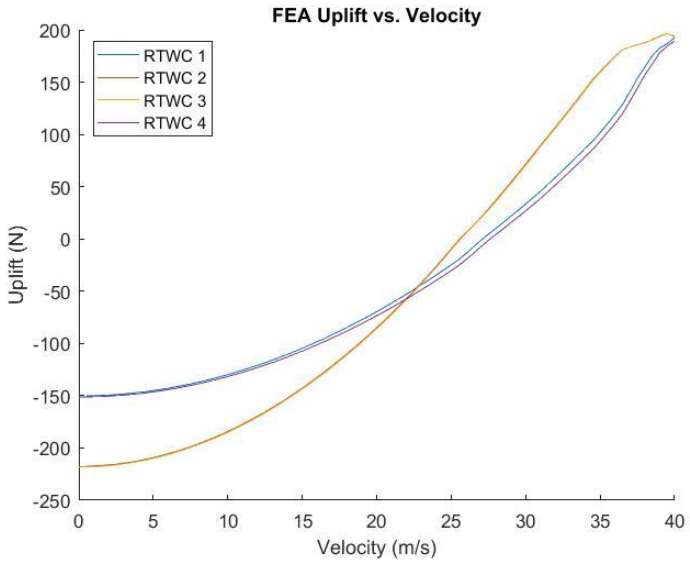

Figure 3.10 FEA generated uplift – velocity curves

Validity of the simplification for the roof behaviour as a series of simply supported beams is demonstrated in the difference in load attributed to the interior and exterior RTWCs.

This observable difference is due to the distribution of the weight of the roof trusses and sheathing, the pretension, and wind induced suction over the roof.

The increase in initial difference between the results of the unretrofitted and retrofitted FEA from approximately 40 N to 65 N indicate that, though more of the interior cables pass through tributary area allocated to the interior RTWCs, the pretension appears to be almost equally distributed. This is because the current retrofit configuration channels most of the tension from the external cables through the interior cable in line with it, rather than distributing this tension equally among the internal cables. Since this particularly heavily loaded internal cable lies between the interior and exterior trusses on either side of the roof, it distributes most of the retrofit tension equally between the interior and exterior RTWCs, and the load sharing between these connections in both the unretrofitted and retrofitted structures are therefore similar.

The addition of the retrofit system however significantly changes the uplift – velocity relationship of the windward RTWCs by contributing a pretension force and stiffness. While the pretension force simply increases the initial compressive force at the RTWCs, the added stiffness of the retrofit system transfers load from the RTWCs as displacement occurs. The sum of these effects increases the velocity at which the average net tension is experienced in the windward RTWCs by approximately 7 m/s, and increases the failure velocity by approximately 10 m/s.

As observed in the unretrofitted uplift – velocity relationship, prior to failure the interior RTWCs achieve ultimate failure and begin to transfer load to the exterior RTWCs and, in

this case, the retrofit system. This causes an observable increase in uplift at the exterior RTWCs just prior to failure.

3.4.4 Displacement – Velocity Curves

Figure 3.11 below describes displacement as a function of velocity for the windward RTWCs.

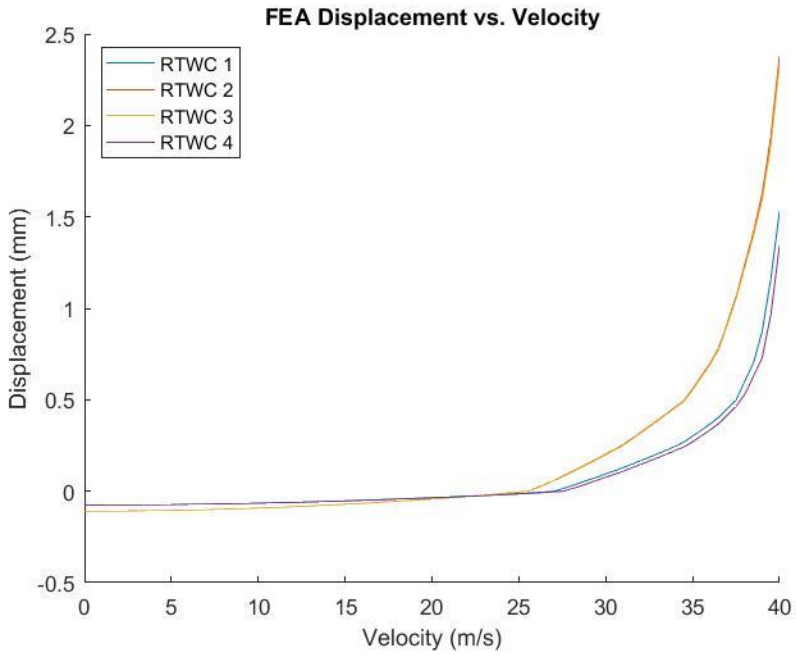

Figure 3.11 FEA generated displacement – velocity curves

Again, since the roof behaves similar to three simply supported spans, the interior RTWCs attract more uplift than the exterior RTWCs and experience correspondingly larger displacement. Since the tension from the retrofit is equally distributed between the interior and exterior RTWCs, the displacement of exterior and interior RTWCs relative to one another is similar to that experienced in the unretrofitted FEA. Unlike the unretrofitted FEA however, the added stiffness of the retrofit system decreases the rate at which this displacement accumulates.

There is a small difference in the velocity at which net tension occurs in the model, suggesting that although the retrofit stiffness appears to be equally distributed between the interior and exterior RTWCs, there may exist some unevenness that favours the exterior RTWCs. A similar phenomenon can also be observed in the previously shown Figure 3.3 and is also possibly evidenced by the difference in initial load seen in that figure.

As all the windward RTWCs were modelled using the same force – displacement relationship, the initial failure of the interior RTWCs is closely followed by the ultimate failure of the roof, at $v = 40$ m/s.

3.4.5 Tension – Velocity Curves

Figure 3.12 below shows the tension – velocity curves for the external cables of the retrofit system, normalized to remove the effect of pretension.

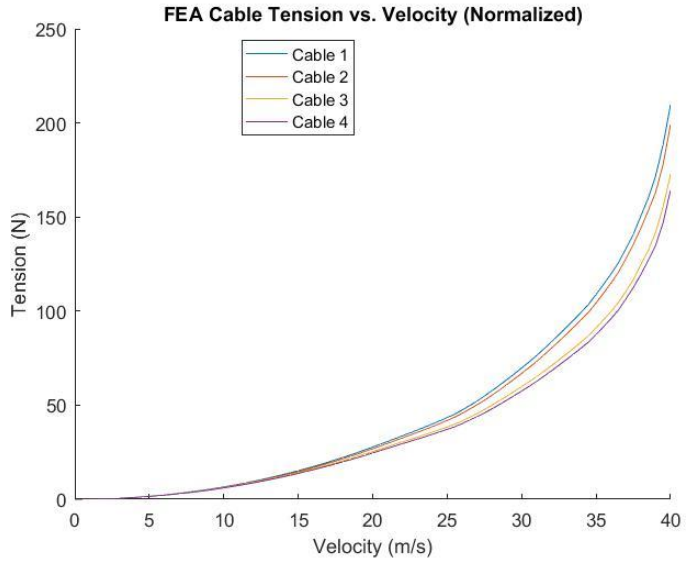

Figure 3.12 FEA generated normalized external cable tension – velocity curves

The change in tension experienced in the cables is primarily dependent on the displacement of the RTWCs, but can also acquire some additional tension from local deflections in the

sheathing. Referring to the demand-capacity ratios used to optimize the retrofit system, it is evident that the retrofit system is well within the elastic range for the wind speeds considered in this paper, and its stiffness can be assumed to be constant. This means that the shape of the tension – velocity curve is proportional to the average windward RTWC displacement – velocity profile, normalized such that there is no initial displacement.

The most noticeable feature of the above figure is the difference in tension between the windward cables 1 and 2, and the leeward external cables 3 and 4. This is a result of modelling the cable – roof interaction as a vertical displacement constraint along the windward edge of the roof to simulate friction. As a point on the roof beneath the cable begins to deform, the corresponding point in the cable element must deform as well. Though the elongation of both sides of the retrofit system are equal, the lengths of the retrofit system on either side of the area of maximum deflection are not. This induces greater strain on the windward cables allowing them to experience slightly greater tension than the leeward cables, effectively simulating the expected effects of friction over the roof.

3.4.6 Load Sharing – Velocity Curves

To understand the interaction of the retrofit and RTWCs, the total change of force in either load path can be compared to the total change of wind load. Figure 3.13 below shows this ratio for the sum of change in both the retrofit and RTWCs.

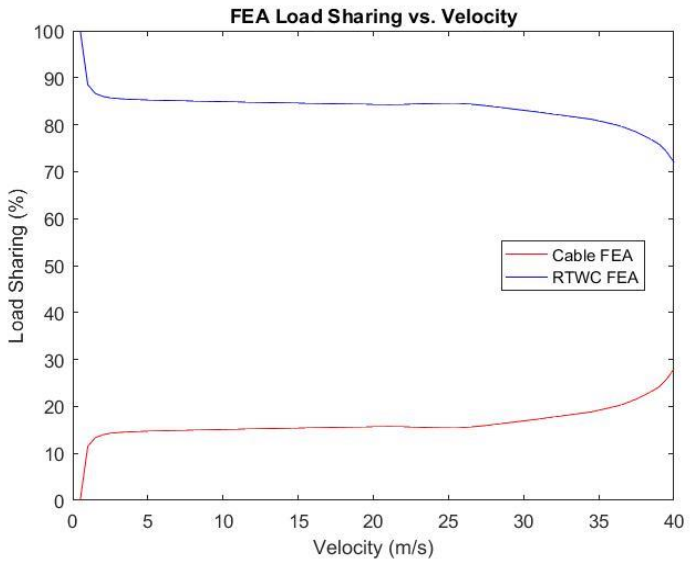

Figure 3.13 FEA generated load sharing – velocity curves

The load sharing ratio is a measure of the relative stiffness of the two load paths. Since retrofit stiffness is assumed to be constant, the rate at which the share of the retrofit load changes will be inversely proportional to the rate at which the RTWC share changes. As discussed, the transfer of load from the RTWCs to the retrofit system is dependent on the average displacement of the windward RTWCs, which is characterized as the events where net tension is first experienced and yield. The curves above display meaningful data from upwards of approximately 3 m/s, where before this point the data becomes unbounded as the change in total load is small. After this point, however, the influence of the average displacement – velocity behaviour is clear.

From approximately 3 m/s to the end of the negative stiffness regime at 27 m/s, the rate of load transfer is small as the stiffness of the RTWCs before net tension is significantly greater than that of the retrofit system. The rate of load transfer then increases from 27 m/s until 36 m/s, which is the average yield velocity of the windward RTWCs. Following 36 m/s until initial failure at 40 m/s, the rate of load transfer increases continuously. Though

the FEA concludes at initial failure, it is anticipated that the rate of load transfer continues in this manner and then stabilizes, as the overturning effect of the roof braced by the retrofit system would increase compression in the leeward RTWCs.

3.5 Analysis of Experimental Behaviour

3.5.1 Instrumentation and Test Description

To construct the reduced scale retrofit system, the wire rope is clipped at either end to be connected to eyebolts fastened to the aluminum beam. The external cables are then connected from the aluminum beam through a modified eyebolt to one end of a 400 kg range s-load cell. The other end is connected to a turnbuckle and rod assembly, which provides the required pretension of 200 N while allowing for a 15˚angle. This assembly is then bolted through the flange of either the windward or leeward 3 in. x 3 in. x ¼ in. steel angles that run the width of the model platform, simulating the piles that would be used in a full scale implementation. A photo of the windward side of the reduced scale test specimen fitted with the retrofit system is shown in Figure 3.14.

Figure 3.14 Windward face of the retrofitted reduced scale test specimen

As with the unretrofitted test, the model was positioned 4.5 m from the aperture of the contraction making a 90˚angle between the incident wind flow and the windward face of the structure. As well, the displacement of each RTWC is recorded by laser displacement transducers and wind velocity was measured with a pitot tube placed upstream at eave height. Prior to wind load application, the turnbuckles of the connection assembly were adjusted and until the s-load cells reported the prescribed pretension of 200 N.

Data was collected over four discrete 90 second periods where the fan speed was progressively increased. Figure 3.15 shows the velocity time history and average for each period of recording.

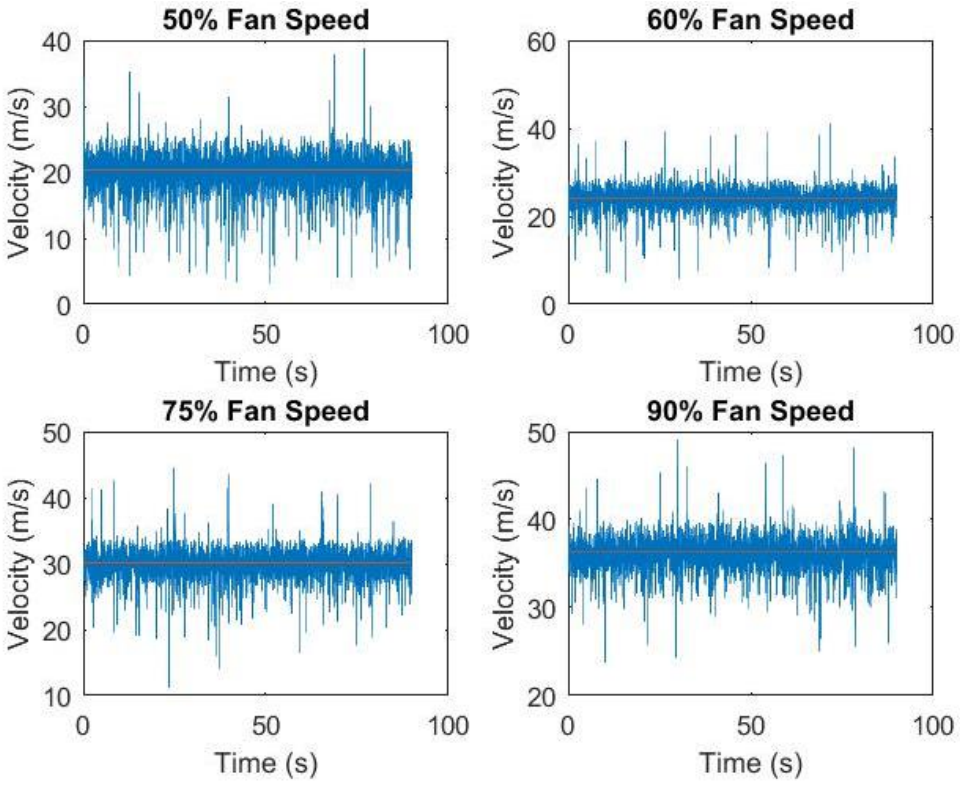

Figure 3.15 Velocity time history for various fan speeds

The velocity statistics for each fan speed are as recorded in Table 3.1 below.

Fan Speed (%)	Mean Velocity (m/s)	Standard Deviation (m/s)	COV
50	20.38	0.63	0.03
60	24.20	0.57	0.02
75	30.12	0.47	0.02
90	36.27	0.43	0.01

Table 3.1 Wind velocity statistics for each fan speed

These statistics indicate that the incident wind flow subjected to the model was relatively constant. Further, a correlation coefficient value of 0.9999 between fan speed and mean velocity indicates that losses of velocity through the contraction are minimal.

3.5.2 RTWC Displacement Analysis

Displacement was recorded at all RTWCs but is only significant at the windward connections. Displacement was collected as a 90 second time history for each of the four fan speeds applied, where an average displacement is calculated and plotted against velocity. Figure 3.16 below shows the velocity – displacement curves for the windward RTWCs.

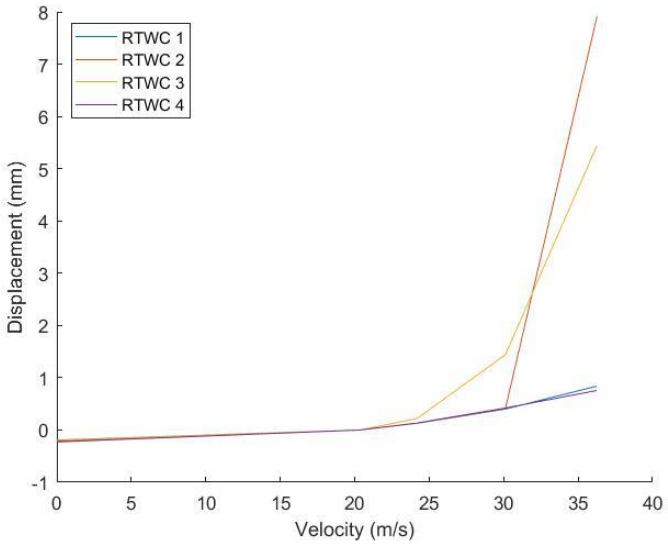

Figure 3.16 Displacement – velocity curves

From $v = 0$ m/s to $v = 20.4$ m/s, RTWCs 1, 3, and 4 experience similar displacement while RTWC 2 appears to be behave stiffly where only slight displacement. In this region, the RTWCs are likely recovering the negative displacement from the compression of the roof weight and retrofit pretension. Beginning at $v = 20.4$ m/s the windward RTWCs begin to experience net tension, and after $v = 24.2$ m/s, RTWC 3 rapidly lose stiffness and begin to deflect, transferring load to the exterior RTWCs and RTWC 2. This causes a minimal increase in deflection in the latter RTWCs until $v = 30.1$ m/s, where RTWC 2 quickly approaches ultimate failure and initiating further deflection in RTWC 3. As the interior RTWCs approach failure, the load allocated to them from tributary area is transferred to the retrofit system, rather than the exterior RTWCs.

The failure modes for RTWC 2 and RTWC 3 were identified through post-failure inspection as all-nail split and nail pullout failures respectively. Given these failures modes, the brittle behaviour of RTWC 2 and the ductile behaviour of RTWC3 observed in the displacement – velocity curves are reasonable.

3.5.3 External Cable Tension Analysis

The external cable tension is recorded for the two windward cables 1 and 2, as well as the two leeward external cables 3 and 4 of the retrofit system. Initial recordings allowed for the adjustment of the pretension prior to wind application, and subsequent measurements captured the total tension in the cables. However, to portray actual tension accumulation as a function of velocity, the following tension – velocity curves in Figure 3.17 below are zeroed to the respective pretension of each cable.

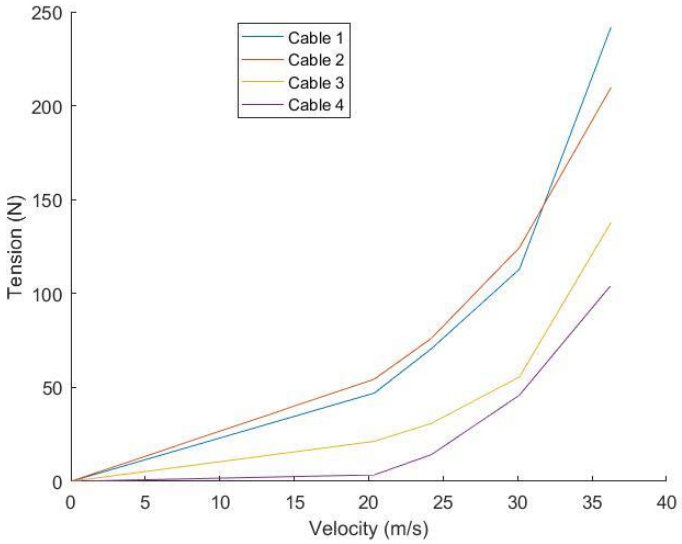

Figure 3.17 Normalized average external cable tension – velocity curves

External cable tension increases proportionally to RTWC displacement as velocity increases. However, the curve presents a notable difference in tension between the windward and leeward external cables, attesting to the significant action of friction between the roof and in internal cables. The internal cables are routed through small 'U' channels of aluminum placed along the path of the cables so as to transfer load to the roof at discrete locations and reduce the chance of cables slipping out of line or off the roof. These channels along with the significant friction incurred at the corners of the roof where the cables change angle, account for an approximately 58 % reduction in tension between the average of windward and leeward external cables at $v = 36.3$ m/s.

3.5.4 RTWC Uplift Estimation

RTWC uplift is not directly measured in the test, so an estimation of uplift in the RTWCs is established by solving the typical 2D force – displacement relationship for the measured displacements at each velocity stage. Further, as the weight of the roof and pretension is overcome at approximately $v = 20.4$ m/s, it can be assumed that in this region the RTWCs

experience compression corresponding to the inverse of the initially recorded displacement. Therefore, Figure 3.18 below shows the resulting uplift – velocity curve where displacement and RTWC load prior to $v = 20.4$ m/s is considered compression.

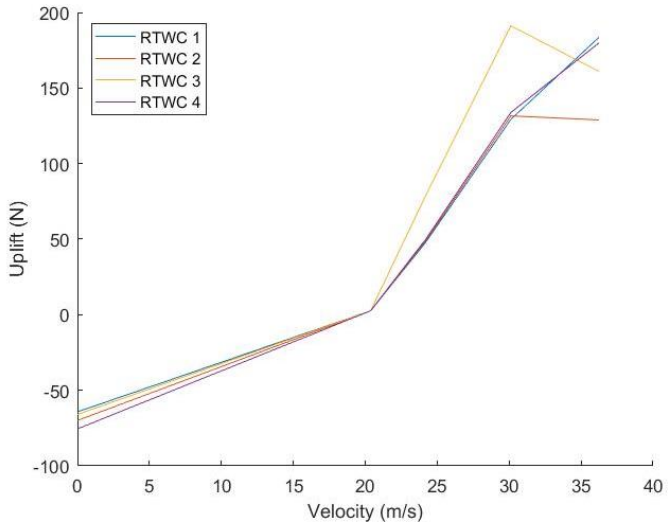

Figure 3.18 Uplift – velocity curves

From $v = 0$ m/s to $v = 24.2$ m/s, RTWCs 1, 3, and 4 experience a similar decrease in compression when recovering roof weight and pretension induced negative displacement. The lack of compression in RTWC in this region is simply indicative of its lack of displacement and not necessarily its true loading condition. While the approach to ultimate failure capacity is more readily observable for RTWC 3 than RTWC 2 from the above set of curves, it is important to note that the resolution of velocity points is limited. Given more velocity data points, the ultimate failure capacity of RTWC would be observable between $v = 30.1$ m/s to $v = 36.3$ m/s. However, the remaining RTWCs demonstrate uplift consistent with the corresponding displacement.

Combining the displacement and uplift data from Figures 3.17 and 3.18 respectively produces the uplift – displacement curves for the windward RTWCs seen in Figure 3.19 below.

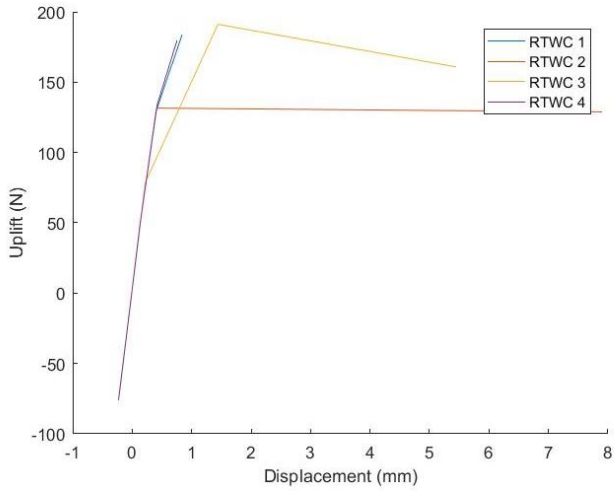

Figure 3.19 Uplift – displacement curves

The response of the RTWCs is made clear in the above set of curves. Again, both RTWCs 1 and 4 are seen to approach the ultimate failure capacity after RTWCs 2 and 3 have failed, and better resolution in velocity data points would allow the profile of RTWC 2 to develop a more characteristic shape.

3.5.5 Load Sharing – Velocity Curves

The load shared between the RTWCs and the retrofit can be evaluated using the recorded tension in the external cables and the estimated force in the RTWCs. Since RTWC force is an estimation, the addition of the cable tension and RTWC force are likely not equal to the applied wind load. To improve accuracy, the load sharing in Figure 3.20 below uses the difference between the total applied load and the total external cable tension as the estimated RTWC load. This is because the external cable tension and pressure distribution were directly measured in and are likely more reliable.

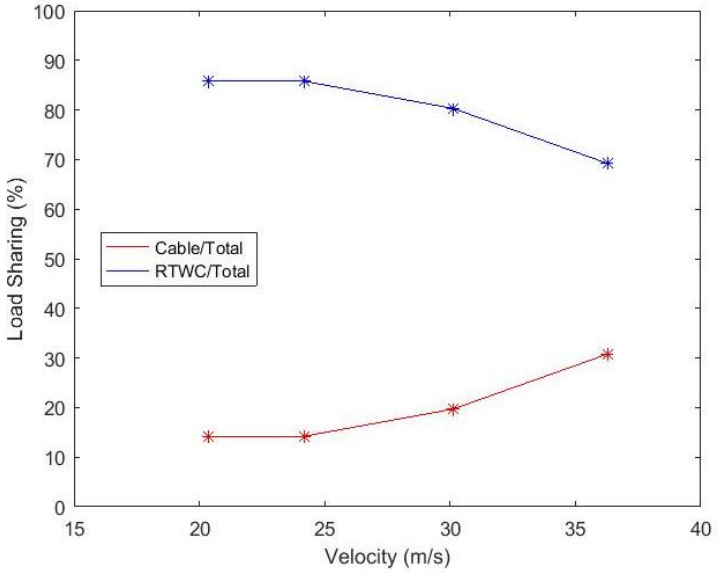

Figure 3.20 Estimated average load sharing between RTWC and retrofit

The share of the total load in both load paths is evaluated at each velocity step achieved in the experimental test. As observed in the FEA derived load sharing – velocity curves, the individual stages of the displacement – velocity curves can be identified by the rate at which load sharing changes. Prior to the occurrence of average net tension in the windward RTWCs at 24 m/s, the RTWCs are comparatively stiffer than the retrofit and change in load sharing is minimal. At velocities greater than 24 m/s, RTWC stiffness significantly decreases producing a greater change in load sharing until average yield behaviour occurs in the windward RTWCs at 30 m/s that accelerates this change. Though resolution is poor due to the low number of sample velocities, the shape of this curve is as expected due to the progressive loss of stiffness in the RTWCs as displacement occurs, and also validates the assumption that the retrofit stiffness is constant.

3.6 Post – Failure Finite Element Analysis

Similar to the initial FEA results of the unretrofitted structure, there exist obvious dissimilarities between the FEA and experimental results. This can be attributed to the variable nature of wood products, and in particular toe-nailed connections. To understand the effect of variable RTWC properties on the structural performance and to produce a numerical model that more accurately portrays the behaviour of the structure, individual RTWC force – displacement relationships are assigned to the windward RTWCs. These relationships are piecewise linear functions that are demarcated by a series of points representing negative force – displacement regime, yield, ultimate failure, residual plasticity, and full withdrawal.

As with the unretrofitted structure, the negative stiffness regime and full withdrawal length are relatively constant parameters, and the point at which residual plasticity leads to full withdrawal cannot be fully examined by the FEA due to negative stiffness. Therefore, to reduce the number of variables, only the yield and ultimate failure are manipulated. A parametric optimization is then performed by iteratively changing the load and displacement values at these points, with the objective of producing FEA derived displacement – velocity curves that acceptably match those produced experimentally. Displacement – velocity is chosen as the objective as it was the RTWC property directly measured. The optimized RTWC properties can then be used to produce FEA results that approximate the experimentally observed behaviour, and potentially validate the more useful uniform RTWC FEA method.

3.6.1 Displacement – Velocity Curves

To better replicate the behaviour of the structure in FEM, post-failure inspection is used to assess the failure mode and better characterize the RTWC force – displacement relationships for modelling. Following the experiment, RTWC 2 and RTWC 3 are found to have failed via a brittle all-nail split and a ductile nail pullout respectively. As failure was not observed in any of the other RTWCs, the typical 2D force – displacement relationship is assumed to be accurate to model these connections. Similar to the post-failure analysis exercise performed for the unretrofitted structure, specific objectives were created for the parametric optimization to ensure good agreement with the experimental data. These were namely (i) to ensure that net tension in the windward RTWCs occur at approximately 20 m/s, (ii) that RTWC 3 begins a ductile failure at approximately 24 m/s, and (iii) that RTWC 2 experiences brittle failure at approximately 30 m/s.

To verify that post-failure parametric study is successful, a comparison of the experimental and post-failure FEA displacement – velocity curves are featured in Figure 3.21 below. Since the experiment was stopped short of total RTWC failure, the red line in Figure 3.21 b) indicates where the data ends in Figure 3.21 a).

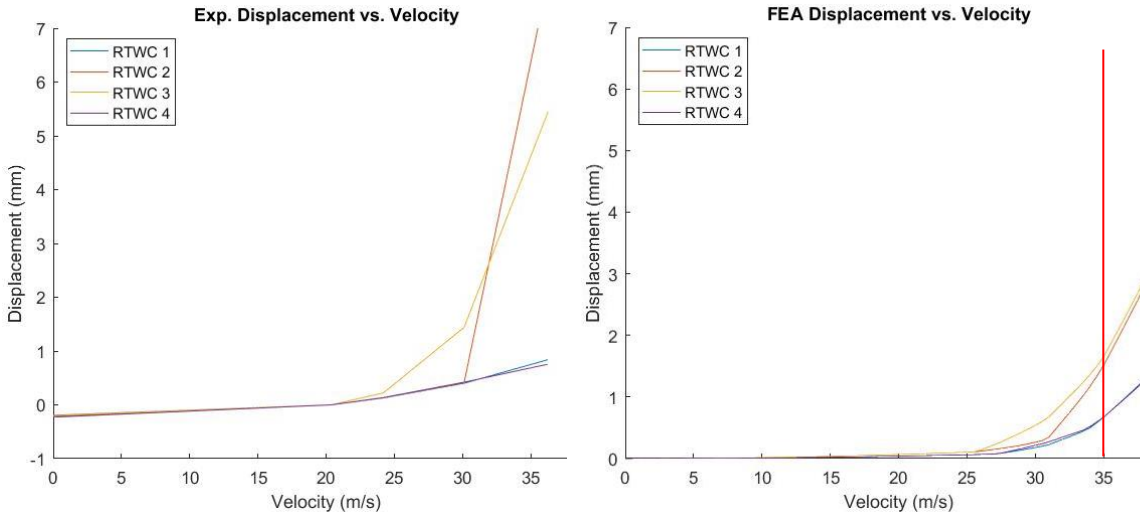

a) b)

Figure 3.21 Displacement – velocity curves from a) experimental and b) FEA results

A comparison of the above figures indicate that indeed, these objectives are satisfactorily met. However, due to model and manual parameter manipulation limitations, some minor aspects of experimental displacement – velocity curves proved difficult to replicate. Chief among these is that the FEA predicts failure of all RTWCs to occur at a particular velocity, whereas the experimental results indicate that the interior RTWCs failed well before the exterior RTWCs would have.

This issue was previously encountered in the post-failure analysis of the unretrofitted structure, and is likely due to the FEA being unable to permit sufficient rotation of lateral bracing members at trusses 1 and 4, to allow large enough deflections to the interior RTWCs. In both the FEA and the test specimen, the difference between interior and exterior RTWC displacement increases with velocity until a certain point at which the full stiffness of the lateral bracing system engages and load is distributed through stiff beam – weak spring behaviour. However, this appears to occur at a much greater difference in the test specimen such that it allows the interior RTWCs to completely fail before full lateral

stiffness can engage. This suggests that the test specimen can be more accurately modelled using non-linear link elements as the lateral bracing connections.

Again, similar to the post-failure analysis of the unretrofitted structure, the unit weight of the sheathing and roof truss materials were reduced such that the velocity at which the windward RTWCs began to experience net tension was decreased to match the experimental results. The resulting unit weights of the materials remain realistic and typical for low moisture content, where the SPF in the roof truss members was reduced to 4.0 kN/m^3 and the plywood sheathing reduced to 5.0 kN/m^3.

3.6.2 Uplift – Velocity Curves

Once the displacement – velocity curves have satisfactorily met the objectives of the parametric optimization, an estimate of the RTWC uplift can be produced. Figure 3.22 below shows the resulting uplift – velocity curve for the windward RTWCs.

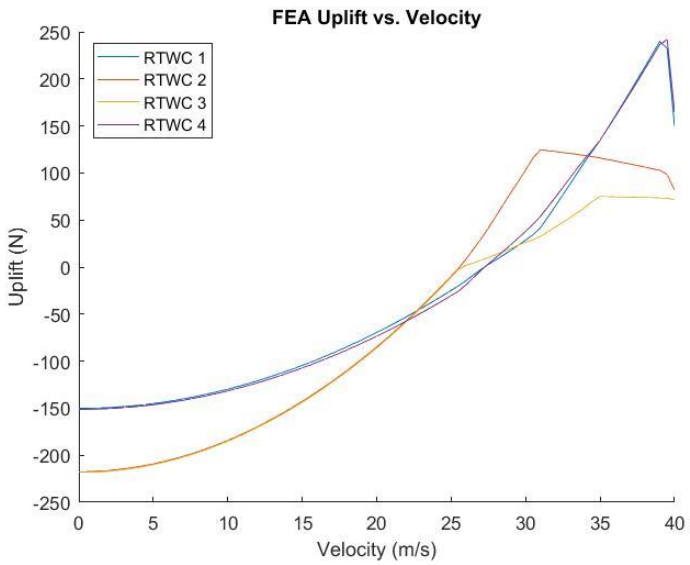

Figure 3.22 Uplift – displacement curves for RTWCs simulating observed failure modes

Since the exterior RTWCs 1 and 4 were modelled using the average 2D toe-nailed connection force – displacement relationship, prior to failure these connections develop the expected full ultimate failure force of approximately 200 N. However, to accommodate early failure of both RTWCs 2 and 3, the load parameters of both yield and ultimate failure were reduced to values uncharacteristically low of that expected by testing individual toenail samples. As discussed in the analysis of the unretrofitted structure, the main reasons for this are the conditions on site that impede fabrication quality, and the potential increase in internal pressure due to displacement of the windward edge of the roof that was not measured. However, applying the proposed solutions of a factor to artificially reduce expected RTWC tensile resistance, and the continuous monitoring of differential pressure across the roof would allow the input load parameters to be closer to values seen in the sample toe-nail connection tests.

3.6.3 Uplift – Displacement Curves

Despite the reasons for the lower than expected values of the load parameters, the uplift – displacement curves of the windward RTWCs, shown below in Figure 3.23, accurately portray the relative difference in stiffness between the connections.

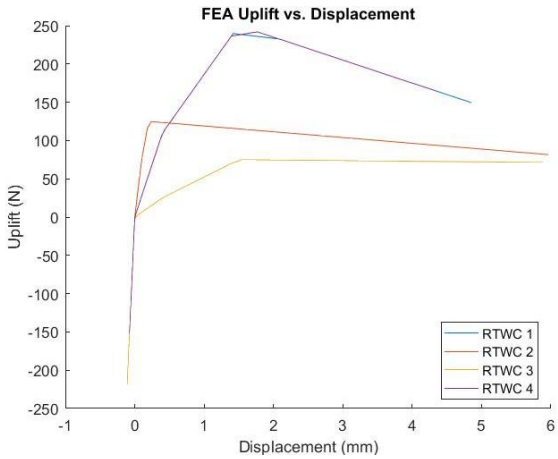

Figure 3.23 Force – displacement relationships simulating experimental failure modes

The characteristics of each windward RTWC piecewise linear force – displacement relationship are shown in Table 3.2 below.

Stage Demarcation Point	RTWC 1		RTWC 2		RTWC 3		RTWC 4	
	F (N)	D (mm)	F (N)	D (mm)	F (N)	D (mm)	F (N)	D (mm)
Negative Stiffness	1000	-0.5	1000	-0.5	1000	-0.5	1000	-0.5
Zero	0	0	0	0	0	0	0	0
Yield	110	0.4	100	0.4	50	0.4	110	0.4
Ultimate Failure	200	1.5	150	0.8	100	1.5	200	1.5
Residual	70	7.5	70	7.5	70	7.5	70	7.5
Full Withdrawal	0	10	0	10	0	10	0	10

Table 3.2 Windward RTWC piecewise linear force – displacement relationships

The optimized force – displacement relationships as outlined validates observations made in post-failure analysis of RTWCs 2 and 3.

RTWC 2 experienced a brittle splitting failure though all nails on both sides of the connection at a relatively low velocity. The above Table 3.2 presents a yield force and displacement that is close to the average. However, this is immediately followed by ultimate failure at a displacement smaller than expected, suggesting the presence of a considerable wood split in the connection. Since all-nail split failures tend to have a large ultimate failure capacity, it makes sense that this parameter was significantly greater in RTWC 2 than RTWC 3.

By contrast, the all-nail pullout failure at RTWC 3 generated yield and ultimate failure at comparatively low wind velocities, while generating displacements for these events that are comparable to that of the average toenail connection. As recorded in the sample connection tests, the most likely failure mode to occur, and therefore contribute the most

to the average behaviour, is the all-nail pullout failure. Since the load parameters could be artificially low due to reasons discussed in the previous section, the near average values of displacement in RTWC 3 suggest a validation of post-failure observations.

3.7 Comparison of Initial and Post-Failure Finite Element Analysis to Experimental Data

The comparison of results for both initial and post-failure FEAs to experimental results is required to determine the accuracy of these methods, and validate them for future use in determining test specimen behaviour. Given the large variability of toenail connection behaviour, the ability to examine failure modes for use in post-failure FEA will invariably give this method an accuracy advantage when compared to simply assuming the average force – displacement relationship of a toenail connection applies all RTWCs, as in the initial FEA. However, the ability to reliably predict the behaviour of the test specimen is of far greater use. Therefore, this section will seek to validate both methods of analysis as accurate, and provide suggestions for improvement.

3.7.1 Equilibrium Ratio

To measure how accurately each analysis method predicted total applied load, a ratio comparing the total uplift due to wind load to the sum of RTWC tension is determined, where the measure of accuracy can be interpreted as the proximity of the ratio to unity. Calculation of the ratio is as outlined in the equation below.

$$Eq.\ Ratio\ (V_i) = \frac{{}^1\!/_2\,\rho V_i \iint C_p(x,y)\cdot dxdy}{\sum RTWC(V_i) + \sum CABLE(V_i)}$$

The ratio is calculated for each velocity step, V_i, recorded in the test. To determine the total applied force, the dynamic pressure is multiplied by the area integral of the pressure coefficient distribution over the area of the roof, adjusted to consider roof inclination. The total force measured consists of RTWC force estimate and the measured retrofit cable tension. The RTWC estimate is the summation of the solution to the force – displacement curves assigned to the RTWCs by the two analysis methods for the average displacement during a particular velocity step. From this equation, Figure 3.24 can be constructed, as shown below.

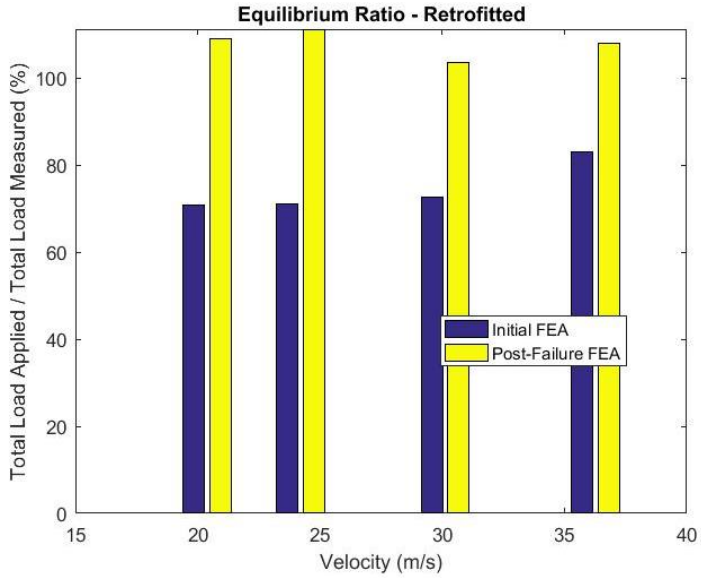

Figure 3.24 Equilibrium ratio at sample velocities for initial and post-failure FEA results

The presented bar chart indicates a significant apparent difference in the accuracy of these analysis methods. The difference is due to the previously discussed effects of material weight, reduced RTWC construction quality on site, and windward edge separation. Though these are theoretical systematic errors, the effects of which can be significantly reduced through better modelling. This is encouraging as the post-failure analysis method appears to be highly accurate, and the difference between the two methods are fairly

constant, suggesting that the use of one force – displacement relationship to model all RTWCs can produce results consistent with methods that use different relationships. Though the post-failure FEA proved much more accurate than the initial FEA in this exercise, better modelling of the identified systematic errors can significantly improve the accuracy of the more useful initial method.

3.7.2 Load Sharing – Velocity Curves

Another means of validating the accuracy of both methods is to compare the FEA derived load sharing to that observed in the experimental results. Figure 3.25 below shows this comparison.

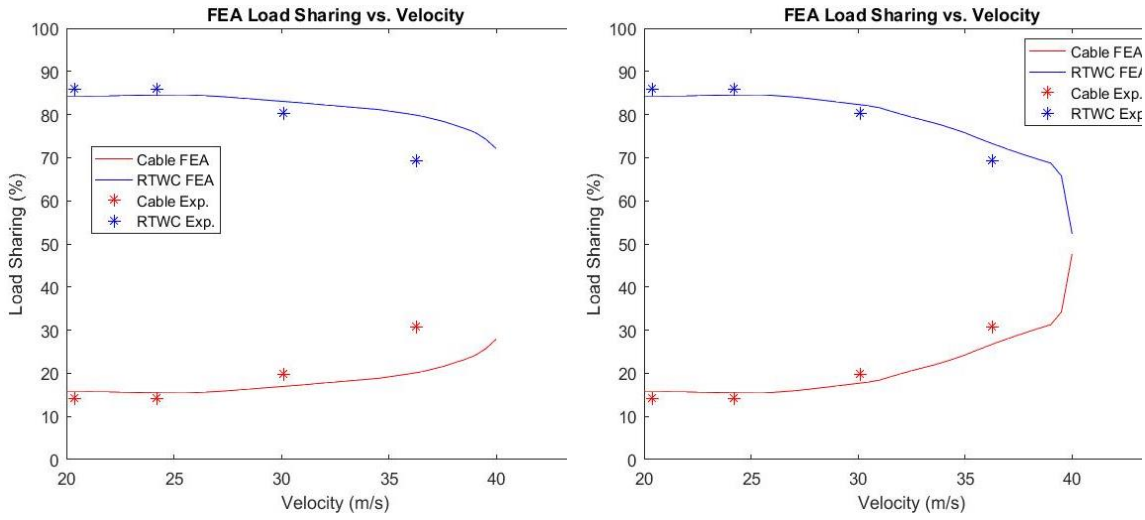

a) b)

Figure 3.25 Load sharing – velocity curves from a) initial and b) post-failure FEA results

Recalling the load sharing analysis previously discussed, the three phases of toenail withdrawal affect how load is distributed between the two load paths. Therefore, optimization of the yield and ultimate failure parameters are reflected in the significant differences between the above two figures. Since the RTWCs share the same stiffness

properties prior to positive displacement, and relatively similar yield stiffness as both RTWCs 1 and 4 are modelled using average 2D toe-nail connection properties, the small difference between the FEA and experimental results at 20 m/s, 24 m/s, and 30 m/s is fairly similar between Figure 3.25 a) and b). However, as the load sharing curve approaches greater velocities, the load sharing accuracy decreases as the post-failure analysis concluded that the interior RTWCs were modelled too stiff in the initial FEA. Conversely, since the post-failure FEA optimized the stiffness of the interior RTWCs, Figure 3.25 b) demonstrates greatly improved accuracy in the near yield and post-yield force – displacement regimes.

Though the post-failure FEA presents notable accuracy improvements in the load sharing velocity – curves, the initial FEA was able to accurately predict values of load sharing in the compression and pre-yield force – displacement regimes and displayed trends consistent with the experimental data. Again, adoption of corrective measures to reduce expected RTWC tensile resistance will reduce the stiffness of the RTWCs in an initial model and improve accuracy of this method in future applications.

3.8 Comparison of Structural Response with and Without Retrofit System

The improvement of the retrofit to the small scale structure is quantified as the increase in wind velocity at which certain RTWC events occur, and examines both the initial and post-failure FEA results as well as the experimental data. As outlined before, these events are the (i) onset of net tension in RTWCs, (ii) occurrence of localized RTWC failure, and (iii) total roof failure.

Table 3.3 below shows the difference in velocity at which the windward RTWCs first experience net tension, inducing separation.

Initial Separation	**Initial FEA**	**Post-Failure FEA**	**Experimental**
Without Retrofit	18.0 m/s	17.0 m/s	15.3 m/s
With Retrofit	23.0 m/s	21.0 m/s	20.4 m/s
Difference	5.0 m/s	4.0 m/s	5.1 m/s
% Difference	21.7 %	19.0 %	33.3 %

Table 3.3 Difference in velocity at which initial separation of windward RTWCs occurs

The difference presented is largely due to the addition of the retrofit induced pretension force. The presence of this force effectively delays the displacement – velocity behaviour of the RTWCs, and increasing the velocity at which subsequent events occur.

Following initial separation in the windward RTWCs, initial RTWC failure occurs in one or both of the interior RTWCs. Table 3.4 below presents the difference in velocity at which this event occurs.

Initial RTWC Failure	**Initial FEA**	**Post-Failure FEA**	**Experimental**
Without Retrofit	31.5 m/s	24.0 m/s	21.1 m/s
With Retrofit	36.0 m/s	32.0 m/s	30.1 m/s
Difference	4.5 m/s	8.0 m/s	9.0 m/s
% Difference	12.5 %	33.3 %	42.7 %

Table 3.4 Difference in velocity at which initial failure of the windward RTWCs occur

Since the initial FEA had overestimated the stiffness of the RTWCs in both models with and without the retrofit, the initial RTWC failure velocity is noticeably greater than for the post-failure FEA and experimental values. Despite this, the increase in velocity difference in both the FEA and experimental values are a result of load being transferred from the

RTWCs to the retrofit system. As the retrofit load share increases with velocity, it will further delay the onset of subsequent events.

As mentioned, after the initial failure of an interior RTWC, load is transferred to adjacent RTWCs and induces total roof failure. It is important to note that total roof failure is considered to be the event at which all RTWCs reach ultimate failure capacity rather than roof overturning, as the presence of the retrofit effectively eliminates this catastrophic failure mode. Table 3.5 below shows the velocity, and difference in velocity, at which this event occurs.

Total Failure	**Initial FEA**	**Post-Failure FEA**	**Experimental**
Without Retrofit	31.5 m/s	23.8 m/s	24.1 m/s
With Retrofit	40.0 m/s	40.0 m/s	40.5 m/s *
Difference	8.5 m/s	16.2 m/s	16.4 m/s *
% Difference	27.0 %	68.1 %	68.1 % *

* Estimation as per post-failure analysis percentage difference

Table 3.5 Difference in velocity at which initial failure of the windward RTWCs occur

As further load sharing reduces the load accumulation experienced at the windward RTWCs, the displacement – velocity behaviour of the RTWCs becomes increasingly extended, consequently increasing the difference in velocity from the previous events. Since total failure was never achieved during experimental testing, the total failure velocity was estimated based on the percentage difference of the more accurate post-failure FEAs.

It should be noted here that the prediction of wind speed at which the reported displacement events occurred is markedly more accurate from the initial FEA of the structure with retrofit than without. The percent difference between these wind velocities derived from the initial FEA models with and without the retrofit system, and the experimentally derived velocities is presented in Table 3.6 below.

Prediction Difference	**Initial Separation**	**Initial RTWC Failure**	**Total RTWC Failure**
Without Retrofit	17.6 %	49.0 %	30.7 %
With Retrofit	12.7 %	19.6 %	1.3 %

Table 3.6 Difference between initial FEA and experimental wind velocities

The majority of the dissimilarity between the velocities derived from the initial FEA of the unretrofitted structure and experimental results is assumed to be due to the inherently varied properties of nailed wood connections. Khan and Kopp (2012) present toenailed connection specimens with the total sample COV for ultimate capacity of approximately 65%. Further, only 40% of samples experienced the same failure mechanism, of which the unique force-displacement relationship and associated properties are wholly reliant upon. Moreover, the work of Khan and Kopp (2014) discusses how the redundant effect of load sharing between roof trusses amplifies the inconsistency of the mechanical properties of toe nailed connections by redistributing uplift load as the connections lose stiffness.

This is contrasted by the relatively close similarity between the velocities derived from the initial FEA of the retrofitted structure and the experimental results. The reason for increased accuracy is attributed to the mechanical properties of the retrofit system. As the roof distributes load from the RTWCs to the retrofit system, the stiffness of the cabling tends to dominate the structural behaviour of the roof. In this condition, the comparatively consistent mechanical properties of the steel and aluminum comprising the retrofit system afford the initial FEA of the retrofitted structure a more accurate prediction of behaviour.

In conclusion, the addition of the retrofit substantially increased the velocity at which the abovementioned RTWC events occur. By applying a pretension force and progressively transferring load away from the RTWCs through load sharing, the retrofit system greatly increased the resistance of the structure to wind failure.

3.9 Retrofit Stiffness Improvement

3.9.1 Description of Alternate Retrofit Configuration

The configuration of the retrofit system heavily relies on the bending stiffness of the beam to evenly distribute the tension from the external cables through to the internal cables. During the experimental test, it was noted that the beam was experiencing significant deflection at both ends and in the middle indicating that the beam was not transferring adequate tension to the corresponding internal cables. This can lead to localized failures such as shingle or sheathing damage as the slack internal cables can allow for deformation in the underlying structure.

To remedy the excessive deformation in the beam, an alternative retrofit configuration is developed that routes the internal cables through the beam. Theoretically, the tension is then distributed through the beam as axial force rather than shear and bending, and any deflection would be from cable elongation. A schematic of the original and alternative retrofit configurations are shown in Figure 3.26 below.

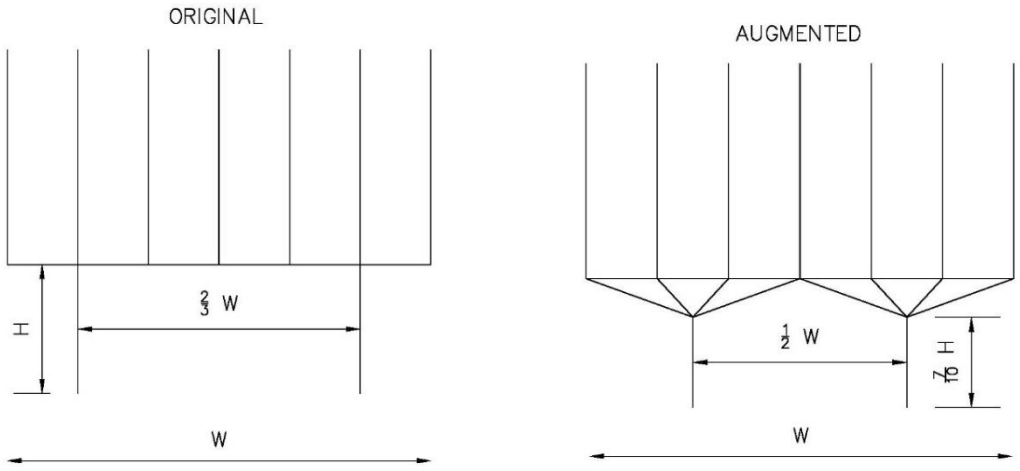

Figure 3.26 Geometry of original and augmented cable configurations

3.9.2 Performance improvement

To test the potential efficacy of the alternate configuration, a copy of the reduced scale FEM was altered to route the internal cables through the aluminum beam. The model of the alternate configuration was subjected to the same realistic loading conditions as previously applied, and the response of various components were compared to those of the original model. Specifically, this exercise looks to examine improvement in two important response features, namely overall structural stiffness and tension distribution.

3.9.2.1 Retrofit Stiffness

As the two FEMs are subject to the same loading conditions, improvement in the overall stiffness of the retrofit system can be observed as the ratio between the average windward RTWC deformation and the average tension in the windward external cables. Figure 3.27 below presents the displacement as a function of velocity for the former parameter.

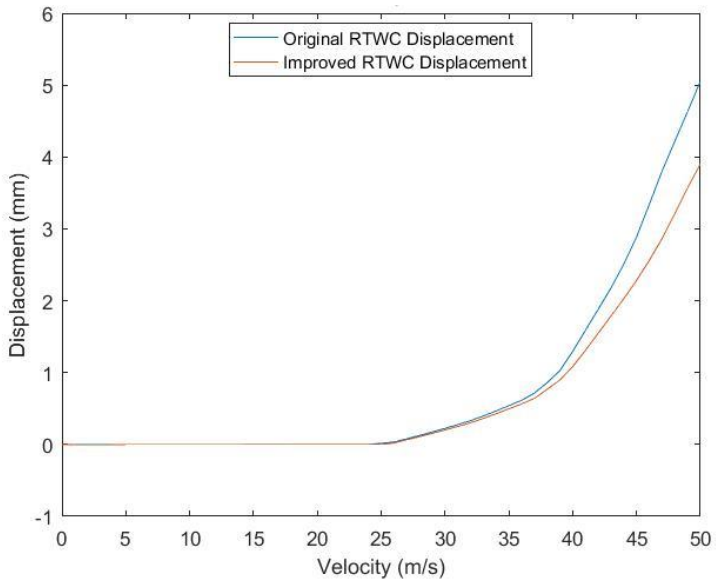

Figure 3.27 Average displacement – velocity curves for the windward RTWCs

Deflection begins to occur in both models at approximately 25 m/s, since the pretension is the same. After this point however, the rate of displacement decreases in the improved model, and at 50 m/s there is 1.1 mm difference in displacement.

Conversely, Figure 3.28 below shows the relatively unchanged average normalized tension – velocity curve for the windward external cables. This indicates that the improved retrofit configuration has an increased stiffness.

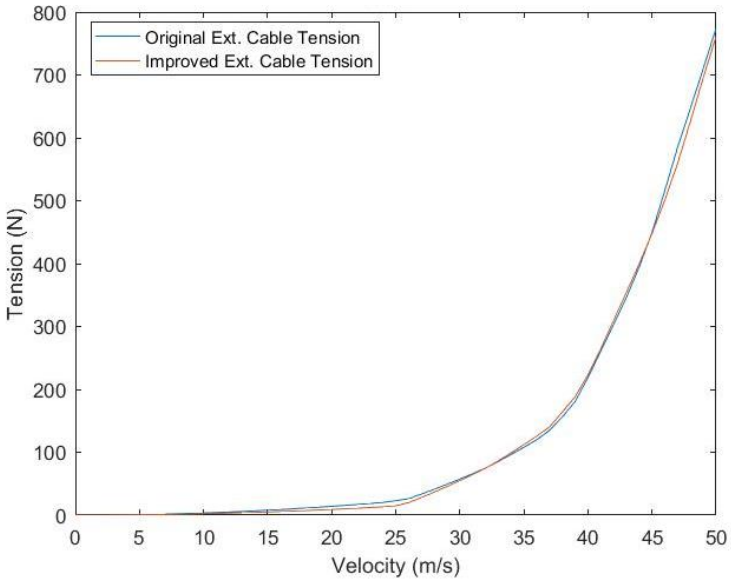

Figure 3.28 Average normalized tension – velocity curves for windward external cables

To quantify this improvement to overall system stiffness, the normalized average tension and average RTWC displacement are plotted in Figure 3.29 below.

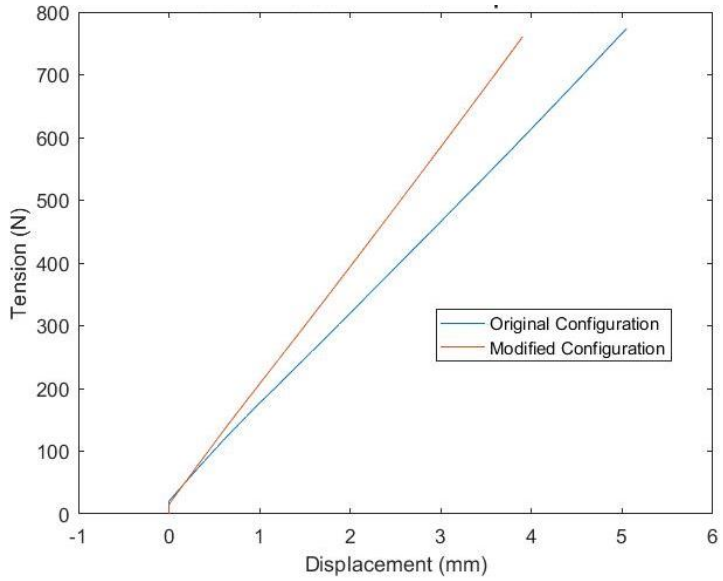

Figure 3.29 Average tension – displacement at windward external cables and RTWCs

For both the modified and original configurations, the system stiffness is highly linear. Using linear regression, the modified system stiffness is 195.12 N/mm, while the original

system stiffness is 153.12 N/mm. This results in an approximate 26.8% improvement to overall retrofit stiffness, key in allowing the retrofit system to offer protection under greater wind load.

3.9.2.2 Tension Distribution

While pretensioning the external cables during the experimental test, the rigid beam is observed to deflect. This leads to noticeably slack internal cables over the roof, particularly those in the middle. Though relatively inconsequential for this test given that measures are taken to ensure only RTWC failure, slack internal cables allow for roof cladding and sheathing components to deform and potentially fail. Enhancing the stiffness of the tension distribution system will allow for more even tension sharing between the internal cables. Figure 3.30 below shows a bar graph presenting the relative distribution of pretension amongst the internal cables for the original and improved configurations.

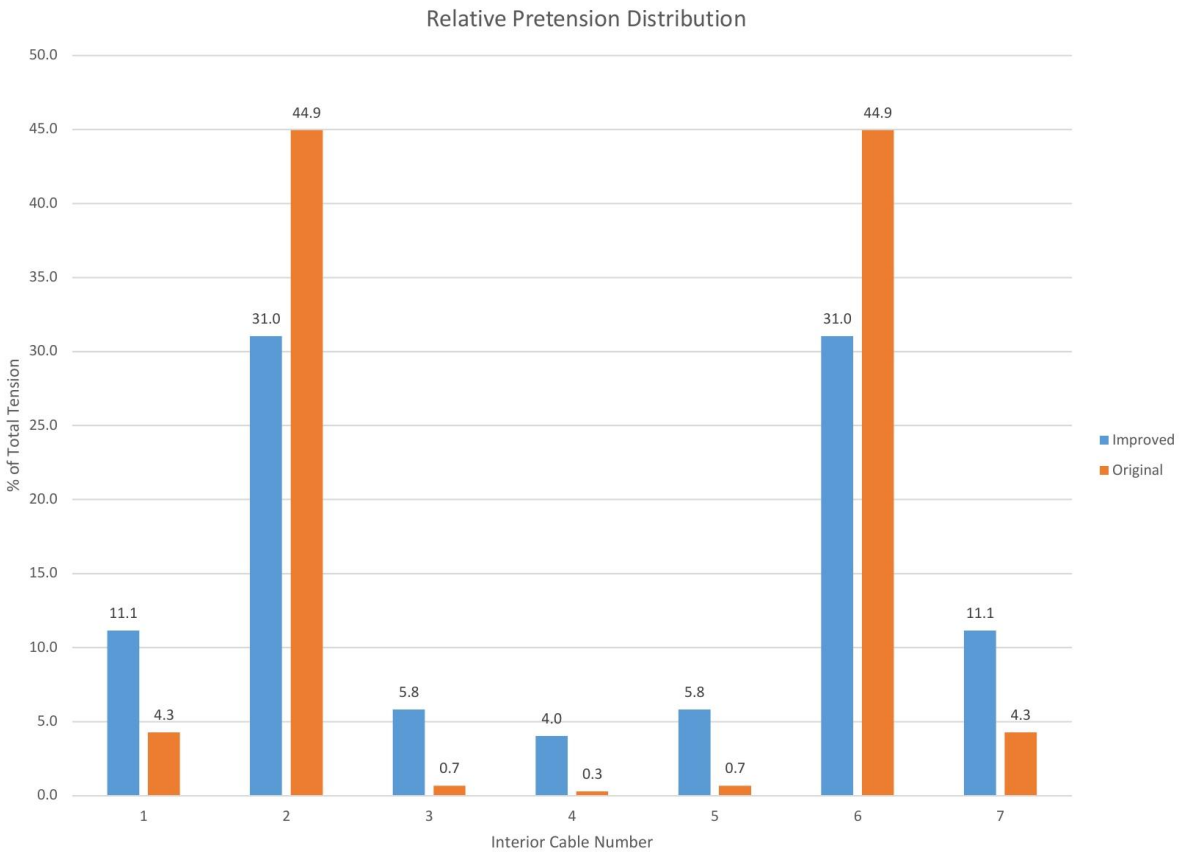

Figure 3.30 Relative distribution of pretension in internal cables

As observed experimentally in the original configuration, the three middle internal cables had shared almost none of the pretension, while the two cables in lines with the external cable experienced 89.8 % combined. In contrast, the improved configuration offers a significantly better pretension spread, allowing for 15.6 % of the total pretension force to be transferred through the middle three cables.

The tension distribution at pretension is different than when the windward RTWCs approach failure. Figure 3.31 below present a bar graph of the relative distribution of tension in the internal cables for the original and improved configurations at 50 m/s.

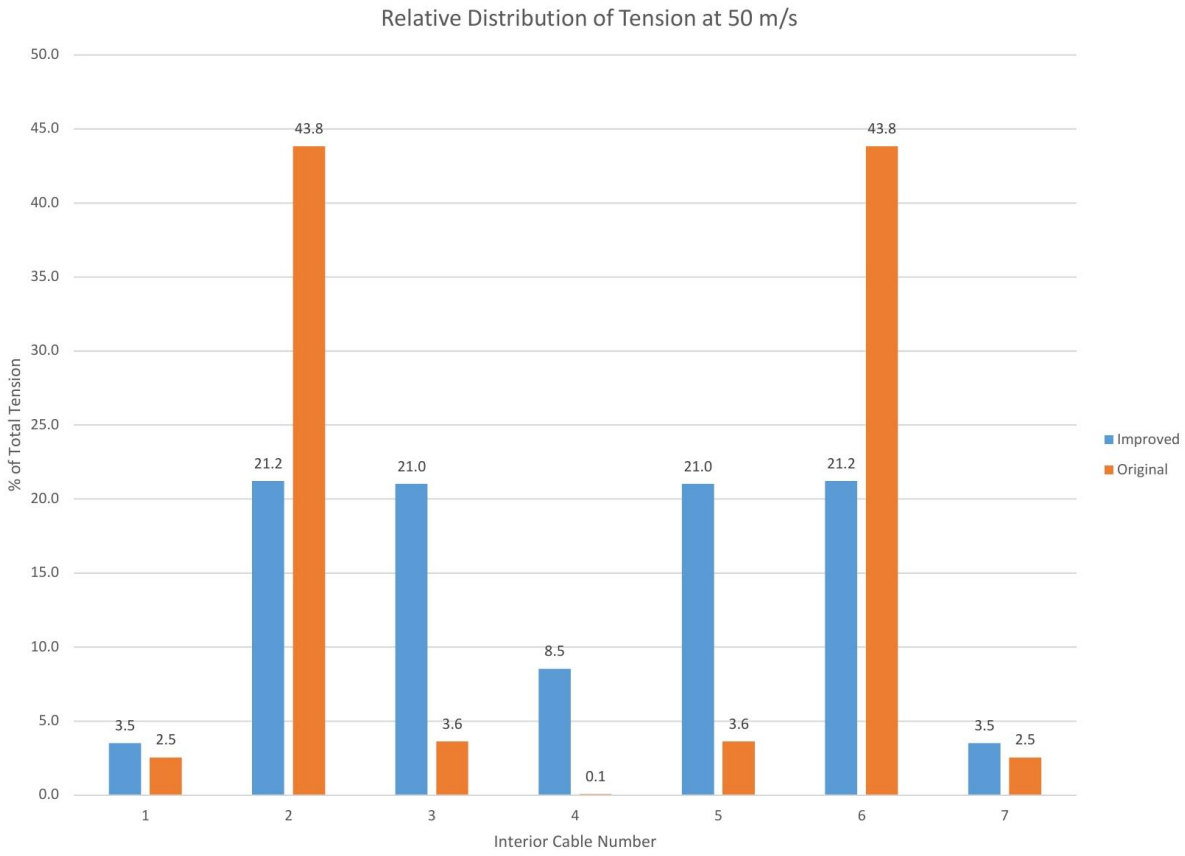

Figure 3.31 Relative distribution of tension in internal cables at 50 m/s

Note that the distribution from the original configuration changes only slightly, by transferring tension from cables 1 and 7 to cables 3 and 5. However, under full wind load, the improved configuration performs better than at rest by distributing tension almost symmetrically about the external cables. By providing significantly improved tension distribution across a sizeable portion of the roof, the modified configuration has effectively mitigated the issue of slack internal cables.

Further research should investigate the optimal dimensions of the improved configuration through an iterative optimization process, where the spacing and length of the external cables can be changed to further improve the distribution of tension across the internal cables and improve system stiffness.

3.10 Conclusions

Following the investigation of the test specimen as the control variable, a scaling exercise similar that governing the roof components is conducted to design a reduced scale version of the retrofit. The retrofit is then applied to the test specimen and the combined performance is assessed and compared to that of the control variable.

Similar to the previous investigation, there are differences in the predicted and observed failure velocity, as well as load sharing behaviour when compared to a full scale house. Again however, the cause of these differences are understood and suggestions are made for future improvement, and a numerical analysis using post-failure observations more accurately captures the behaviour.

Both the numerical and experimental results are used to compare the behaviour of the test specimen with and without the retrofit system. Most importantly, the addition of the retrofit significantly improved the velocity at which initial separation, initial RTWC failure, windward RTWC failure all occur.

The findings of this investigation are as follows:

- All of the conclusions from the previous investigation of the test specimen alone have been noted to occur with the addition of the retrofit. To summarize these points
    - Further investigation into improving the lateral roof stiffness of the reduced scale model would better simulate the RTWC load sharing of a full scale structure, but is not necessary if used purely for comparative purposes.

  - Application of a reduction factor to RTWC strength and continuous monitoring of differential pressure throughout the test can improve the accuracy of RTWC load parameters

  - Post-failure analysis succeeds in numerically approximating the observed behaviour of the test specimen, but since the potential increase in internal pressure is not recorded, only the relative stiffness of the RTWCs are accurate

- All significant RTWC displacement events occurred at significantly higher wind velocities with the addition of the retrofit. Though the test environment was not able to produce the require wind speed to observe total windward RTWC failure, the post-failure FEA concludes that this would have occurred at 40.5 m/s. This would be a 68.1% increase in velocity at the same event in the test specimen alone.

- At a given wind velocity, load sharing between the retrofit system and RTWCs is directly governed by RTWC displacement due to the constant stiffness of the retrofit system. However, increasing pretension and retrofit stiffness will increase the velocity at which RTWC displacement events occur uniformly and linearly respectively.

- Observation and FEA analysis reveal that the current configuration of the retrofit system does not adequately distributed the tension developed in the external cables to the interior cables. A proposed solution is to route the interior cable through the rigid bar to a node, such that the rigid bar is exclusively in tension. Comparison of FEAs with both configurations concludes that routing the cables through the rigid

bar significantly increases both the tension distribution, as well as totally retrofit stiffness.

The ability of the retrofit system to act as a second load path in addition to providing a pretension force results in the clear benefit observed in both the numerical and experimental results. Further, the increased velocities at which separation and initial RTWC failure occur are key in preventing water infiltration damage. It is important to note that though total windward RTWC failure may occur, the more catastrophic failure of the whole roof via rotation about the leeward RTWCs is inherently prohibited by the presence of the retrofit system.

3.11 References

Baskaran, A. and Dutt, O., 1997. Performance of roof fasteners under simulated loading conditions. Journal of Wind Engineering and Industrial Aerodynamics, 72(0), 389-400

Bimberg, U., and Bimberg, O. (1997), U.S Patent No. 5623788. Washington, DC: U.S. Patent and Trademark Office.

Computers and Structures, Inc. (2009). SAP 2000 V. 14: Integrated Software for Structural Analysis and Design. Berkley, California, USA.

Federal Emergency Management Agency (FEMA), 2010. Wind Retrofit Guide for Residential Buildings. Federal Emergency Management Agency.

Jacklin, R., El Damatty A. A., Dessouki, A. A., 2014. Finite-Element Modeling of a Light-Framed Wood Roof Structure. Wind and Structures, Vol. 19 No. 6, 603-621

Morrison, M. J. (2010). *Response of a Two-Story Residential House Under Realistic Fluctuating Wind Loads*. (PhD Thesis). London, Ont.: Department of Engineering, The University of Western Ontario.

Luzzi, J., 1999. U.S Patent No. 5881499. Washington, DC: U.S. Patent and Trademark Office.

Rosenkrantz, J. D., El Damatty, A. A., 2016. Wind load parameters of a structural test using real wind load at the WindEEE Dome. 4th American Association for Wind Engineering Workshop, May 31st 2016

Stewart, M. G., 2003. Cyclone damage and temporal changes to building vulnerability and economic risks for residential construction. Journal of Wind Engineering and Industrial Aerodynamics, 91(5), 671-691

van de Lindt, J., Graettinger, A., Gupta, R., Skaggs, T., Pryor, S., and Fridley, K., 2007. Performance of wood-frame structures during Hurricane Katrina. Journal of Performance of Constructed Facilities, 21(2), 108-116.

4 Conclusion

4.1 Summary

The chief concern of this research is the further development of a roof harness retrofit system studied by Jacklin and El Damatty (2014) as a temporary method of mitigating damage to traditionally built light-framed wood structures in high wind speed events. The retrofit acts as a secondary vertical load path while providing a pretension force that compresses the structure beneath, reducing the uplift experienced at STTCs and RTWCs.

The current research extends the previous numerical and experimental work by subjecting a reduced scale version of a whole LFWS using wind to generate RTWC failure. To create an environment capable of destructive testing, a three dimensional linear contraction was developed. A reduced scale test specimen is then developed to meet the geometric and failure velocity requirements of the test environment, while simulating the behaviour of a full scale LFWS.

The test specimen is subjected to wind load until failure, and the observed behaviour is then compared with the results of a numerical model. Differences between the numerically and experimentally determined responses are then used to alter the numerical model such that it approximates the observed response and provides an estimate of the actual RTWC properties. The process is then repeated with a reduced scale version of the retrofit system, and the numerical and experimental responses are compared to those of the test specimen alone. The comparison shows that the retrofit provides a significant benefit in mitigating damage to the RTWCs. An alternative retrofit configuration is then presented, with marked improvement in tension distribution and overall stiffness.

4.2 Key Findings of the Current Work

In pursuing the primary goal of validating the effectiveness of the proposed retrofit system, a method of expanding the capabilities of wind tunnels to include reduced scale destructive testing was also developed. Initial tests of the experimental setup were aimed at understanding the wind profile, pressure distribution over the roof, and load imparted to the RTWCs, and lead to a number of conclusions:

- The incident wind flow resembles a jet, and provides a maximum velocity of approximately 36 m/s at full fan speed uniformly across the wind field, with very low values of turbulence intensity. The low turbulence intensity is uncharacteristic of land-based terrain classifications, and there is no meaningful development of a boundary layer with respect to the height of the structure. Though the development of a more realistic flow is important to the future development of this testing method, flow remediation efforts are not required due to the comparative nature of the current study.
- The pressure distribution over the roof presents significant concentrations of suction along the windward edge and on the leeward side of the peak as expected. However, the distribution is markedly different from those produced over similar roofs in wind tunnel studies using suburban wind profiles. This is a result of the uniform incident profile, and again, flow remediation efforts are not required due to the comparative nature of the current study.
- Significant uplift force is measured at the RTWCs as a result of the pressure distribution, distributed according to tributary area as the RTWCs were fixed. The

accuracy of the measurements is verified by comparing the total RTWC uplift to the integral of the pressure across area of the roof.

Concluding that the testing environment was capable of producing considerable effects on the prototype of the test specimen the RTWCs, sheathing, and roof truss components were scaled down to simulate the behaviour of a full scale LFWS and ensure the roof failed at an achievable velocity. The destructive test of this new roof focussed on observing the failure mode of the roof and validating the corresponding numerical model, and resulted in the following conclusions:

- Theoretically, scaling the capacity of structurally pertinent members of a LFWS to approximating the behaviour of a slightly different structure can be successful. However, capacity scaling was not applied to the lateral bracing connections of the test specimen, resulting in a weak lateral roof stiffness that caused the roof to behave like three separate simply supported spans rather than the stiff beam – weak spring behaviour observed in a full scale structure. Though this limits the ability of the research to make accurate predictions regarding a full scale structure, it is not critical to the success of a comparative study.
- The test specimen was successful in displaying the desired overturning failure mode, and the characteristic non-linear shape of the displacement – velocity RTWC curves was observable in the recorded data. The effect of the weak lateral roof stiffness was also observable in the recorded data.
- The numerical model predicted a higher failure wind speed than observed, due to an underestimation of the internal pressure and an overestimation of RTWC tensile resistance. In future tests, it is recommended that the differential pressure across

the roof be continuously monitored and a reduction factor be applied to the RTWC load parameters. However, the failure mode of the model was similar to the observed failure mode of the test specimen, which could be validated with the adoption of recommendations to improve estimations of pressure and RTWC resistance.

- The numerical model was updated by optimizing the RTWC properties such that the resulting RTWC displacement – velocity curve was similar to that observed in the test specimen. Though this method still neglects the errors in internal pressure and RTWC resistance estimation, the resulting optimized RTWC properties indicate the actual relative stiffness of the RTWCs in the test specimen and provide an accurate portrayal of the observed response.

A similar test is run using an identical roof along with a scaled version of the retrofit system. Like the previous experiment, observation of the potential failure model and validation of the numerical model were the focus of this exercise. However, an investigation of the load sharing dynamic between the RTWCs and the retrofit system as well as a comparison of the performance between the test specimen alone and with the retrofit were also conducted. The findings of this exercise are detailed below:

- As the test specimen was unchanged between this experiment and the previous, the same observations were made regarding:
    - Lack of lateral roof stiffness causing simply supported beam behaviour,
    - Expected failure mode and RTWC behaviour,
    - Overestimation of RTWC resistance and underestimation of internal pressure,

  - Accuracy of the post-failure adapted numerical model

- Structure performance was defined as the velocity at which particular displacement events occurred in the windward RTWCs. The addition of the retrofit was effective in increasing the velocity at which these events occurred, as compared to the test specimen alone, by providing both a pretension force that added greater initial RTWC compression and a second load path. Though total windward RTWC failure was not observed during the experiment, an estimate using results of the highly accurate post-failure adapted numerical model would suggest that this event would occur in the test specimen at 40.5 m/s. This would be a 68.1% increase over the test specimen alone.

- The function of the retrofit as a second load path allowed uplift to be shared between the RTWCs and the retrofit. Since the stiffness of the retrofit is approximately constant, load sharing at a given wind velocity depends on the variable stiffness of the RTWCs which is a function of displacement. This was observed in the experimental and numerical results.

- During the experiment, poor tension distribution between the external and internal cables was observed as bending in the rigid bar. A solution was proposed to route the cables through the rigid bar such that the rigid bar would only experience compression. A comparison of numerical analyses using both the original and alternate internal cable configurations revealed a significant improvement to both the tension distribution and overall stiffness of the retrofit system.

4.3 Recommendations for Future Work

Though the work presented is exhaustive, developing a relatively novel testing method requires more research than can be provided in this thesis. Additionally, the retrofit system is still a new technology and further work is required to mature it to a marketable product. Therefore, recommendations for further study are prepared as follows:

- Development of the wind field generated by the contraction such that a controllable profile is generated. Using roughing elements such as blocks and a wire grid would help introduce turbulence and provide a more characteristic pressure distribution over the roof. A more robust testing scheme, detailed below, and a more realistic wind field would no longer require expensive comparative testing.
- Testing and scaling the lateral bracing components of the test specimen to better simulate the stiff behavior of a full scale roof. Increasing the lateral stiffness of the test specimen would allow for the stiff beam – weak spring behaviour and associated load sharing to occur, as observed in a typical LFWS roof.
- Facilitating easier pressure data collection such that this can be recorded on every test, or finding a relationship between windward edge separation and change in internal pressure. This would allow for a better prediction of failure velocity, and a more accurate post-failure estimate of RTWC properties.
- A more robust model of the base LFWS through either:
    - Further reduction of the size of nails, connections, and other roof components such that more detail of the full scale structure can be accommodated. Key features of a full scale LFWS such as gable trusses and

tighter truss spacing significantly change the behaviour of the roof, and can be accommodated if the size and strength of components decrease.

    - Full scale, or near-full scale, testing at a facility that can accommodate a large LFWS, and produce sufficient wind speed to generate the required failure.

- Testing and scaling of STTCs for isolated sheathing failure experiments. More research into the ability of the retrofit in preventing STTC failure will prove critical to the maturation of the system.
- Analysing the stresses incurred at overhangs and eaves due to the retrofit system, and the development of mitigation techniques. Overhang stress limits the amount of pretension that can be applied to the retrofit, so development of techniques such as cables risers or diverters will be critical to function.
- Experimental testing of the proposed internal cable configuration to validate the numerical results. The potential increase in tension distribution and overall stiffness will be of greater importance if testing for STTC failure.

Curriculum Vitae

Name Joshua D. Rosenkrantz

Post-secondary Education and Degrees

The University of Western Ontario
London, Ontario, Canada
2010-2014 BESc.

The University of Western Ontario
London, Ontario, Canada
2014-2017 MESc.

Related Work Experience

Structural EIT
Thornton Tomasetti Canada Inc.
2017 - Present

Teaching Assistant
The University of Western Ontario
2014-2016

Junior Designer / Inspector
Sigmund Soudack and Associates Inc.
Summer 2013 & 2014

Junior Project Manager, 407 Median Project
Brennan Construction
Summer 2012

Publications

Rosenkrantz, J. D., Enajar, A., and El Damatty, A. A.. 2016. Structural modelling and verification methods to develop a cable roof harness retrofit system. *5th International Natural Disaster Mitigation Specialty Conference*, Canadian Society for Civil Engineering, London, Ontario, Canada, 9 p. paper in proceedings.

Rosenkrantz, J. D., and El Damatty, A. A.. 2016. Wind load parameters of a structural test using real wind load at the WindEEE Dome. *4th American Association for Wind Engineering Workshop*, American Association for Wind Engineering, Miami, Florida, USA, 47 p. paper in proceedings.